(1)

UNCLASSIFIED

SECURITY CLASSIFICATION OF THIS PAGE (When Data Entered)

REPORT DOCUMENTATION PAGE		READ INSTRUCTIONS BEFORE COMPLETING FORM
1. REPORT NUMBER AFIT/CI/NR 88- 118	2. GOVT ACCESSION NO.	3. RECIPIENT'S CATALOG NUMBER
4. TITLE (and Subtitle) THE EFFECTS OF PLY DROPOFFS ON THE TENSILE BEHAVIOR OF GRAPHITE/ EPOXY LAMINATES		5. TYPE OF REPORT & PERIOD COVERED MS THESIS 6. PERFORMING ORG. REPORT NUMBER
7. AUTHOR(s) RAYMOND KEVIN CANNON		8. CONTRACT OR GRANT NUMBER(s)
9. PERFORMING ORGANIZATION NAME AND ADDRESS AFIT STUDENT AT: MASSACHUSETTS INSTITUTE OF TECHNOLOGY		10. PROGRAM ELEMENT, PROJECT, TASK AREA & WORK UNIT NUMBERS
11. CONTROLLING OFFICE NAME AND ADDRESS		12. REPORT DATE 1988 13. NUMBER OF PAGES 176
14. MONITORING AGENCY NAME & ADDRESS (if different from Controlling Office) AFIT/NR Wright-Patterson AFB OH 45433-6583		15. SECURITY CLASS. (of this report) UNCLASSIFIED 15a. DECLASSIFICATION/DOWNGRADING SCHEDULE

16. DISTRIBUTION STATEMENT (of this Report)

DISTRIBUTED UNLIMITED: APPROVED FOR PUBLIC RELEASE

17. DISTRIBUTION STATEMENT (of the abstract entered in Block 20, if different from Report)

SAME AS REPORT

18. SUPPLEMENTARY NOTES

Approved for Public Release: IAW AFR 190-1
LYNN E. WOLAVER 20 July 88
Dean for Research and Professional Development
Air Force Institute of Technology
Wright-Patterson AFB OH 45433-6583

19. KEY WORDS (Continue on reverse side if necessary and identify by block number)

20. ABSTRACT (Continue on reverse side if necessary and identify by block number)

ATTACHED

DD FORM 1 JAN 73 1473 EDITION OF 1 NOV 65 IS OBSOLETE

UNCLASSIFIED

SECURITY CLASSIFICATION OF THIS PAGE (When Data Entered)

THE EFFECTS OF PLY DROPOFFS ON THE TENSILE BEHAVIOR OF GRAPHITE/EPOXY LAMINATES

by

RAYMOND KEVIN CANNON

Submitted to the Department of Aeronautics and Astronautics
on May 26, 1987 in patial fulfillment of the
requirements for the Degree of Master of Science

ABSTRACT

The effects of ply dropoffs on the stress-strain behavior, fracture modes and fracture strength of graphite/epoxy laminates in tension were investigated. Seven different layups with ply dropoffs were manufactured and tested to failure in uniaxial tension. Test variables included the number, order, angular orientation, and effective ply thickness of dropped plies. With six of the ply dropoff laminates, one side of the laminate was flat, with the outer plies of the other side of the laminate curving over the ply dropoff from the undropped, or thicker, section to the dropped section. This type of laminate is geometrically unsymmetric, and therefore bending stresses are induced in the laminate during testing. The analysis method developed was a one-dimensional model which allows the calculation of first ply failure of a ply dropoff laminate taking into account this induced bending effect. The seventh ply dropoff laminate was made such that the outer plies surrounding the dropped plies tapered in on both sides such that the laminate was geometrically symmetric. The stress-strain behavior of the ply dropoff laminates was closely approximated by those of the flat laminates having the same layups as the dropped and undropped sections. The failure stresses and modes of the ply dropoff laminates were equal and similar to, respectively,that of the flat laminate having the same layup as the dropped section of the ply dropoff laminate, within data scatter. Of the number, order, angular orientation, and effective ply thickness variables studied, only the order seemed to affect the ply dropoff laminates in comparison with the flat laminates. Laminates with all dropped plies adjacent to each other in the center of the laminate tended to delaminate away from the rest of the laminate in the undropped section. Failure stresses were still unaffected, however.

Thesis Supervisor: Paul A. Lagace

Title: Associate Professor of Aeronautics and Astronautics

THE EFFECTS OF PLY DROPOFFS ON THE TENSILE BEHAVIOR OF GRAPHITE/EPOXY LAMINATES

by

RAYMOND KEVIN CANNON
B.S., United States Air Force Academy
(1981)

SUBMITTED IN PARTIAL FULFILLMENT
OF THE REQUIREMENTS FOR THE
DEGREE OF

MASTER OF SCIENCE IN
AERONAUTICS AND ASTRONAUTICS

at the

MASSACHUSETTS INSTITUTE OF TECHNOLOGY
May 1987

Signature of Author_____
Department of Aeronautics and Astronautics
May 26, 1987

Ceritifed by_____
Professor Paul A. Lagace
Thesis Supervisor

Accepted by_____
Professor Harold Y. Wachman
Chairman, Departmental Graduate Committee

THE EFFECTS OF PLY DROPOFFS ON THE TENSILE BEHAVIOR OF GRAPHITE/EPOXY LAMINATES

by

RAYMOND KEVIN CANNON

Submitted to the Department of Aeronautics and Astronautics
on May 26, 1987 in patial fulfillment of the
requirements for the Degree of Master of Science

ABSTRACT

The effects of ply dropoffs on the stress-strain behavior, fracture modes and fracture strength of graphite/epoxy laminates in tension were investigated. Seven different layups with ply dropoffs were manufactured and tested to failure in uniaxial tension. Test variables included the number, order, angular orientation, and effective ply thickness of dropped plies. With six of the ply dropoff laminates, one side of the laminate was flat, with the outer plies of the other side of the laminate curving over the ply dropoff from the undropped, or thicker, section to the dropped section. This type of laminate is geometrically unsymmetric, and therefore bending stresses are induced in the laminate during testing. The analysis method developed was a one-dimensional model which allows the calculation of first ply failure of a ply dropoff laminate taking into account this induced bending effect. The seventh ply dropoff laminate was made such that the outer plies surrounding the dropped plies tapered in on both sides such that the laminate was geometrically symmetric. The stress-strain behavior of the ply dropoff laminates was closely approximated by those of the flat laminates having the same layups as the dropped and undropped sections. The failure stresses and modes of the ply dropoff laminates were equal and similar to, respectively,that of the flat laminate having the same layup as the dropped section of the ply dropoff laminate, within data scatter. Of the number, order, angular orientation, and effective ply thickness variables studied, only the order seemed to affect the ply dropoff laminates in comparison with the flat laminates. Laminates with all dropped plies adjacent to each other in the center of the laminate tended to delaminate away from the rest of the laminate in the undropped section. Failure stresses were still unaffected, however.

Thesis Supervisor: Paul A. Lagace

Title: Associate Professor of Aeronautics and Astronautics

ACKNOWLEDGMENTS

I would like to take this opportunity to thank the many people who have contributed so much to this thesis and to my stay at MIT. First of all, I would like to thank the Air Force for sponsoring me and MIT for accepting me into this program. The challenge was great and the rewards were many.

I am very thankful to my advisor, Professor Paul Lagace. Besides putting in a great deal of effort, expertise, and insight into the thesis itself, Paul was a great motivator. Whenever things were going badly, a talk with Paul would help me get things turned around.

While the Air Force and MIT got me into this program, my office mates saw me through it. Whether it was technical advice for research or the classroom, or just keeping things fun and interesting, my friends in the office never let me down. Thanks very much to Lenny who took me under his wing when I first arrived, Doug, Mike K., Pierre, Mike B., Peter, John B., John S., and especially to Kevin, without whom this thesis would still not be done.

I had a great deal of assistance from two undergraduates from beginning to end of the thesis, Stephanie and Kara. My sincere thanks goes to you for not only doing a lot of the "grunt" work required in the lab, but for also being real contributors in every aspect of the project. I would also like to thank Adam and Charles for coming to my rescue during the last month of the project when so much still needed to be done.

There would be no TELAC without the people who really run the lab. Many thanks to Al Supple and Carl Varnerin for getting me through the manufacturing, testing, and so many other details which go into an experimental program. Thanks go to Ping Lee and Debra Smith for taking care of the administrative matters.

DEDICATION

To my wife, Leona, and son, Jonathan

TABLE OF CONTENTS

TABLE OF CONTENTS (continued)

LIST OF FIGURES

LIST OF TABLES

LIST OF DATA TABLES

NOMENCLATURE

CLPT	Classical Laminated Plate Theory
E_L	longitudinal modulus
GPa	Gigapascals ($=10^9$ pascals)
KN	Kilonewtons ($=10^3$ newtons)
M	moment resultant
MPa	Megapascals ($=10^6$ pascals)
mm	millimeters
N	stress resultant
w	z-direction displacement
κ	curvature
π_p	total potential energy
$\sigma_{11}^{[\theta_i]}$	longitudinal stress in ith ply
$\sigma_{22}^{[\theta_i]}$	transverse stress in ith ply
$\sigma_{12}^{[\theta_i]}$	shear stress in ith ply
σ_f	failure stress
ν	Poisson's ratio

CHAPTER 1

INTRODUCTION

The use of composites has grown tremendously in the past decade. Industries as diverse as recreational, sporting, automotive, and aerospace have found good use of the improved strength to weight and stiffness to weight ratios which composites can offer over more conventional materials. Golf club shafts, hockey sticks, and tennis racquets reinforced by or made of advanced composites are now commonplace to the sports enthusiast. It is becoming more and more common to see composite racing bicycle frames in the local bicycle shop. Composite driveshafts and leaf springs have been in production in American automobiles for several years. Formula type and Grand Touring Prototype (GTP) racecars use composite monocoque chassis. Lotus expects to have the first production car with a full composite monocoque chassis sold in the United States in late 1990 [1]. What is particularly encouraging about some of these later developments in the use of composites is that they are being used in primary structural applications, laid up from preimpregnated tape or cloth rather than molded chopped fibers. This gives a composite structure in its strongest and stiffest form.

Nevertheless, the aerospace industry has been the prime mover in composite materials, mainly because of the great importance of weight savings. Initial aircraft applications were secondary structural applications, such as access doors,

fairings, and flaps. Tail sections and wing skins are common in such aircraft as the General Dynamics F-16 and the McDonnell-Douglas F-18. The Beech Starship is a new, all composite, business class civilian aircraft currently awaiting certification by the FAA. This aircraft represents a huge jump forward in the use of composites. Another very desirable property of composites which make them particularly well suited to the aerospace industry is that the stiffness, strength, and coefficient of thermal expansion can be "tailored" to optimize the structure for the type of loads it will carry. A space structure can be made with a zero coefficient of thermal expansion to eliminate the problems caused by large swings of temperature in space. Bending-twisting coupling can be tailored into forward-swept wings allowing the increased aerodynamic performance of this configuration to be taken advantage of without the divergence problem which occurs with isotropic material. This is currently being demonstrated with the X-29.

With many real world structures, the load which must be carried is not uniform throughout the structure. An example of this is an aircraft wing, where the root of the wing carries much higher loads than the tip. For this reason it would be too conservative to design the entire structure to the highest load. Ideally, each area of the structure is designed to be able to carry only the load which it will see. This is often done by varying the thickness of the structure. With metals, it might be done by machining, casting, or various forming

methods. With composites it is often done by terminating plies at various points to achieve the desired thicknesses. These terminated plies are called ply dropoffs. These ply dropoffs are essentially a discontinuity which act as a stress riser both in the plane and out of the plane, even with strictly in plane loading. Out-of-plane, or interlaminar, stresses can lead to delamination in a composite material due to the relative weakness of the material in the out of plane direction when compared with the strength along the fibers. Delamination can in turn lead to early failure in the structure when compared with that predicted from in-plane considerations.

The purpose of this investigation was to determine the effects of ply dropoffs on the strength of graphite/epoxy laminates loaded in tension. This was done by conducting a series of experiments on statically loaded tensile coupons with and without ply dropoffs. In Chapter 2 of this document, previous work done in this area and the related topic of free edge induced interlaminar stresses is described. The experimental work performed, including ply dropoff characteristics, specimen manufacturing, and testing methods are described in Chapter 3. A derivation of the analysis used to predict the strength effects of ply dropoffs on laminates is presented in Chapter 4. In Chapter 5, the results of the experimental study, including stress-strain behavior, fracture stresses, fracture modes, and the analysis are presented. Chapter 6 contains a discussion on the effects of the ply dropoffs on fracture stresses and failure modes. Finally,

conclusions from this work and further recommendations are made in Chapter 7.

CHAPTER 2

SUMMARY OF PREVIOUS WORK

2.1 Interlaminar Stresses and Delamination

Delamination is a damage mode peculiar to laminated composites where the plies of the composite separate at a ply interface. Delaminations are caused by out-of-plane, or interlaminar, stresses. These interlaminar stresses occur in a multidirectional composite wherever there is a gradient field, such as at a ply dropoff, free edge, hole, or bonded or bolted joint [2]. The most studied case in this area has been that of the free edge.

Classical Laminated Plate Theory (CLPT) is based on the assumption that a state of plane stress exists for a thin, symmetric laminate when subjected to in-plane loads. In any multidirectional layup, elastic properties such as Poisson's ratio, Young's modulus, and coefficients of mutual influence differ among the various angular orientations [3]. Since CLPT imposes strain continuity through the thickness of the laminate, in-plane stresses must differ in the plies. The CLPT solution cannot hold near the gradient field. This is most easily seen with the case of the free edge. Figure 2.1 is a drawing of a laminate with a free edge uniaxially loaded in the x-direction. The free edge is in the y-z plane of the laminate, and therefore in-plane stresses σ_{22} and σ_{11} must be zero on this face. With CLPT, however, it is predicted that

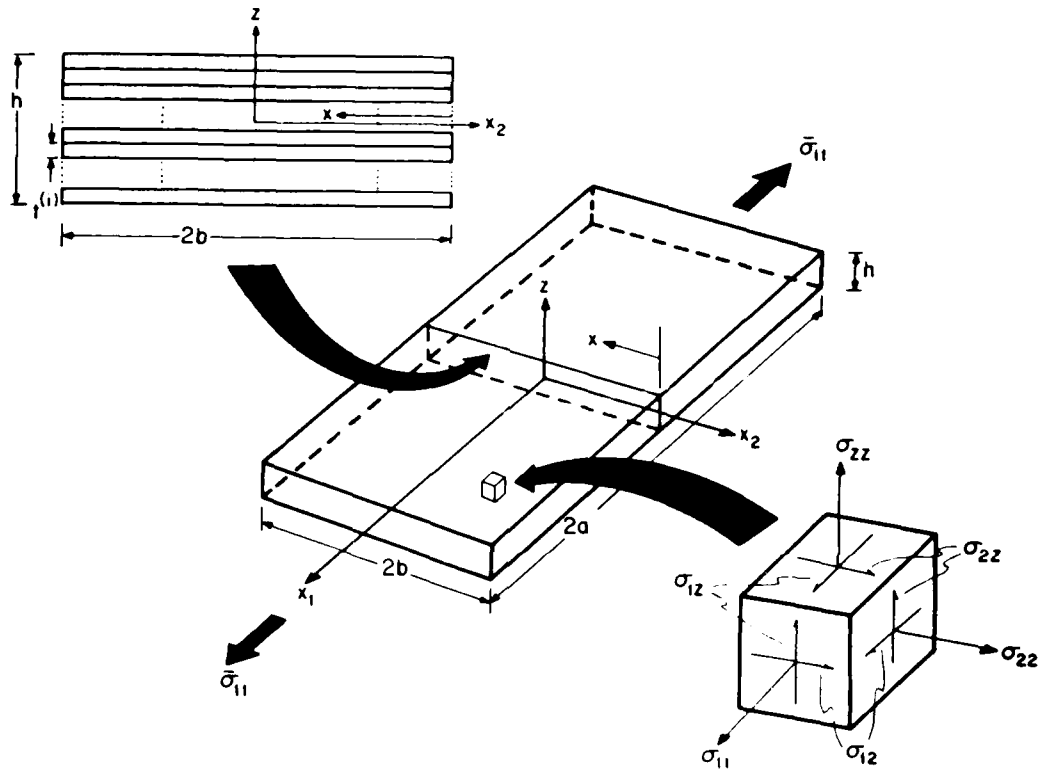

Figure 2.1 Laminate with Free Edge Uniaxially Load

these stresses are not zero in the plies themselves, but only in an average sense through the thickness of the laminate. As can be seen in Figure 2.2, σ_{12} equal to zero on the free edge means that the couple caused by σ_{12} on the other edges must be reacted by some other force to remain in equilibrium. The only force that can counteract this couple is σ_{1z} acting on the edge, or boundary layer, at the lower ply interface [4]. This same boundary layer effect will occur at any gradient field.

Calculating these interlaminar stresses has been the topic of many research papers. Pipes and Pagano used a finite difference scheme in a 1970 paper which initiated much of the interest in this area [5]. Many authors have used finite element methods (FEM) to model the interlaminar stress problem [6,7,8,9]. Whitney assumed stress functions which satisfied differential equilibrium and found fair agreement with some elasticity solutions although compatability was not satisfied [10]. Pipes and Pagano experienced a divergence problem using a Fourier series method [11]. Lagace and Kassapoglou [12,13] determined the interlaminar stresses in the free edge problem by assuming stress functions which satisfy differential and integral equilibrium, and minimizing the complementary energy. Excellent agreement with numerical solutions were obtained with the benefi of thick laminate capability and greatly reduced computational time over that of FEM.

After the interlaminar stress distributions are calculated, a failure, or delamination initiation, criterion is needed to determine the effects of these stresses. The

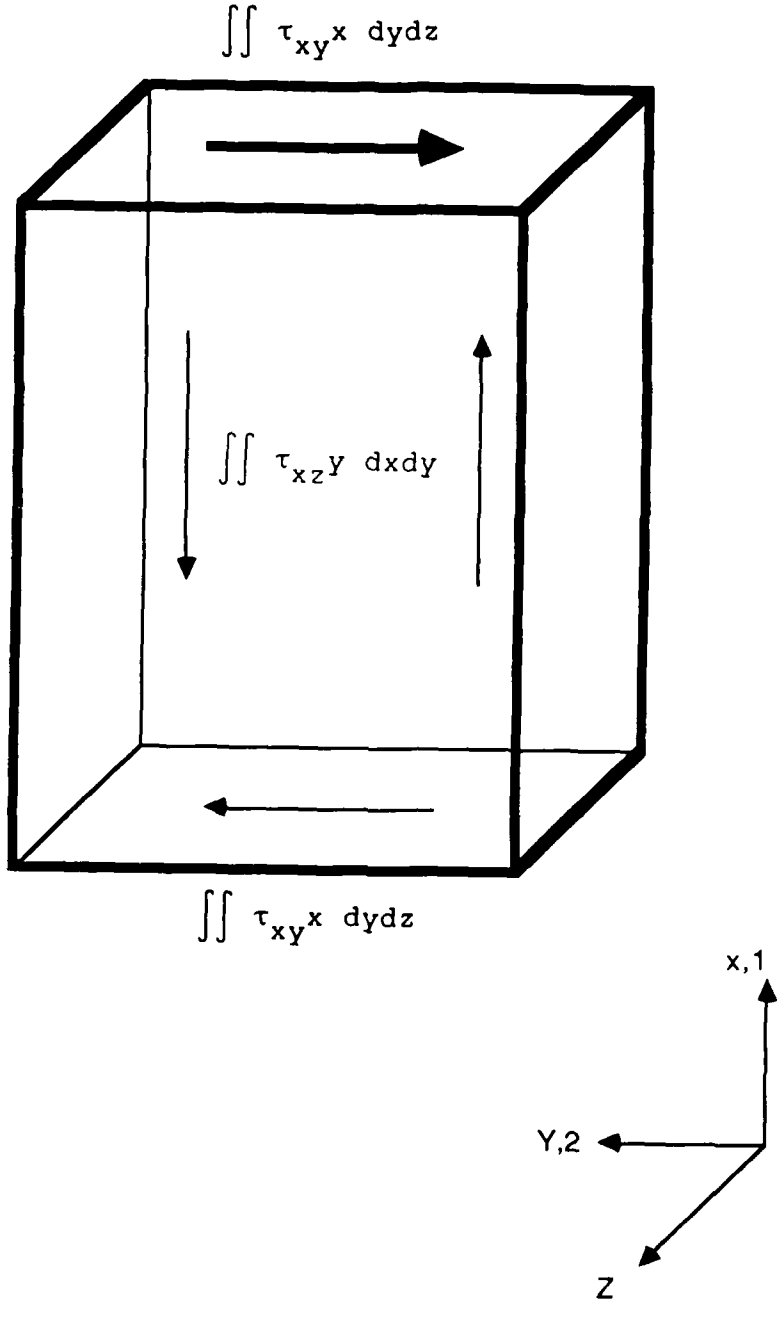

Figure 2.2 Interlaminar Shear Stress From Free Edge

interlminar shear and normal stresses calculated at the point of the free edge far exceed the strength of the matrix, which is similar to the case of the point at the edge of a hole where the in-plane stress, σ_{11}, exceeds the ultimate stress of the material. Since failure does not occur the moment this point stress value exceeds the strength of the material, it was reasoned that failure is due to an average stress over a specified region. Whitney and Nuismer [14] introduced this concept of an average stress criterion in a study of the failure of notched composites. Kim and Soni [15,16] applied an average stress criterion to delamination initiation, first by averaging the interlaminar normal stress, σ_{zz}, over an arbitrarily chosen dimension of one nominal ply thickness. Delamination initiation was predicted when the averaged σ_{zz} value reached the interlaminar normal strength parameter, which was estimated as the transverse strength of a unidirectional ply. In another study, Kim and Soni averaged the interlaminar shear stress, σ_{1z}, over the nominal ply thickness and used the in-plane shear stregth to approximate the interlaminar shear strength of the laminate. Reasonable agrreement with experimental data was achieved with both of these studies.

The Quadratic Delamination Criterion (QDC) proposed by Lagace and Brewer [17] is an average stress criterion which takes account of σ_{1z} and tensile σ_{zz}. Compressive σ_{zz} values are not believed to cause delamination. The effect of ply thickness on delamination initiation due to interlaminar stresses at the free edge was also studied in this

investigation. It has been experimentally shown that initiation will occur at lower values of applied far-field stress for laminates with larger ply thicknesses. This was explained mathematically by noting that the interlaminar stress distributions spread out with respect to distance from the free edge as ply thickness increases, while the value of stress at the free edge and the shape of the stress distribution remains constant. Since the stresses are averaged in the QDC failure criterion over an averaging dimension which remains constant, the average interlaminar stress components contributing to delamination increase for a given far field stress.

Several others [18,19,20] have used a fracture mechanics approach for predicting delamination initiation. With this approach, the delamination is modeled as an interlaminar crack. The basic idea behind this approach is that delamination occurs if and only if the strain energy released as the delamination grows is sufficient to provide the energy needed to create the new surface. Strain energy available for release is typically determined by finite element analysis.

2.2 Interlaminar Stresses With Ply Dropoffs

While the effects of interlaminar stresses and delamination have been studied quite extensively in the area of the general free edge problem, very little work has been done in the area of ply dropoffs. Similar to the free edge problem, gradient stress fields also occur due to ply dropoffs and therefore need to be studied further. Ply dropoffs are used

quite frequently in the aerospace industry to tailor thickness, stiffness, and strength. Therefore, it is important to gain a more thorough understanding of the strength effects of ply dropoffs in composite laminates.

The Navy has funded several projects in the area of ply dropoffs, dealing more specifically with composite panels designed for the vertical stabilizers of the F-18. These investigations were performed by the Northrop Corporation and the University of Wyoming and included experimental and analytical work. Grimes and Dusablon [21] and Adams [22] performed an experimental investigation based on a 30 ply $[(\pm 45)_5/0_{16}/90_4]_C$ layup, where the $[\ ]_C$ notation denotes a condensed notation scheme used for ease of wriiting. Three variations were tested, the flat (undropped) laminates, a ply dropoff laminate with two 0^o plies dropped off (referred to as PDO #1) and a ply dropoff laminate with two sets of $\pm 45^o$ plies dropped off(PDO #2). All plies were dropped off symmetrically. The panels were tested in compression testing both statically and in fatigue, as well as under various temperature and humidity conditions. For the static tests, there was very little variation in strength between the flat specimens and PDO #1 and #2. Note, however that these ply dropoffs are relatively benign cases, with only two 0^o or four 45^o plies dropped off in a 30 ply laminate.

Ramkumar and Adams [23] continued this study by combining the effects of porosity and holes drilled at the ply dropoffs. The same laminates, in addition to $[0]_{24}$, $[90]_{24}$, and $[\pm 45]_{6S}$,

were used in this study. Reduced pressure during the cure cycle was used to create additional porosity in the laminates. Porosity had no effect on the failure strains of the laminates with ply dropoffs but did reduce failure strains in the flat specimens. Holes drilled at ply dropoffs greatly reduced failure strains, regardless of porosity.

Adams, Ramkumar, and Walrath [24] performed an analytical study on the same problem using a three-dimensional nonlinear finite element analysis of PDO #1. Manufacturing stresses and moisture absorption were taken into account. The grid used was rather coarse, two layers of elements were used for the 0^{o} dropped ply, and only the top half was modeled, even though the laminate was not geometrically symmetric. It was felt that a good representation of the macroscopic, structural effect of the ply dropoffs was achieved. The results showed concentrations of in-plane stress in the area of the ply dropoff and correlated well with the experimental room temperature results. The model showed small interlaminar stresses around the ply dropoff region relative to that of the in-plane stresses.

DiNardo and Lagace [25] conducted an investigation into the effects of ply dropoffs on the buckling and postbuckling behavior on composite plates. Both experimental and analytical work was done with flat (no dropoff) plates, plates with ply dropoffs, and plates with angle changes in the same location as the ply dropoffs, that being along a centerline perpendicular to the loading direction. Several layups with ply dropoffs

were considered, including a single 0^{o} ply dropped off, double 0^{o} plies dropped off both symmetrically and unsymmetrically, angle plies dropped off symmetrically, 0^{o} and angle plies dropped off symmetrically, and entire sublaminates $([\pm 45/0]_{S})$ dropped off. Two methods of analysis were used, both looking at the linear buckling behavior of the plates. One method used a "superelement" formulated with a Rayleigh-Ritz assumed deflection method. Each plate used one such element to model each half of the plate. The second method used a hybrid stress finite element method.

DiNardo and Lagace found that ply dropoffs have significant effects on both the buckling load and deflection shapes of buckled plates. It was found both with the analysis and by experiment that the buckling loads for the ply dropoff cases were bounded by the buckling loads for the basic plates having the same layups as the individual halves of the plate with the ply dropoff. The ply dropoffs complicated the deflection shapes, as well as moving the maximum lateral deflection of the plate from the center towards the center of the dropped section. The buckling behavior of the plates with the dropoffs depended largely on the ratio of the D_{11} terms of the dropped and undropped sections. Plates with ply dropoffs which had dropped and undropped sections with identical or similar D_{11} terms had exhibited similar deflection, strain, and failure behavior. In general, failure loads were dependent on the thickness of the thinnest section of the plate.

More closely related to the topic at hand, Wu and Webber

[26] performed an analytical investigation upon the effects of ply dropoffs via FEM by developing a quasi-three dimensional isoparametric element. They modeled a configuration with the ply dropoffs on the outside of the laminate with a plane of symmetry about the center of the laminate such that the displacements and strains do not vary across the width of the specimen in the transverse direction away from any free edges. The assumed displacement fields limit the applicability of this element to balanced, symmetric laminates. Three laminates were analyzed, $[0_4]_S$, $[0/90/0_2]_S$, and $[-+45/0_2]_S$. The first two plies in each half laminate were dropped off on the outside of the laminate, where only half of the laminate is modeled due to symmetry. The model predicted high in-plane (σ_{11}) and interlaminar (σ_{1z} and σ_{zz}) peak stresses in the corner region of the step. These peak stresses were reduced when a more realistic case was modeled with a glue fillet added at the tip of the ply dropoff. The three laminates above are listed in descending order of peak stresses, with the $[0_4]_S$ laminate having the highest peak stresses.

Kemp and Johnson [27] also conducted an analytical study in the area of ply dropoffs in compression and tension. They used a two-dimensional isoparametric element for the finite element analysis used to predict stresses. Two modes of failure initiation were analyzed. The maximum stress criterion was used for the pure resin regions modeled around the inidividual plies and the three-dimensional Tsai-Wu criteria was used for in-plane failure. Two layups were analyzed,

$[\pm 45/0/90/0_{nD}/90/0/-+45]$ (case 1) and $[0/90/\pm 45/0_{nD}/-+45/90/0]$ (case 2) in both symmetric and total configurations, where the laminates in the total configuration were half the thickness of the symmetric configuration and flat on one side. The symmetric configuration laminates were geometrically symmetric. The subscript nD denotes the number of plies dropped off where n is equal to one, two, or three. One other variable was added to the analysis. which the authors called the aspect ratio and was defined as the ratio of height to length of the triangular region of resin ahead of the dropped ply. Values of 1/3, 1/4, 1/5, and 1/6 were used. Tensile results of the first laminate listed above in both the symmetric and total configuration were presented and discussed with n equals 3 and an aspect ratio of 1/3.

The results presented showed that the ply dropoff does significantly affect the stress distribution and contributes to the formation of interlaminar shear and normal stresses. The peak values of the interlaminar stresses occur at the ply dropoff and decay when moving away from the dropoff to a value of zero, as predicted by CLPT, away from this boundary layer. The shear-in distance, defined as the axial length required to transfer load to dropped plies, for interlaminar shear stress was found to be equal to 20h for 1 ply dropoff, where h equals the ply thickness, and an additional 5h for each additional dropped ply. Shear-in distance for interlaminar normal stress was about half that of interlaminar shear stress. The failure criterion for out-of-plane failure indicated a failure at the

upper interface at the ply dropoff for all unsymmetric laminates and about half of the symmetric laminates, with the remaining failures occurring at the lower interface at the ply dropoff. Decreasing aspect ratio increased strain to failure. This was the first failure event predicted in most cases, although the analysis predicted tension intralaminar failures at the upper corner of the ply of the case 2 layup with an aspect ratio of 1/3. The authors noted that material nonlinearity might need to be taken into account to realistically predict failure strains due to the known softening of the neat resin before failure.

Curry, Johnson, and Starnes [28] performed an experimental and analytical study on the effects of ply dropoffs on graphite/epoxy laminates loaded in tension and compression. Laminates considered were $[(\pm 45/0/90)_S(N_D)(\pm 45/0/90)_S]_T$ layups where N_D represents eight different sublaminates. Six of these sublaminates were unidirectional layups of 90^o and 0^o, each with two, four, or eight plies. The last two sublaminates were $[\pm 45/0_2]_S$ and $[\pm 45/0/90]_S$. Therefore, undropped laminate thickness ranged from 18 to 24 plies, while all dropped end thicknesses were 16 plies. All laminates with ply dropoffs were fabricated with one side of the laminate flat and one side tapering in from the undropped end of the specimen to the dropped end. Bending-extension coupling was thus created due to the geometric eccentricity of the midplanes of the dropped and undropped sections. A finite element analysis was performed to determine the three-dimensional state of stress in

the laminates in the region of the ply dropoff. Three failure criteria were used to predict the failure load and mode. The three-dimensional tensor polynomial failure criterion and individual fiber/matrix criteria developed by Hashin were used for intralaminar failure, the interlaminar criteria were based on the matrix failure modes developed by Hashin, and strength criteria for neat resin were taken from data by Chamis.

The results of this study were that the strength of laminates with ply dropoffs was less than that of its dropped section, the compression specimens exhibited a lower strength than a tension specimen of the same configuration and width, and that the reduction in strength is directly related to the axial stiffness change between the thick and thin sections of the laminate. The failure criteria were accurate in predicting the regions of critical stress, but were quite conservative in predicting the failure load.

It is clear from a review of work completed to date in the area of ply dropoffs that more work needs to be done in this area to understand what is really happening, particularly in the case of tension loaded laminates, where very little work has been done. Methods must be developed to predict the strength, and possible strength and stiffness reduction effects, of laminates with ply dropoffs for more efficient design of aerospace structures. The goal of this investigation is therefore to experimentally determine the effects of ply dropoffs on the strength of a composite structure loaded in

tension. Analysis methods are developed to determine any strength reduction effect caused by the ply dropoffs due to induced bending.

CHAPTER 3

THE EXPERIMENT

3.1 Material and Specimen Choice

The graphite/epoxy used in this investigation was Hercules AS4/3501-6. The material was furnished as a continuous roll of unidirectional tape with a nominal width of 305 mm. The epoxy system of the preimpregnated tape or prepreg was in a semi-cured state and hence stored in freezers at $-18^{o}C$ or below until used. The elastic properties of unidirectional AS4/3501-6 are listed in Table 3.1.

The specimen used in this study was the standard coupon used at TELAC [29]. This coupon, shown in Figure 3.1, measures 350 mm long by 50 mm wide. Glass/epoxy loading tabs 75 mm long were bonded to the ends of the specimen with FM-123-2, a film adhesive from American Cyanimid. The loading tabs were precured 3M type 1002 with a layup of alternating 0^{o} and 90^{o} plies. The thickness of the loading tabs was a function of the thickness of both ends of the coupon. This is described in more detail in Section 3.3, Specimen Manufacture. The tab thickness to specimen thickness ratio is that recommended by the American Society for Testing and Materials, which is between 1.5 to 1 and 4 to 1 [30]. The length of the test section is 200 mm.

TABLE 3.1

ELASTIC PROPERTIES OF AS4/3501-6 GRAPHITE/EPOXY

E_{11}	142 GPa
E_{22}	9.81 GPa
E_{33}	9.81 GPa
G_{12}	6.0 GPa
G_{13}	6.0 GPa
G_{23}	4.8 GPa
ν_{12}	0.30
ν_{13}	0.30
ν_{23}	0.34

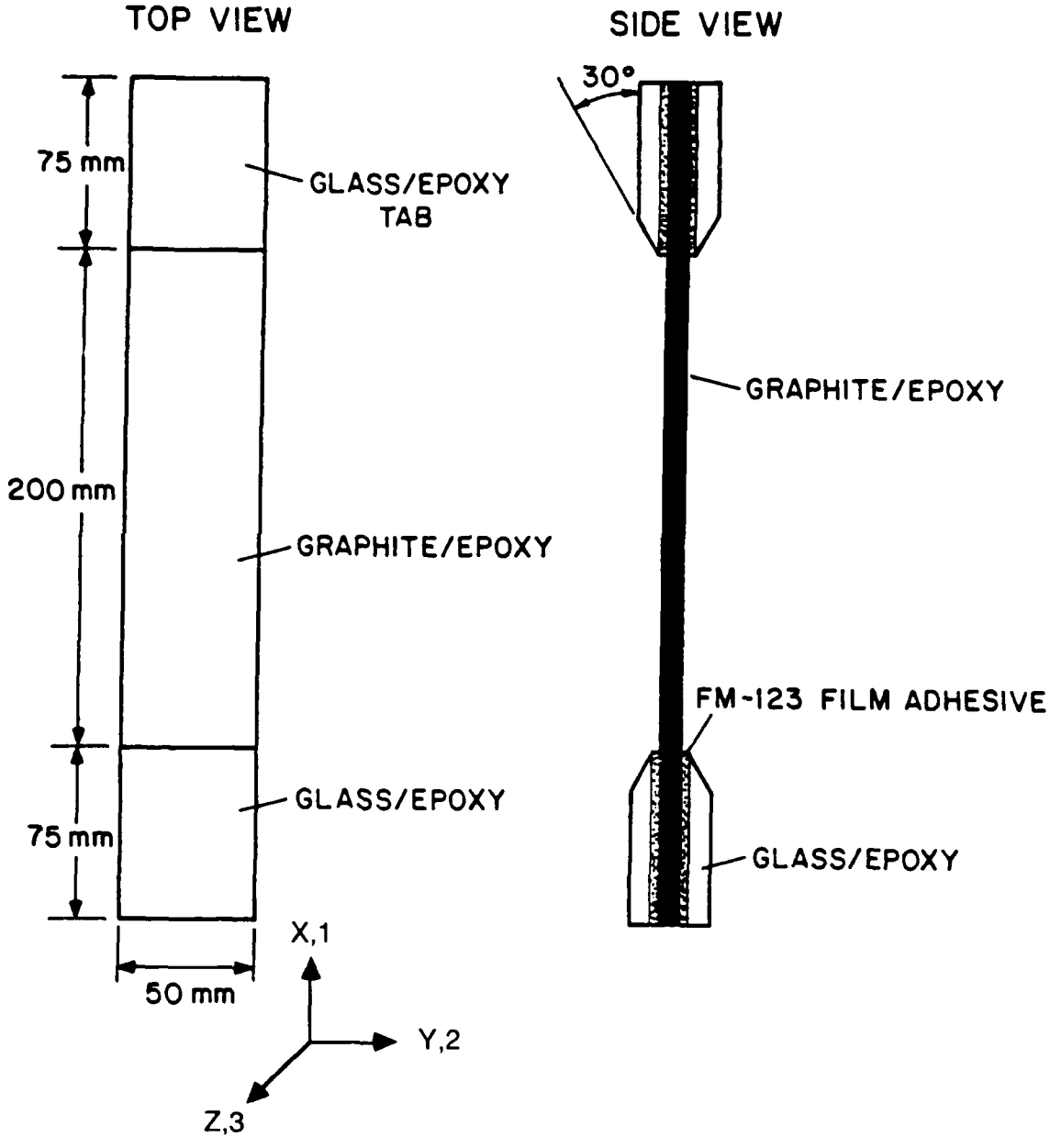

Figure 3.1 Characteristics of the Standard TELAC Tensile Coupon

3.2 Experimental Test Program

A wide range of laminates was tested during this program to demonstrate various effects of the presence of ply dropoffs. Most of the laminates were chosen to correspond to a previous study by DiNardo [25] dealing with the compressive behavior of composite plates with ply dropoffs. The current experimental program consisted of five families of laminates. Most of these laminates were based on the $[\pm 45/0]_S$ laminate, a commonly used and relatively well understood layup. More importantly, these laminate families do not have a tendency to delaminate due to free edge effects. This helps to isolate effects of the ply dropoffs from those of the free edges. Also, 90^o plies were left out in order to reduce the likelihood of transverse crack formation. The fifth group of laminates was based on the $[\pm 15/0]_S$ laminate, which was specifically chosen for its tendency to dalaminate at the free edge [31]. This allowed for comparison between laminates with a tendency toward in-plane and out-of-plane failure, and the effects of ply dropoffs on each.

Each of these families has specimens with and without dropped plies. In a coupon with dropped plies, the thick section of the coupon is referred to as the "undropped" section and the thin end is referred to as the "dropped" section. For each specimen with dropped plies, coupons without dropped plies with layups corresponding to those of both the dropped and undropped section were fabricated and tested for comparison

purposes.

Several factors were considered important in choosing these layups, including the number of plies dropped off, the orientation of the plies dropped off, the arrangement of the dropped plies within the laminate, and the effective ply thickness. Laminates were selected such that these effects could be isolated. All of the laminates tested contained internal ply dropoffs only, that is the plies which are dropped off have covering contoured plies over them such that the dropped ply is not exposed. This was done for realism as most structural designs using ply dropoffs use internal ply dropoffs.

Four different classes of ply dropoffs were considered for this investigation to isolate the effects of the factors listed above. These were a single 0° ply dropped off, two 0° plies dropped off symmetrically, angle plies ($\pm 45^{\circ}, \pm 15^{\circ}$) dropped off symmetrically, 0° and angle plies dropped off symmetrically, and an entire sublaminate ($[\pm 45/0]_s$) dropped off.

Side views of the coupon configurations with ply dropoffs used in this investigation are shown in Figure 3.2. Most of the specimens made were of the type shown in Figure 3.2a. These specimens have one flat side. The other side is not flat due to the ply dropoffs. The plies laid up on top of the terminating plies curve over the ply dropoff and then become flat again over the dropped section of the coupon. Note that even though the specimens are laid up symmetrically, with both the dropped and the undropped sections having a symmetric

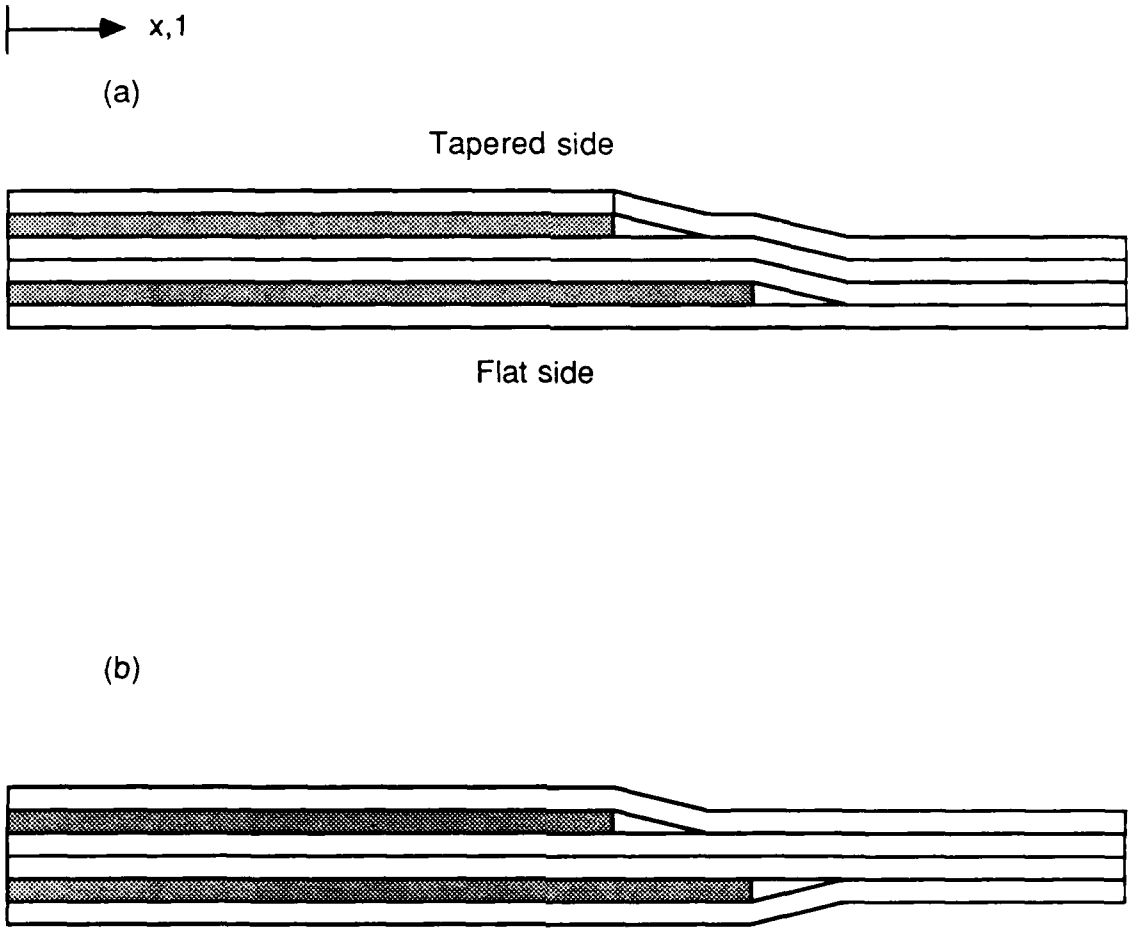

Figure 3.2 Side View of Coupon Configurations for (a-Top) Coupon With Ply Dropoffs With One Flat Side; and (b-Bottom) Coupon With Ply Dropoffs With Contiguous Neutral Axis

layup, the entire coupon is not geometrically symmetric. The midplanes of the dropped and undropped section do not coincide. While thicker loading tabs were used on the dropped end of the specimen to minimize loading eccentricity, some bending is still likely to be induced.

The motivation behind the specimen shown in Figure 3.2b was to make a geometrically symmetric laminate. With this laminate, the midplanes of the dropped and undropped sections are the same. Therefore when the laminate is loaded extensionally in the test machine, a loading eccentricity, and therefore bending, does not occur. It should be noted, however, that the specimen in Figure 3.2a is more realistic of actual structures. The specimen in Figure 3.2b was used experimentally to help isolate the effects of the ply dropoff from one more variable, that being induced bending. This proved to be a more difficult laminate to manufacture. More details of the fabrication of this laminate are given in section 3.3 on Specimen Manufacture.

Table 3.2 is a complete list of the specimens used in this investigation. The subscript "S" denotes that the laminate is symmetric about the midplane for the flat coupons. Although the specimens with ply dropoffs do not have a common midplane, the "S" subscript still means that the laminate is laid up symmetrically. The "S" applies to the dropped plies as well as the undropped plies, and also applies to each section separately. The subscript "T" stands for total and means that the total laminate has been specified. The subscript "D"

TABLE 3.2

TEST PROGRAM SUMMARY

Laminate	Letter Name	Type[a]	Comments
$[\pm 45/0]_S$	J	F	Basic Laminate
$[\pm 45/0_D/0/-+45]_T$	K	PD	Single 0° ply dropped
$[\pm 45/0/-+45]_T$	M	F	Models dropped section
$[\pm(45_2)/0_2]_S$	A	F	Basic laminate
$[\pm(45_2)/0/0_D]_S$	E	PD	0° plies dropped
$[+45/+45_D/-45/-45_D/0/0_D]_S$	F	PD	0°, angle plies dropped
$[\pm(45_2)/0]_S$	C	F	Models dropped section
$[(\pm 45)_2/0_2]_S$	G	F	Basic laminate
$[\pm 45/(\pm 45)_D/0_2]_S$	H	PD	Angle plies dropped
$[\pm 45/(\pm 45)_D/0/0_D]_S$	I	PD	0°, angle plies dropped
$[\pm 45/0_2]_S$	L	F	Models dropped section
$[\pm 45/0]_{2S}$	B	F	Basic laminate
$[\pm 45/0/(\pm 45/0)_D]_S$	D	PD	Sublaminate dropped
$[\pm(15_2)/0_2]_S$	Q	F	Basic Laminate
$[+15/+15_D/-15/-15_D/0/0_D]_S$	P	SPD[b]	0°, angle plies dropped
$[\pm 15/0]_S$	R	F	Models dropped section

[a]laminate types: flat (F), ply dropoff (PD)

[b]SPD indicates geometrically symmetric ply dropoff specimen

denotes that the associated ply or sublaminate are terminated at the midline of the section, perpendicular to the direction of the applied load. For example, a $[\pm 45/(\pm 45)_D/0/0_D]_S$ laminate would have an undropped section layup of $[(\pm 45)_2/0_2]_S$ and a dropped section layup of $[\pm 45/0]_S$.

The laminates used in this experiment are placed into five groups in Table 3.2. The first group is based around the $[\pm 45/0]_S$ laminate. The second laminate in the first group, $[\pm 45/0_D/0/-+45]_T$ has one 0^o ply dropped off from the basic laminate. The third laminate in this group, $[\pm 45/0/-+45]_T$ matches the dropped section of the second laminate. Note that the undropped section of the second laminate is the same as the $[\pm 45/0]_S$ laminate, the first layup in this group.

The second group of specimens in Table 3.2 is based around the $[\pm(45_2)/0_2]_S$ laminate. This is actually the same layup as the basic laminate of the first with double the effective ply thickness. The second laminate in this group, $[\pm(45_2)/0/0_D]_S$, has two 0^o plies dropped symmetrically, whereas the $[+45/+45_D/-45/-45_D/0/0_D]_S$ laminate has both angle plies and 0^o plies dropped symmetrically in an alternating fashion. The first laminate in this group models the undropped section of both of the laminates with ply dropoffs. The fourth laminate in this group, $[\pm(45_2)/0]_S$ models the dropped section of the $[\pm(45_2)/0/0_D]_S$ laminate. Note that the dropped section of the $[+45/+45_D/-45/-45_D/0/0_D]_S$ is modeled by the basic laminate of the first group, the $[\pm 45/0]_S$ laminate.

The third group of laminates is similar to the second, the

difference being that the 45^{o} plies are alternated instead of being doubled. The basic layup in this group is the $[(\pm 45)_2/0_2]_S$ laminate. The second laminate in this group, $[\pm 45/(\pm 45)_D/0_2]_S$ has angle plies dropped, while the third laminate in this group, $[\pm 45/(\pm 45)_D/0/0_D]_S$ has both angle plies and two 0^{0} plies dropped off symmetrically. The undropped sections of both the laminates with ply dropoffs in this section are modeled by the basic lanminate in this group, $[(\pm 45)_2/0_2]_S$. The dropped section of the $[\pm 45/(\pm 45)_D/0_2]_S$ laminate is modeled by the fourth laminate listed in this group, $[\pm 45/0_2]_S$. The dropped section of the $[\pm 45/(\pm 45)_D/0/0_D]_S$ laminate is modeled by the basic laminate of the first group, $[\pm 45/0]_S$.

The fourth group of laminates in Table 3.2 is based around the first laminate of this group, the $[\pm 45/0]_{2S}$ layup. This is also related to the basic $[\pm 45/0]_S$ of the first group, but with twice the plies. Instead of making the plies double thickness, as in the second group, the thickness has been doubled by doubling each half of the laminate as a unit, rather than by doubling the individual plies. This allows comparison of single ply effective thickness, double ply effective thickness, and stacking sequence effects. The ply dropoff laminate in this group is a $[\pm 45/0/(\pm 45/0)_D]_S$ layup with half of its plies dropped off symmetrically as a sublaminate group. The undropped section of this laminate is modeled by the basic laminate of this group, while the undropped section of this laminate is modeled by the basic laminate of the first group,

$[\pm 45/0]_S$.

The fifth family of laminates in this group in Table 3.2 is similar to that of the second group but with two differences. The first is that the $\pm 45^o$ angle plies of the second group are replaced by $\pm 15^o$ plies. This was done to create a laminate with a greater tendency to delaminate. Previous experiments with flat laminates have shown this greater tendency to delaminate over that of the $[\pm 45/0]_S$ family [31,32] The second difference is that the laminates with dropped plies in this group were laid up symmetrically, that is both sides were made to curve around the ply dropoff region rather than having one side flat and one side curve around the dropped region. This was done to minimize any load eccentricity and thus induced bending effect which might be caused by the loading of a geometrically unsymmetric (one side flat) laminate. Details on fabrication of these specinmens are contained in section 3.5. The basic laminate of this group then is the $[\pm(15_2)/0_2]_S$ layup, which corresponds to the undropped section of the laminate with the ply dropoffs in this group, the $[+15/+15_D/-15/-15_D/0/0_D]_S$ layup. This latter laminate has angle plies and two 0^o plies dropped off symmetrically in an alternating fashion. The undropped section of this laminate is modeled by the third laminate in this group, $[\pm 15/0]_S$.

3.3 Specimen Manufacture

All procedures except those directly pertaining to ply

dropoffs were done according to standard procedures developed at TELAC [29]. The methodology of manufacturing the laminates with ply dropoffs had already been developed within TELAC by DiNardo [25]. The important point dealing with the manufacturing of ply dropoffs which came out of this study was that constructing these laminates requires a great deal of care to prevent voids from forming. The general manufacturing methodology is as follows. The plate is laid up in the conventional manner up until the layer of the terminated ply. The terminated ply is half the length of a normal ply in the x direction. The undropped plies are then laid up on top of the terminated ply or plies. Each of these plies is carefully smoothed down by hand over the ply dropoff region. The entire laminate is carefully smoothed down by hand, again paying particular attention to the region over the ply dropoff.

The laminate is cured according to standard procedure, except that no top caul plate is used since the upper surface is not flat. Care must be taken to ensure that cure materials on top of the laminate are flat so as not to cause any wrinkling on the laminate surface. After cure and postcure, a milling machine equipped with a diamond grit cutting wheel and water cooling system is used to cut the plate into coupons. This allows the ply dropoff region to be examined at two widthwise points per coupon under a microscope.

A detailed summary of these procedures and modifications made for ply dropoff manufacturing follows.

The graphite/epoxy is supplied in rolls of semi-cured

unidirectional preimpregnated tape or "prepreg" with a nominal width of 305 mm. To prevent curing of the matrix before layup, the prepreg is stored in freezers at a temperature below $-18^{o}C$. One hour prior to manufacture, the roll is removed from the freezer and left in a sealed bag. This warm-up procedure prevents condensation from forming on the composite and helps to make the prepreg more pliable. The prepreg is cut and stacked ino uncured laminates in an air conditioned "clean room". The air conditioning keeps the temperature below $25^{o}C$ and the relative humidity low. When handling the prepreg, surgical gloves are worn to avoid contamination by skin oil. The prepreg is cut into shapes which can be placed together to form plies with dimensions of 305 mm by 350 mm. This is accomplished using Stanley razor knives and teflon covered templates to ensure the required precision. When forming the angle plies, the cuts are made to avoid fiber breaks in the ply. The edges of the two pieces which form this angled ply are placed together so the cuts are parallel to the fiber direction. In other words, only matrix joints are present within a laminae. Alignment of the plies during layup is assured by laying one corner of the plies up against a square corner of a layup jig, which defines the good corner of the laminate. This good corner is used subsequently as a reference to ensure alignment during cure and machining of the laminate. Following layup, peel-ply is applied to both sides of the laminate. The peel-ply protects the laminate during the cure and also produces a textured finish to aid in bonding the

loading tabs and strain gages.

Layup of the ply dropoff plates requires the use of special techniques not standardized within TELAC. However, plates with ply dropoffs have previously been manufactured at TELAC by DiNardo [25]. These same procedures were used in the current study.

The plate is laid up in the conventional manner up until the layer of the terminated ply. The terminated ply is half the length of a normal ply in the x direction, as illustrated in Figure 3.3. Aluminum templates were made with a tolerance of ± 0.03 mm to cut the terminated plies to the desired accuracy. When more than two plies are dropped off, the dropoffs were spaced apart from each other (in the x-direction) by 1.5 mm. This spacing allows the top plies to more readily conform to the underlying plies, reducing the likelihood of void or bubble formation. During the actual layup of the plies, considerable care was taken to smooth down the plies as they were laid down, particularly in the region of the ply dropoff. A plastic smoothing tool was used to press down the plies as they were laid down and to smooth out any bubbles or wrinkles in the laminate. At the ply dropoff, each ply was carefully pressed down to conform as much as possible to the underlying plies. These steps permitted the manufacture of quality ply dropoff specimens containing a minimum of voids and other defects. The ply dropoff characteristics are described in Section 3.4. In Figure 3.4, a photomicrograph of a typical specimen in the region of the ply dropoff is shown. The

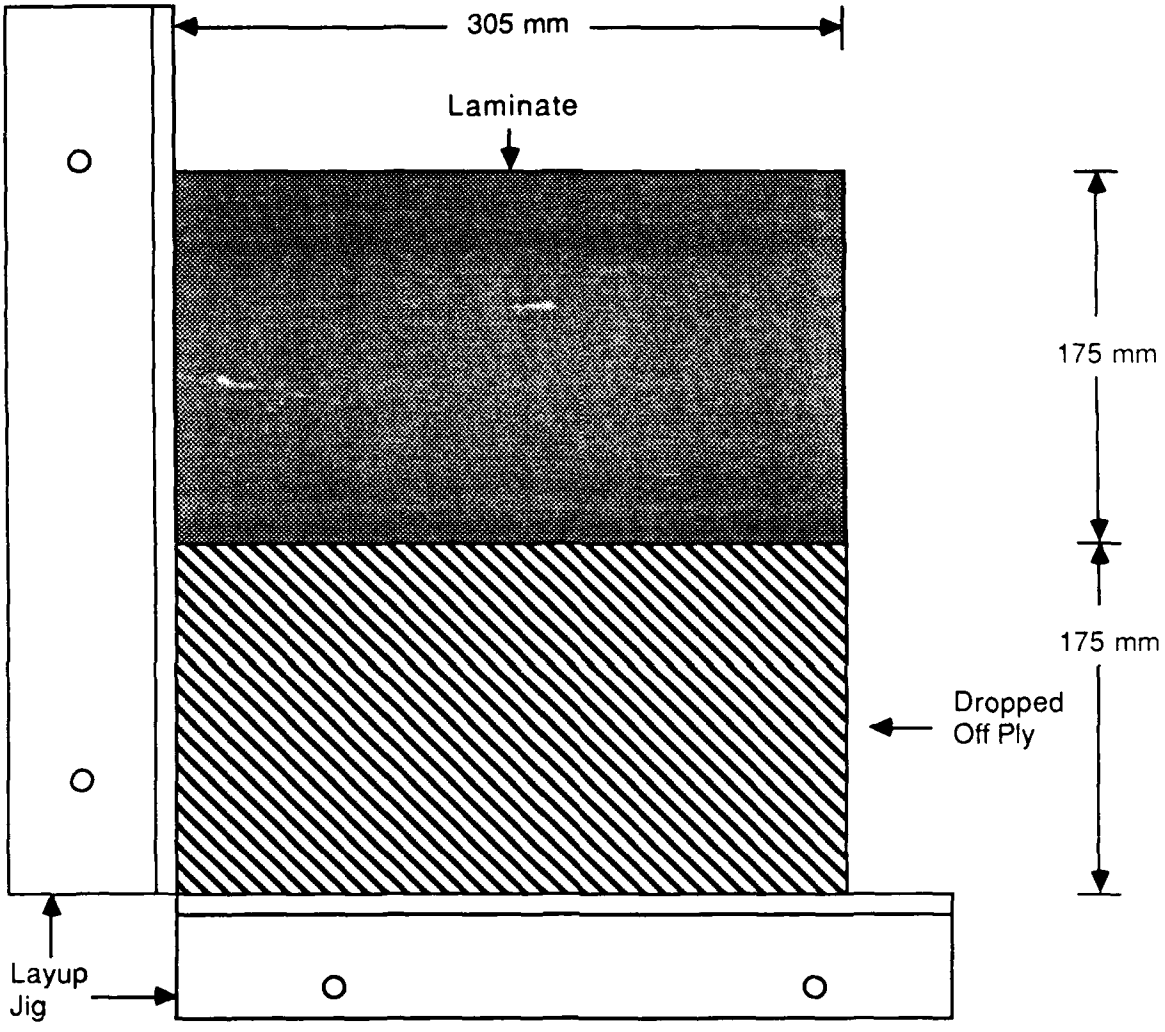

Figure 3.3 Schematic of a Layup With Ply Dropoffs

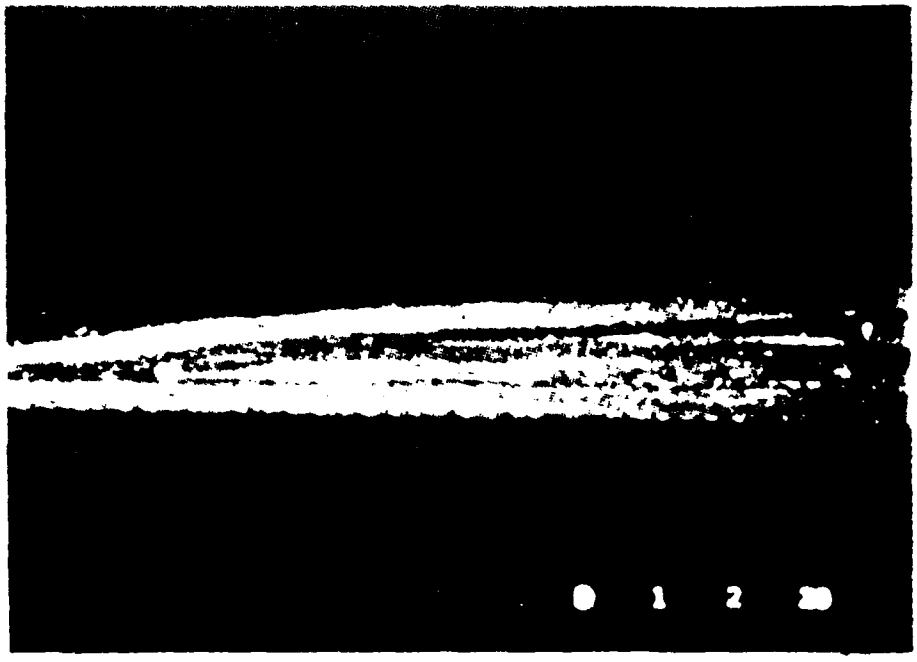

Figure 3.4 Photomicrograph of a Typical Ply Dropoff Region

individual plies and the triangular resin of neat matrix in front of the terminated plies are clearly visible. Microscopic examination of a number of coupons provided assurance that large numbers of voids were not present in the test specimens.

The cure setup for the flat laminates is illustrated in Figure 3.5. The peel-ply covered laminate is placed into a prepared space set up on an aluminum caul plate which is large enough to cure six 305 mm by 350 mm plates at a time. Each laminate is held in place by aluminum dams on two sides, which maintain the good corner and by cork dams on the other two sides. Nonporous teflon is placed on the caul plate, which was previously coated with mold release, to help keep it clean during the cure. The laminate is covered with porous teflon, followed by one layer of paper bleeder for every two plies to absorb excess resin during the cure. This is followed by a sheet of nonporous teflon and an aluminum top plate coated with Frekote 905 mold release. The top plate helps assure that the finished laminate will be flat. The assembly is covered with another piece of nonporous teflon, followed by porous teflon, fiberglass air breather and finally the entire setup is vacuum bagged.

The cure setup used for the ply dropoff specimens was slightly different, as shown in Figure 3.6. Since the top surface of a ply dropoff specimen is, and must not be, flat, the aluminum top plates could not be used. Instead, the top plate was eliminated from the cure setup and pressure was applied directly through the cure materials to the laminate

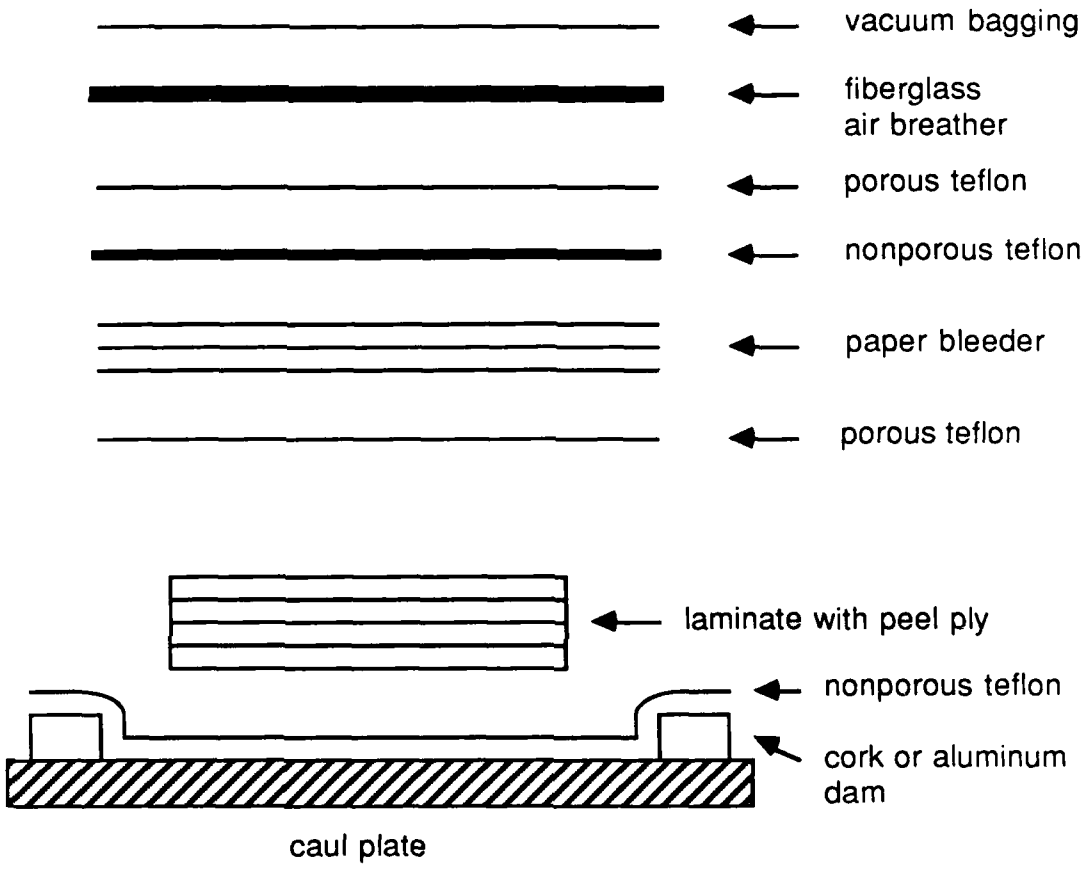

Figure 3.5 Illustration of Cross Section of Cure Setup for Flat Laminates

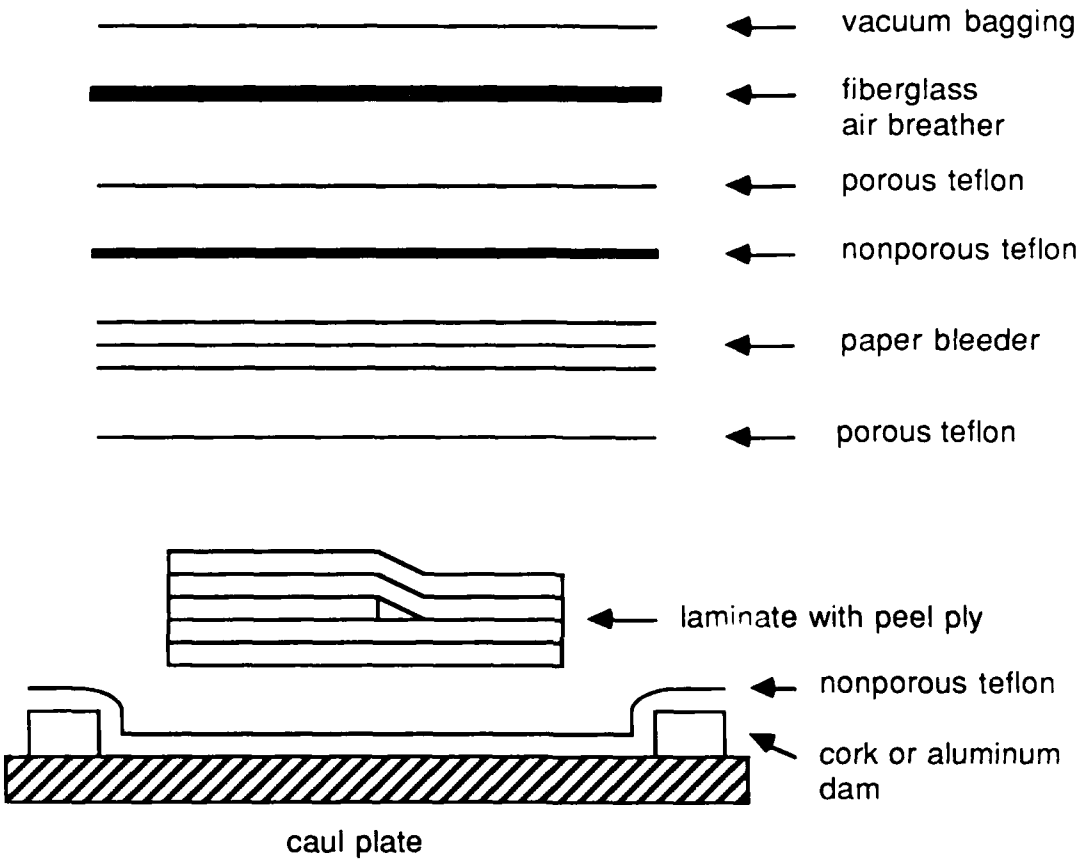

Figure 3.6 Illustration of Cross Section of Cure Setup for Laminates With Ply Dropoffs

during the cure. Particular care was taken with the cure materials to ensure a smooth surface, both with the cure materials, and thereby the laminate itself. Any creases or irregularities in the cure materials would affect the surface finish of the cured plates.

The $[\pm 15/+15_D/-15/-15_D/0/0_D]_S$ specimen required a special cure setup to provide a geometrically symmetric specimen. In other words, these specimens did not have a flat side, but instead had a common midplane in the dropped and undropped region of the specimens with both sides of the undropped plies curving in from the undropped end of the laminate around the ply dropoff and joining up with the dropped end, as illustrated in Figure 3.2b. It can also be seen in Figure 3.2b that these specimens are not exactly symmetric in that the ply dropoffs are laid up in a slightly antisymmetric manner about the midplane such that no two ply dropoffs occur at the same point in the x-direction. This should have minimal affect on the behavior of the laminate with respect to induced bending loads or extension-bending coupling. The cure assembly used for these specimen types is shown in Figure 3.7. Again, 305 mm by 350 mm plates are cured. Spacers manufactured from the same material as the laminates were used both underneath and above the dropped end of the specimen in a thickness equal to half of the total plies dropped off. These spacers were cured before being used. The spacers were wrapped in peel-ply to prevent them from sticking to the laminate. Peel-ply was added to the undropped end of the specimen to compensate for the added

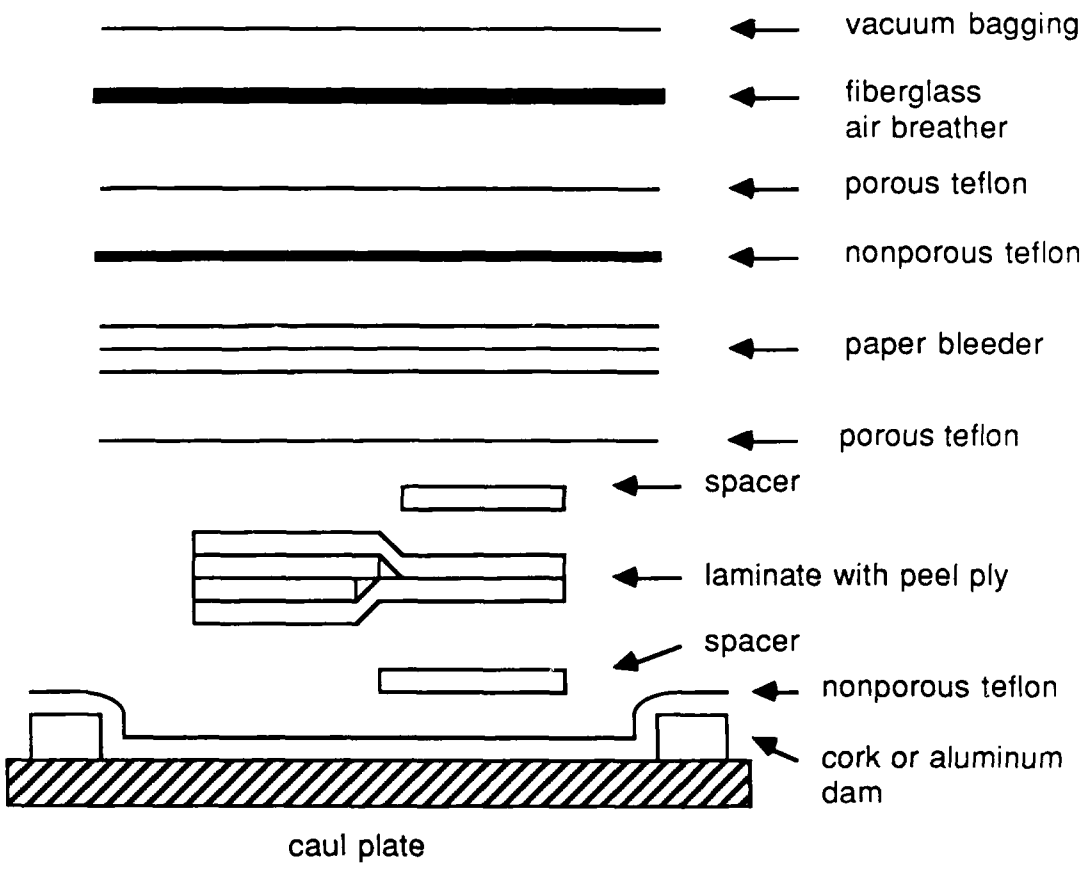

Figure 3.7 Illustration of Cross Section of Cure Setup for Geometrically Symmetric Ply Dropoff Laminates

thickness of the peel-ply on the spacers.

Curing the AS4/3501-6 graphite/epoxy is a two-stage process and is accomplished in a one meter diameter by 1.5 meter long Baron-Blakeslee autoclave. The autoclave pressure is raised to 0.59 MPa with an applied vacuum of 740 mm Hg. When the temperature reaches 117^{o}C, the first stage or "flow stage" occurs. This temperature is held for one hour. The next stage of the cure is a two hour "set stage" at 177^{o}C where most of the chemical crosslinking of the polymer chains in the epoxy occurs. To avoid thermally shocking the composite, all heat-up and cool-down rates were approximately 3^{o}C per minute. The complete autoclave cure cycle is shown in Figure 3.8. All laminates were postcured in an oven at 177^{o}C for eight hours after removal from the curing assembly.

All laminates were cut into five 350 mm by 50 mm specimens with a modified milling machine equipped with a diamond grit cutting wheel and water cooling system. Special attachments were used to ensure straight, parallel edges. Before the specimens were cut, approximately 8 mm was cut from the reference edge of the laminate and discarded. Since excess resin is bled from the laminate edges, removing this strip ensured the specimens cut from the edges of the plates did not contain an excess resin build-up. A thin, leveling strip of glass/epoxy was used underneath the dropped end of the geometrically symmetric laminate to provide a flat cutting surface.

Flat specimens were measured for width at three positions

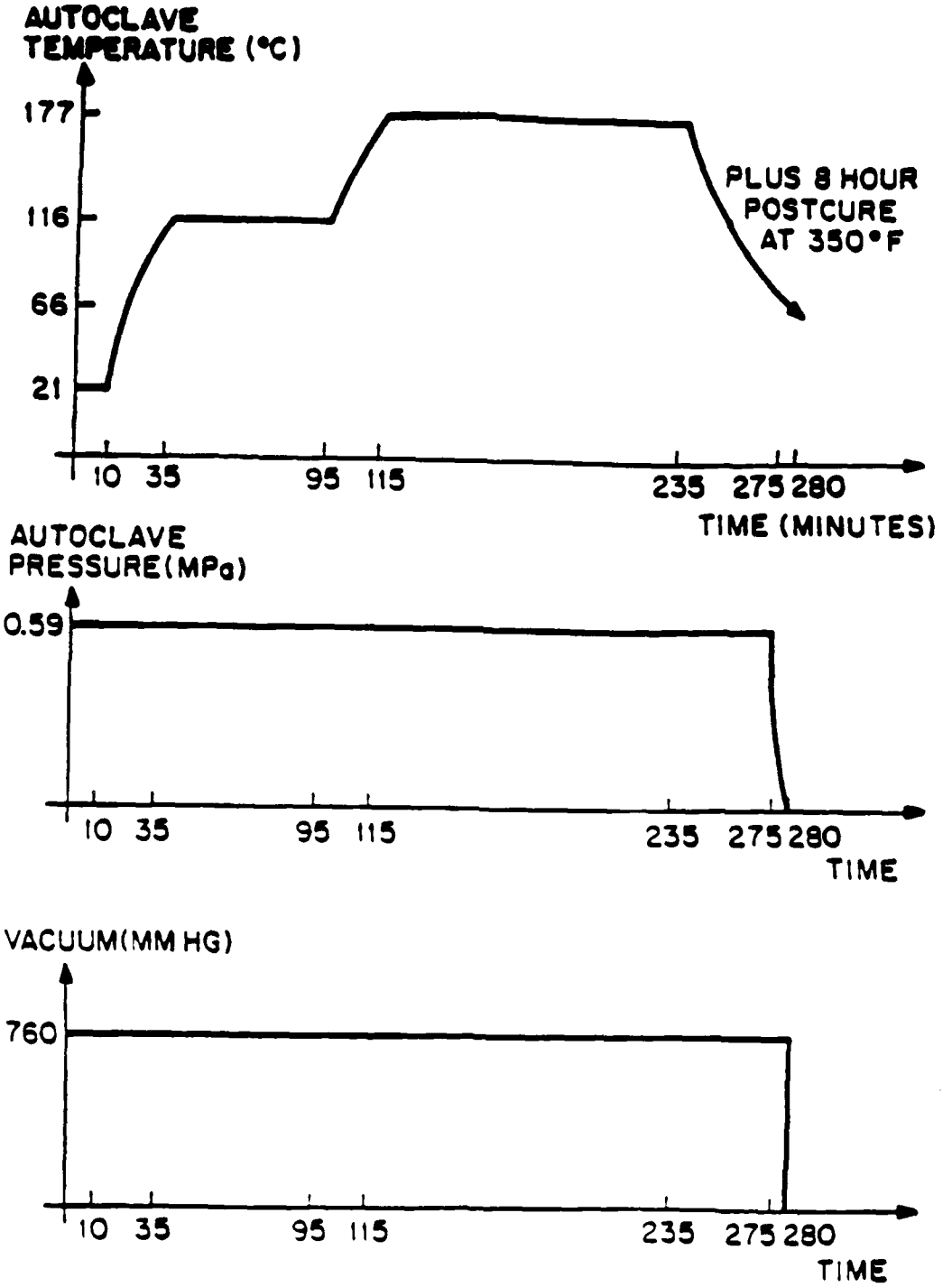

Figure 3.8 Standard Cure Cycle for AS4/3501-6 Graphite/Epoxy

and specimens with ply dropoffs at four locations using calipers. Flat specimens were measured for thickness at nine locations and specimens with ply dropoffs were measured for thickness at twelve locations, six in each of the dropped and undropped sections of the specimens. The exact location of the measurement points is shown in Figure 3.9. The thickness measurements were taken primarily as a quality control check. Application of the peel-ply causes dimpling of the laminate surface which slightly distorts the thickness measurements. Therefore, nominal thicknesses were used in all stress calculations, with a nominal per ply thickness of 0.134 mm. The overall average ply thickness was 0.135 mm with a coefficient of variation of 4.8%. The average ply thickness of the flat specimens was 0.134 mm with a coefficient of variation of 4.3%, while the average thickness for specimens with ply dropoffs was 0.136 mm with a coefficient of variation of 5.0%. The average ply thickness of the dropped section of the specimens with ply dropoffs was 0.140 mm with a coefficient of variation of 4.3%, while the average for the undropped section was 0.132 mm with a coefficient of variation of 3.5%.

Precured glass/epoxy loading tabs 75 mm long by 50 mm wide were bonded to the coupons with American Cyanimid FM-123-2 film adhesive. The tabs were 3M type 1002 with a $[0/90]_{nS}$ layup, where for flat specimens n is determined so as to be sufficient for the loading tab to be 1.5 to 4 times as thick as the laminate, as is recommended by the American Society for Testing and Materials [31]. For specimens with ply dropoffs, the tabs

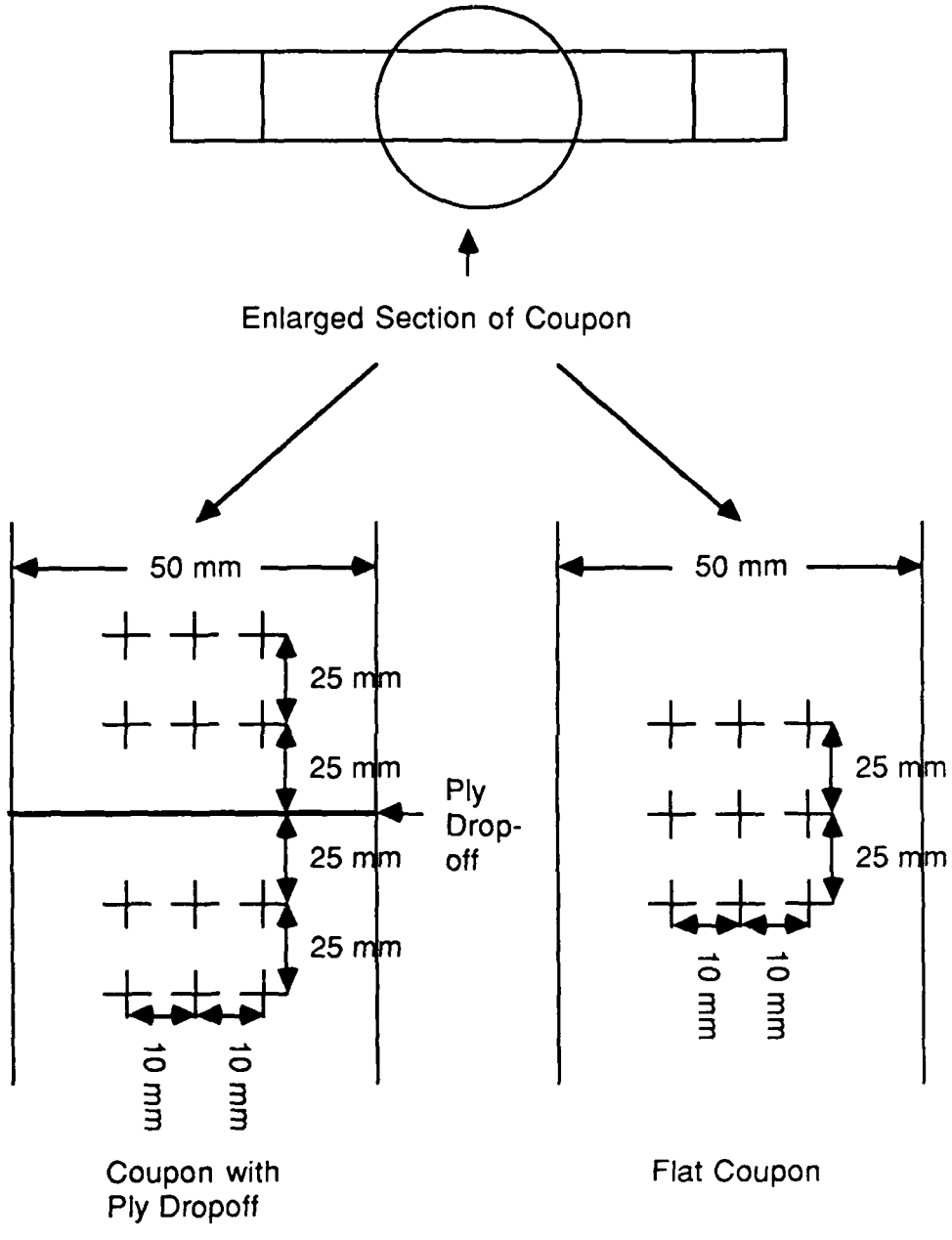

Figure 3.9 Location of the Coupon Measurement Points

at the undropped end of the specimen were scaled the same way as the flat specimens. This same tab thickness was used on the flat side of the dropped end of the specimen, but tab thickness was added to the other side of the dropped end of the specimen to compensate for the additional thickness of the undropped end of the specimen. For the ply dropoff laminate cured to be geometrically symmetric, that is with no flat side, the thickness difference between the dropped and undropped sections was split equally between both sides of the dropped end of the specimen. The purpose of this was to facilitate the bond cure, as described below. The number of tab plies used for all the coupons are listed for the flat specimens in Table 3.3 and for the ply dropoff specimens in Table 3.4. Tab ply thickness equals 0.250 mm.

The adhesive, cut about 4 mm longer and wider than the tab itself, was applied directly to the tab which was then carefully aligned and applied to the coupon. The film, which is stored at $-18^{o}C$, becomes very tacky at room temperature and holds the tab in place on the coupon until curing. The specimens were placed on an aluminum caul plate and covered with porous teflon before placing steel plates on each specimen. Nonporous teflon and then fiberglass air breather were placed on top of the plates and the entire assembly vacuum bagged. The film adhesive was cured for two hours at $107^{o}C$ with an applied vacuum and an autoclave pressure of 0.07 MPa. This provided an absolute pressure of 0.35 MPa on the bonding surface.

TABLE 3.3

NUMBER OF PLIES PER TAB FOR FLAT SPECIMENS

LAMINATE	NUMBER OF TAB PLIES
$[\pm 45/0]_S$	9
$[\pm 45/0/-+45]_T$	9
$[\pm(45_2)/0_2]_S$	15
$[\pm(45_2)/0]_S$	13
$[(\pm 45)_2/0_2]_S$	15
$[\pm 45/0_2]_S$	11
$[\pm 45/0]_{2S}$	15
$[\pm(15_2)/0_2]_S$	15
$[\pm 15/0]_S$	9

TABLE 3.4

NUMBER OF PLIES PER TAB FOR PLY DROPOFF SPECIMENS

LAMINATE	NUMBER OF TAB PLIES		
	Undropped End	Dropped End	
		Flat side	Tapered side
$[\pm 45/0_D/0/-+45]_T$	9	9	9
$[\pm(45_2)/0/0_D]_S$	15	15	17
$[+45/+45_D/-45/-45_D/0/0_D]_S$	15	15	19
$[\pm 45/(\pm 45)_D/0_2]_S$	15	15	17
$[\pm 45/(\pm 45)_D/0/0_D]_S$	15	15	19
$[\pm 45/0/(\pm 45/0)_D]_S$	15	15	19
$[+15/+15_D/-15/-15_D/0/0_D]_S$	15	17[a]	17[a]

[a]geometrically symmetric laminate, both sides taper

3.4 Ply Dropoff Characteristics

Typical photos of the ply dropoff region and schematic representations of the photos are shown in Figures 3.10 and 3.11. For every ply that is dropped off, a triangular region of epoxy is created at the end of the dropped ply due to the fact that the ply placed on top of the terminated ply cannot bend very sharply over the discontinuity. The length of this triangular region is typically about three times the thickness of the dropped ply (a ply has a nominal thickness of 0.134 mm). This triangular region of resin is the area where voids often form, as can be seen in Figure 3.11. As mentioned in the previous section, steps were taken when laying up the dropped plies to minimize void formation. Although some voids did still occur, they were normally found on only one side of the cuts made when machining the plates into coupons, suggesting that the voids were small and roughly spherical.

3.5 Instrumentation of Specimens

Three coupons were tested with photoelastic coating bonded to them, one each of the $[\pm 45/0_D/0/-+45]_S$, $[\pm 45/(\pm 45)_D/0/0_D]_S$, and $[\pm 45/0/(\pm 45/0)_D]_S$ laminates. The purpose of these tests was to obtain a qualitative feel for the stress distribution around different ply dropoff regions. The photoelastic coatings were bonded to the coupons using PC-1 adhesive, a two part adhesive mixed with ten parts of PCH-1 hardener to one part adhesive. The surfaces of the coupon were wiped clean

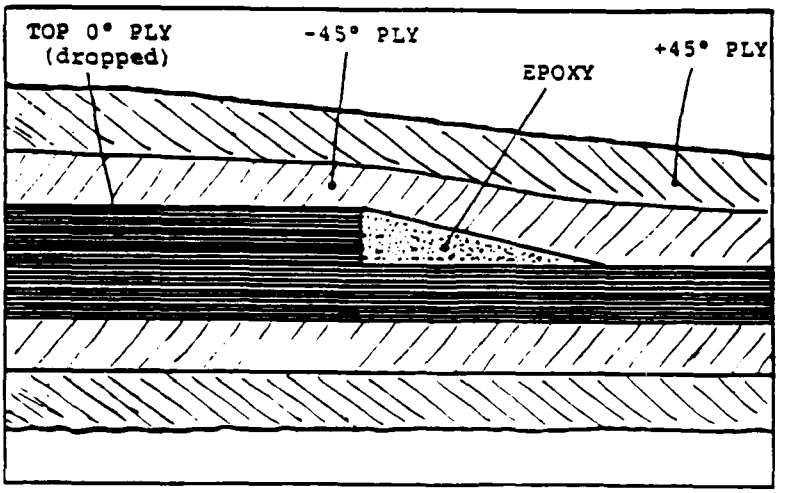

Figure 3.10 Photomicrograph and Schematic Representation of Ply Dropoff

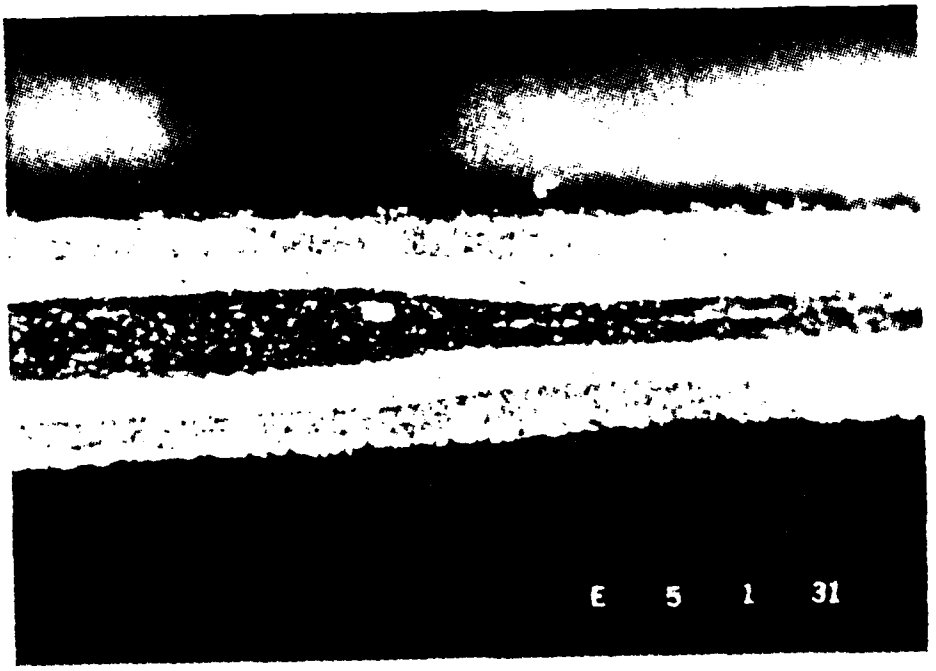

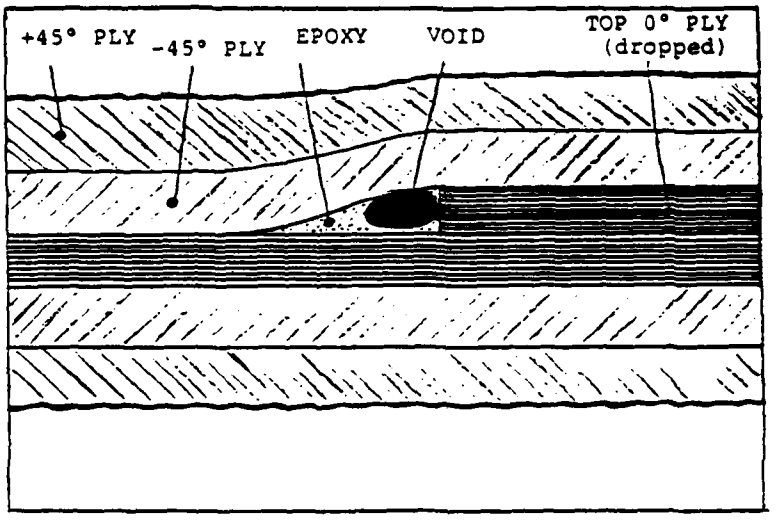

Figure 3.11 Photomicrograph and Schematic Representation of Ply Dropoff With Void

with cheesecloth before bonding. The 1.0 mm thick photoelastic coating was cut with scissors to the size of the test section, 200 mm by 50 mm. The adhesive was allowed to cure for twelve hours at room temperature.

Strain gages were attached to the rest of the coupons. The gages used were type EA-06-125AD-120 with a gage factor of 2.055 and an accuracy of +0.5% and were manufactured by Micro-Measurements Division of Measurements Group, Inc. For the flat (no ply dropoff) specimens, one gage was centered on the test section, as shown in Figure 3.12. For the coupon with ply dropoffs, four strain gages were used. Back to back gages were centered on both the dropped and undropped halves of the coupon, again shown in Figure 3.12. The purpose of the strain gages was to determine the stiffness of the specimens and to detect any bending which might occur in the coupons with ply dropoffs.

3.7 Testing Procedures

All testing was done under monotonic tensile loading using a Material Test System (MTS) 810 equipped with hydraulic grips. A stroke rate of 1.09 mm/minute was used. For a specimen with a 200 mm test section, this equates to a strain rate of approximately 5500 microstrain per minute.

After the specimen was aligned properly in the upper grip using a machinist's square, the grip was closed and the strain gages attached to Vishay conditioners. This free hanging position is defined as the zero load position. The gages were

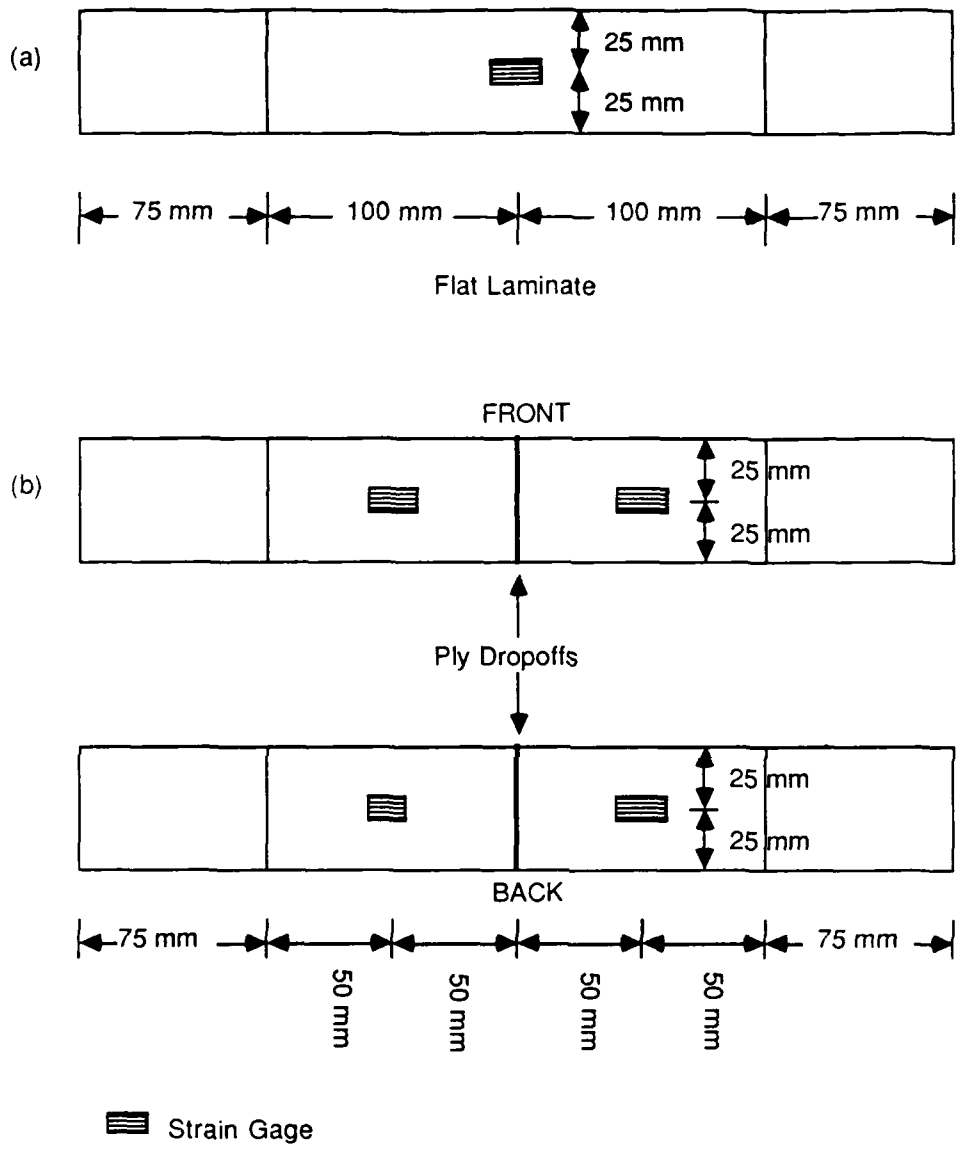

Figure 3.12 Strain Gage Locations for (a) Flat and (b) Ply Dropoff Specimens

calibrated before the lower tab was gripped. Each gage was first balanced so zero strain registered in this zero load position. The proper resistance was then connected in parallel with each strain gage to calibrate the system. A PDP11/34 computer stored the data from the conditioners through analog-to-digital converters.

The data acquisition program was started just prior to the application of the load by the testing machine. All tests were conducted to failure. During the tests, the specimens were inspected visually for signs of cracking, matrix splitting, and delamination and monitored for sounds indicating damage. When sounds were detected, marks were placed at the corresponding point in the data file using a feature offered by the data acquisition software. At failure, the fracture load and stroke were recorded and a photograph was taken of the specimen while it was still mounted in the grips.

3.8 Data Reduction

Following each testing period, the data was stored on floppy disks to form a permanent record. The data was analyzed on computer software written at TELAC [33]. This analysis consisted of editing out points in the data file which were recorded before the test started and after it ended. Thickness and width measurements were added to the data file so that load could be converted to stress. The slope of all the stress and strain data was computed using a program called LIN6. This program uses an algorithm to determine best fit linear regions

of a data set. The longitudinal modulus at the far-field position was determined using this program. Finally, a graph was drawn on a pen plotter showing the stress-strain behavior at all gage positions, as well as the marks which were placed in the data file when noises were heard.

CHAPTER 4

ANALYSIS

4.1 PROBLEM OVERVIEW

All the specimens with ply dropoffs, but one, in the current investigation were laid up with one side flat and the other side tapered over the ply dropoff region from the undropped to the dropped section. This means that the midplanes of the two sections did not coincide. This is the way most structures with ply dropoffs are actually manufactured for reasons such as ease of manufacture and for improved aerodynamics. The problem with this midplane offset is that bending stresses are induced from in-plane loads. This induced bending load is what is analyzed herein. It is very important to note that this analysis does not consider the effect of the interlaminar stresses induced by the ply dropoffs, as was discussed in Chapter 2, but does consider the in-plane stress concentration caused by the loading eccentricity. The objective of this analysis is to determine the failure stress of the specimen taking into account the in-plane stresses caused directly by the tension loading in the x-direction and the induced bending stress due to curvature in the x-direction.

4.2 Assumptions

A drawing of the model used in this analysis is shown in Figure 4.1. Several assumptions were made in deriving the

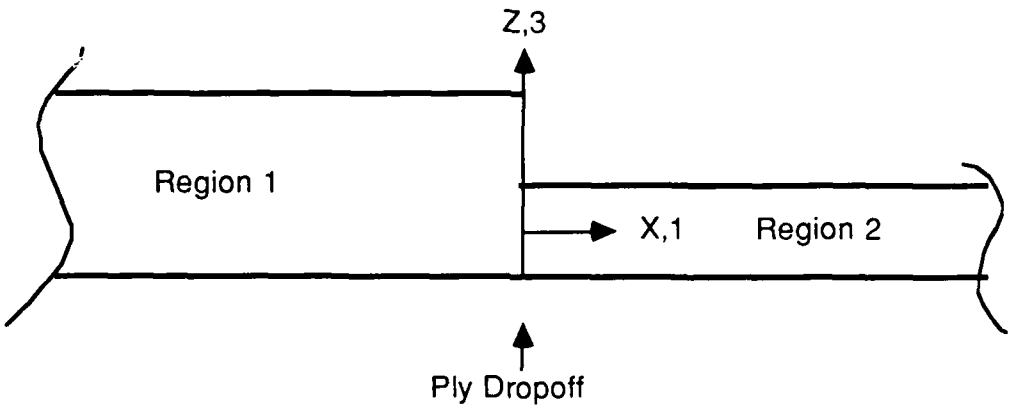

Figure 4.1 Schematic of Analysis Model

bending correction equation. The individual properties of the fiber and matrix are "smeared", that is each ply was considered macroscopically homogeneous. Also, classical laminated plate theory (CLPT) can be applied. Thus, each region is characterized by the elastic matrices calculated from CLPT. The most important assumption is that the model is a one-dimensional model, that is in the energy expression used in deriving the desired equations, bending and extension terms in the x-direction only are included. Bending in the transverse direction is assumed to be negligible.

4.3 Governing Equations

It can be seen from Figure 4.1 that the laminate is divided up into two sections where terms with a "1" subscript refer to the undropped end of the specimen and terms with a "2" subscript refer to the dropped end. Since the ends of the specimens are far away from the ply dropoff area under consideration, the coupon can be assumed to be infinitely long. The total potential energy of the laminate, considering only bending and extension terms in the x-direction, can be expressed as the sum of the potential energy of the undropped and dropped sections:

$$\pi_p = \int_{-\infty}^{0} \left[\tfrac{1}{2} M_1 \kappa_1 + \tfrac{1}{2} N (w_1')^2 \right] dx + \int_{0}^{\infty} \left[\tfrac{1}{2} M_2 \kappa_2 + \tfrac{1}{2} N_2 (w_2')^2 \right] dx \tag{4.1}$$

where N and M are the stress and moment resultants in the x-direction, respectively, w is the out-of-plane displacement, and a single apostrophe indicates a derivative with respect to x. The moment resultants and curvatures can be expressed as:

$$M_1 = D_1 w_1'' + B_1 (A_1^{-1} N) \tag{4.2}$$

$$\kappa_1 = w_1'' \tag{4.3}$$

$$M_2 = D_2 w_2'' \tag{4.4}$$

$$\kappa_2 = w_2'' \tag{4.5}$$

Substituting these expressions into the energy expression gives:

$$\pi_p = \int_{-\infty}^{0} \left[\tfrac{1}{2} D_1 (w_1'')^2 + \tfrac{1}{2} B_1^* N w_1'' + \tfrac{1}{2} N (w_1')^2 \right] dx + \int_{0}^{-\infty} \left[\tfrac{1}{2} D_2 (w_2'')^2 + \tfrac{1}{2} N (w_2')^2 \right] dx \tag{4.6}$$

where

$$B_1^* = B_1 A_1^{-1} \tag{4.7}$$

No bending-extension coupling, or B, terms exist for the dropped region since the reference midplane for the analysis is the midplane of the dropped section and all of the dropped sections were symmetric.

The Principle of Minimum Potential Energy is now applied. This principle states that the set of displacements satisfying the boundary condition which also satisfy the equilibrium equations are those that make the total potential energy of the system stationary. Taking the first variation of the total potential energy yields:

$$\delta\pi_p = \int_{-\infty}^{0} \left[D_1 w_1'' \delta w_1'' + \frac{1}{2} B_1^* N \delta w_1 + N w_1' \delta w_1 \right] dx \tag{4.8}$$

$$\int_{0}^{\infty} \left[D_2 w_2'' \delta w_2'' + N w_2' \delta w_2' \right] dx$$

Integrating this equation with integration by parts gives:

$$\delta\pi_p = \left[D_1 w_1' \delta w_1' - D_1 w_1'' \delta w_1 \right]_{-\infty}^{0} - \int_{-\infty}^{0} D_1 w_1''' \delta w_1 \, dx$$

$$+ \tfrac{1}{2} B_1^* N \, \delta w_1' \Big|_{-\infty}^{0} + N w_1' \delta w_1 \Big|_{-\infty}^{0} - \int_{-\infty}^{0} N w_1'' \delta w_1 dx \qquad (4.9)$$

$$+ \left[D_2 w_2' \delta w_2' - D_2 w_2'' \delta w_2 \right]_{0}^{\infty} - \int_{0}^{\infty} D_2 w_2''' \delta w_2 \, dx$$

$$+ N w_2' \delta w_2 \Big|_{0}^{\infty} - \int_{0}^{\infty} N \, w_2'' \delta w_2 \, dx = 0$$

Since the variation of w_1 and w_2, and therefore their integrals, are arbitrary, this equation may be split into four parts, the first of which deals with terms associated with the variation of w_1:

$$\int_{-\infty}^{0} D_1 w_1''' \delta w_1 \, dx + \int_{-\infty}^{0} N w_1'' \delta w_1 \, dx = 0 \qquad (4.10)$$

Since the variation of w_1 is arbitrary and therefore not equal to zero, the following must be true;

$$w_1''' - \frac{N}{D_1} w_1'' = 0 \qquad (4.11)$$

Similarly, the second part of the energy equation dealing with

the variation of w_2 is:

$$\int_0^\infty D_2 w_2'''' \delta w_2 \, dx + \int_0^\infty N w_2'' \delta w_2 \, dx = 0 \qquad (4.12)$$

yields a comparable equation in terms of w_2:

$$w_2'''' - \frac{N}{D_2} w_2'' = 0 \qquad (4.13)$$

The third and fourth parts of the energy expression are obtained by grouping the coefficients of the variation of w and the first derivative of w. Once again, theese expressions must be equal to zero, resulting in:

$$\left[(D_1 w_1'' + \tfrac{1}{2} B_1^* N) \delta w_1' \right]_{-\infty}^{0} + D_2 w_2'' \delta w_2' \Big|_0^\infty = 0 \qquad (4.14)$$

$$\left[(-D_1 w_1''' + N w_1') \delta w_1 \right]_{-\infty}^{0} + \left[(-D_2 w_2''' + N w_2') \delta w_2 \right]_0^\infty = 0 \qquad (4.15)$$

The following equations are boundary conditions which state that the displacements and slopes are equal at the ply dropoff and equal to zero at the clamped ends of the laminate.

$$w_1(0) = w_2(0) \qquad (4.16)$$

$$w_1'(0) = w_2'(0) \qquad (4.17)$$

$$w_1(-\infty) = w_2(\infty) = w_1'(-\infty) = w_2'(\infty) \tag{4.18}$$

These boundary conditions are used to evaluate the integrals in equations 4.14 and 4.15 from the energy expression, which results in:

$$D_1 w_1'' \Big|_0 + \tfrac{1}{2} B_1^* N - D_2 w_2'' \Big|_0 = 0 \tag{4.19}$$

$$D_1'' \Big|_0 - D_2 w_2'' \Big|_0 = 0 \tag{4.20}$$

Equations 4.11 and 4.13 are ordinary differential equations with the solutions:

$$w_1 = C_1 + C_2 x + C_3 e^{-\omega_1 x} + C_4 e^{\omega_1 x} \tag{4.21}$$

$$w_2 = C_5 + C_6 x + C_7 e^{-\omega_2 x} + C_8 e^{\omega_2 x} \tag{4.22}$$

where

$$\omega_1 = \left[\frac{N}{D_1} \right]^{\frac{1}{2}} \tag{4.23}$$

$$\omega_2 = \left[\frac{N}{D_2} \right]^{\frac{1}{2}} \tag{4.24}$$

The clamped boundary condition of Equation 4.18 implies that

$$C_2 = C_3 = 0 \tag{4.25}$$

$$C_6 = C_8 = 0 \tag{4.26}$$

giving the following equations:

$$w_1 = C_1 + C_4 e^{\omega_1 x} \tag{4.27}$$

$$w_2 = C_5 + C_7 e^{-\omega_2 x} \tag{4.28}$$

Applying the boundary conditions of displacement and slope continuity, equations 4.16 and 4.17, at the ply dropoff to the above equations gives:

$$C_1 = C_5 + C_7 - C_4 \tag{4.29}$$

$$C_4 = -\Delta C_7 \tag{4.30}$$

where

$$\Delta = \left[\frac{D_1}{D_2} \right]^{\frac{1}{2}} \tag{4.31}$$

Equations 4.29 and 4.30 simplify Equations 4.27 and 4.28 to

$$w_1 = C_5 + C_7 \left[1 + \Delta - \Delta e^{\omega_1 x} \right] \tag{4.32}$$

$$w_2 = C_5 + C_7 e^{-\omega_2 x} \tag{4.33}$$

The fourth equation from the energy expression, Equation 4.20 provides no new information with the simplified form of the displacement equation. However it does provide a check. Using Equations 4.32 and 4.33 with Equation 4.19, the third equation from the energy expression, allows C_7 to be solved for.

$$C_4 = \frac{B_1^*}{2(1 + \Delta)} \tag{4.34}$$

Looking at Equations 4.32 and 4.33, it can be seen that C_5 is arbritrary since it exists alone in both the equations and will therefore drop out of the solution. Substituting Equation 4.34 into 4.32 and 4.33 gives:

$$w_1 = \frac{B_1^*}{2} \left[1 - \frac{\Delta}{\Delta + 1} e^{\omega_1 x} \right] \tag{4.35}$$

$$w_2 = \frac{B_1^*}{2(\Delta + 1)} e^{-\omega_2 x} \tag{4.36}$$

Substituting this into Equation 4.2, the moment resultant equation, yields:

$$M_o = \frac{-B_1^* \Delta}{2(\Delta + 1)} N + \frac{B_1^*}{2} N \tag{4.37}$$

which simplifies to:

$$M_o = \frac{B_1^*}{2(\Delta + 1)} N \tag{4.38}$$

Using Equations 4.29 and 4.2 gives:

$$M = \frac{1}{2} \left[\frac{B_1 A_1^{-1}}{\left[\frac{D_1}{D_2} \right]^{\frac{1}{2}} + 1} \right] N \tag{4.39}$$

This equation gives the bending moment resultant M induced by the extensionsal stress resultant N. The D_1 represents the flexural stiffness of the undropped section and D_2 represents the same in the dropped section. The A_1^{-1} is an inverse extensional stiffness term of the undropped section. The B_1 is a bending-extensional coupling term which arises when the A,B, and D matrices of the undropped section are calculated with the undropped section's midplane shifted to that of the dropped section.

4.4 Stress Calculation

All stresses were calculated using a program previously developed at TELAC called Laminated Analysis Software Package (LASP). This program uses CLPT and user input layup and material values to calculate the A,B, and D matrices. Loads

are then applied by the user. In this case, two loading cases were done for each specimen with a ply dropoff which was not geometrically symmetric. In the first loading case, a solution for the dropped end of the specimen is desired, neglecting any of the effect of the ply dropoff and undropped end of the specimen. This is the solution for the flat, control specimen which models the dropped end of the specimen. In this case, a unit stress in the x-direction is applied and CLPT and the Maximum Stress Criterion (described in Section 4.5) are used to determine the failure stress of the laminate. In the second case, the applied loading is adjusted to include the induced bending effect caused by the eccentric loading of the coupon. In this case, a unit value of stress resultant N is applied to the dropped section with the corresponding value of M. This number is the coefficient of M in Equation 4.47. The Maximum Stress Criterion is again used with LASP to determine the failure stress of the dropped section of the specimen. In all cases, in-plane failure would occur in this section rather than in the undropped section since the latter is thicker than the former and thus has more load-carrying capability.

4.5 Failure Criteria

The Maximum Stress Criterion is used to determine the magnitude and type (shear, longitudinal or transverse tension or compression) of ply failure. The allowable ply stresses are [34]:

$$-1468 \text{ MPa} \leq \sigma_{11}^{[\theta_i]} \leq 2356 \text{ MPa}$$

$$-186 \text{ MPa} \leq \sigma_{22}^{[\theta_i]} \leq 49.4 \text{ MPa}$$

$$-105 \text{ MPa} \leq \sigma_{12}^{[\theta_i]} \leq 105 \text{ MPa}$$

the program scales the applied unit stress or stress resultant and applies the above criterion to determine the magnitude and type of first ply failure and in which ply it occurs.

For the specimens without the bending correction, the stiffness properties of the failed ply are zeroed and the analysis is run again. This is continued until the maximum failure stress is found. With the equations developed previously for the problem of induced bending, only first ply failure can be found for the specimens with ply dropoffs. This is due to the fact that after the first ply fails, the midplane of the dropped section will change, making it no longer symmetric and in turn affecting the B and D matrices of both the undropped and dropped ends of the specimen. This is a much more complicated problem. Therefore, the failure stresses of laminates which include the induced bending stresses are a conservative first ply failure only.

It is again important to note that this analysis and failure criteria only deal with in-plane failure of the laminate. Interlaminar stresses are not calculated nor taken into account in the failure criterion.

4.6 Analytical Results

Table 4.1 is a summary of the analytical results for failure. The first column contains the first ply failure stress of the laminate without bending effects being considered. The second column is a list of final failure stresses neglecting any induced bending stresses. The third column lists the first ply failure stress for the specimens with ply dropoffs including the effects of the induced bending stresses. Note that the $[+15/+15_D/-15/-15_D/0/0_D]_S$ laminate was geometrically symmetric and therefore has no loading eccentriciy and therefore no induced bending effect. It can be seen that there is a significant difference between columns three and the first two columns. The first ply failure stresses predicted with the induced bending stresses are typically about half that predicted without these bending stresses.

In addition, a check in the analysis can be made by looking at the longitudinal curvature. Using equations 4.3 and 4.5, the curvature-dispacement relations, with the dispacement equations, equations 4.25 and 4.26, the curvatures can be expressed as:

$$\kappa_1 = \omega_1^2 C_4 e^{\omega_1 x} \tag{4.40}$$

$$\kappa_2 = \omega_2^2 C_7 e^{-\omega_2 x} \tag{4.41}$$

TABLE 4.1

SUMMARY OF ANALYTICAL RESULTS FOR LAMINATES WITH PLY DROPOFFS

Laminate	σ_f (MPa) BASED ON DROPPED SECTION		
	First Ply Failure	Final Failure	First Ply Failure w/ Bending
$[\pm 45/0_D/0/-+45]_T$	464	471	252
$[\pm(45_2)/0/0_D]_S$	464	471	239
$[+45/+45_D/-45/-45_D/0/0_D]_S$	638	785	364
$[\pm 45/(\pm 45)_D/0_2]_S$	866	1178	439
$[\pm 45/(\pm 45)_D/0/0_D]_S$	638	785	364
$[\pm 45/0/(\pm 45/0)_D]_S$	638	785	371
$[+15/+15_D/-15/-15_D/0/0_D]_S$ [a]	2105	2105	[a]

[a] Geometrically symmetric specimen, no bending correction

By setting these equations equal to 1% of the maximum curvature which occurs at the ply dropoff, it can be determined where the curvature becomes insignificant. The equations to solve for this value of x is therefore:

$$x = \frac{\ln(100)}{\omega_{1,2}} \tag{4.42}$$

This distance required for the longitudinal curvature to become insignificant varies from laminate to laminate. The maximum longitudinal distance for the curvature to die out in the dropped section is 25 mm, while that of the undropped section is 70 mm for the $[\pm(45_2)/0/0_D]_S$ laminate. Recalling that the far-field strain gages are 75 mm from the ply dropoff region, the analysis predicts that the gages will not measure any consistent curvature due to the ply dropoffs. Experimental data held this to be true. There was no consistent curvature information to be found from the experimental results.

CHAPTER 5

EXPERIMENTAL RESULTS

5.1 Stress-Strain Behavior

The far-field stress-strain behavior of the specimens tested is discussed in this section. This data was collected from strain gages centered on the front and back of both the dropped and undropped sections of the coupons with ply dropoffs, and centered on one side of the flat specimens, as explained in Chapter 3 and illustrated in Figure 3.12. All stress calculations were computed using load data from the testing machine, the measured width of the specimen, and the nominal thickness of the specimen, equal to the number of plies times 0.134 mm as explained in Chapter 3. Trends of audible sounds detected by ear during testing are also discussed. These audible sounds often correspond to damage and hence changes in the stress-strain behavior of the laminate. The order of discussion is based on the grouping of laminates shown in Table 3.2.

Most of the stress-strain curves can be categorized according to a few basic types of curves. The first type is linear, where the strain increases at a constant rate proportional to the load. A schematic of this type of curve is shown in Figure 5.1. A curve which has a gradual decrease in tangent modulus is said to soften. This type of curve can be seen in Figure 5.2. This figure also illustrates the term

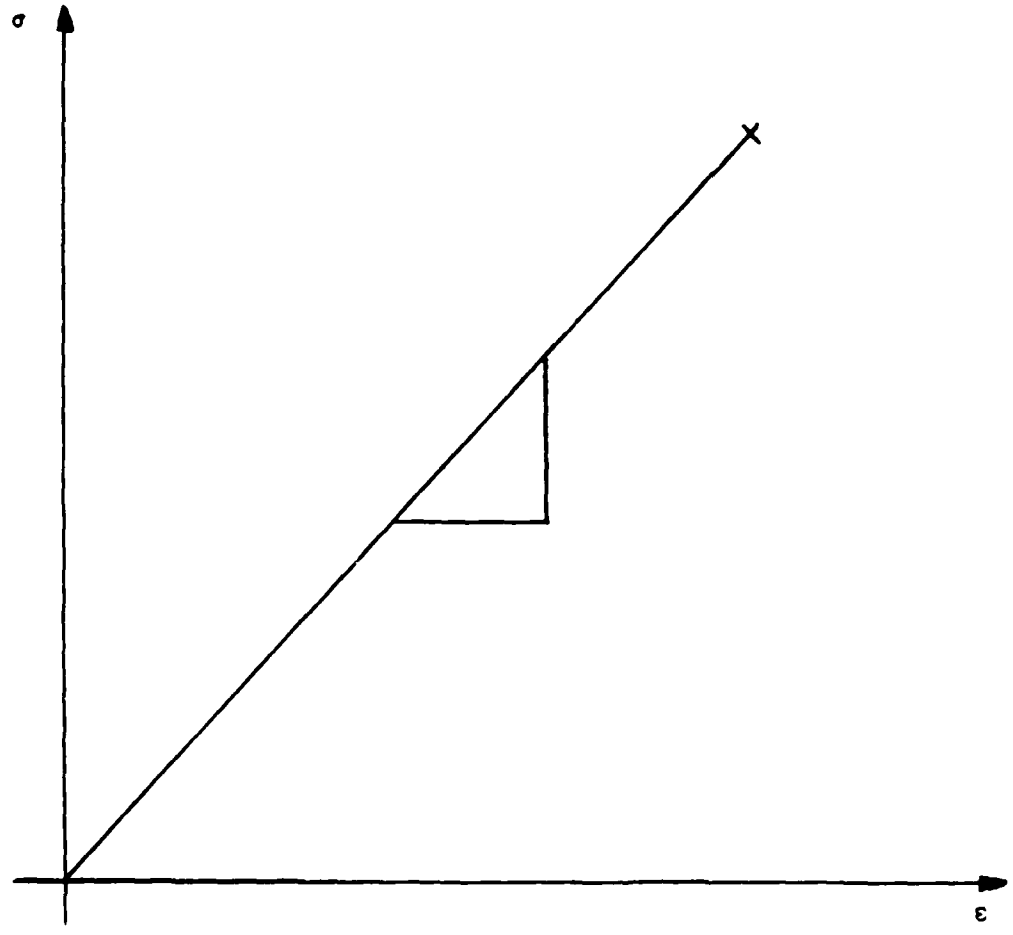

Figure 5.1 Stress-Strain Plot Showing Linear-to-Failure Behavior

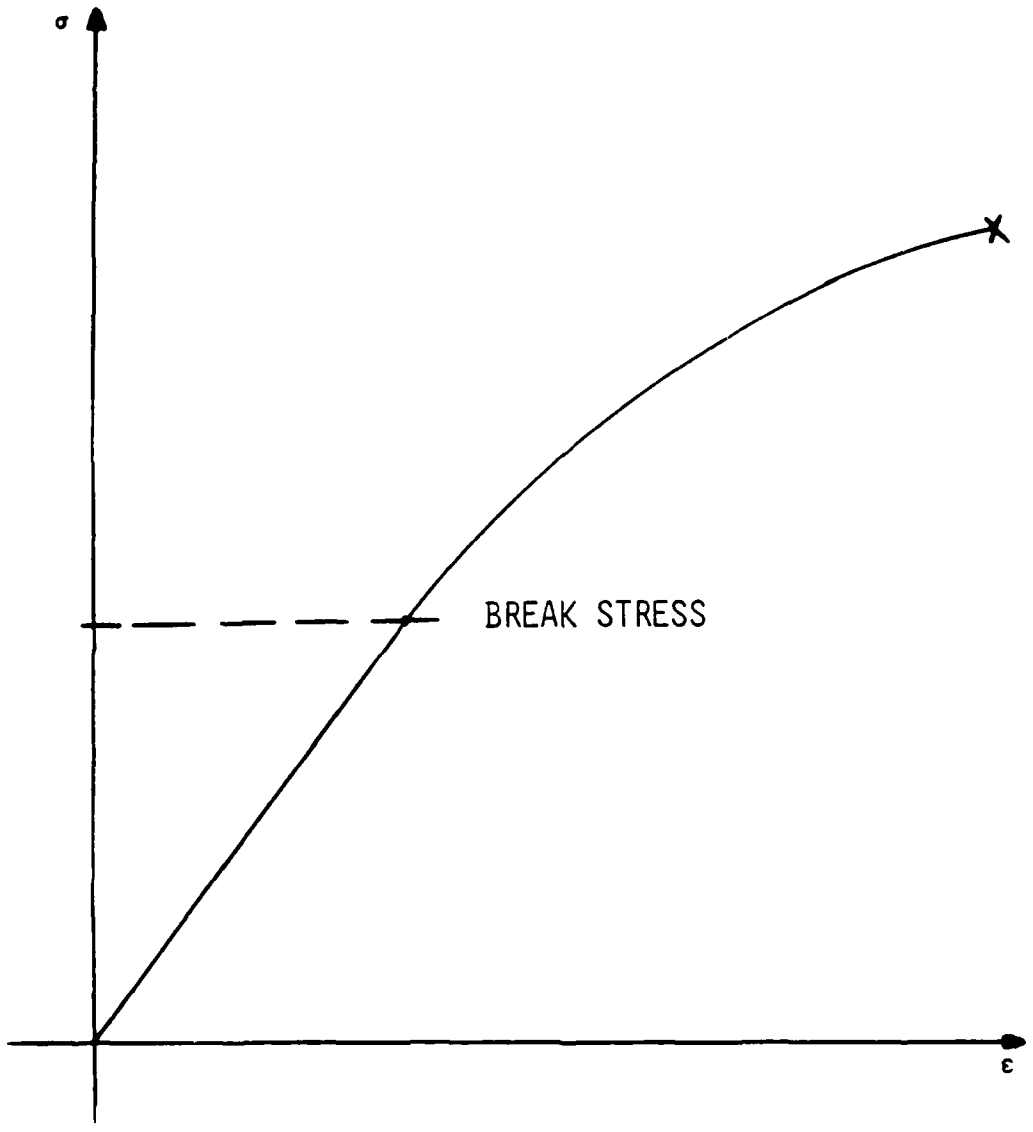

Figure 5.2 Stress-Strain Plot Showing a Reduction in Tangent Modulus ("Softening")

the term break stress, which is the point where a linear curve becomes nonlinear, such as in the softening type of curve [31]. A curve which has a gradual increase in tangent modulus is said to stiffen. This curve is illustrated in Figure 5.3. A discontinuity is a term to describe any irregularity from a smooth curve. There are several common types of discontinuities. A strain discontinuity occurs where strain increases at a constant load, as shown in Figure 5.4. A reversal point, illustrated in Figure 5.5, is a point where both load and strain decrease. A load drop, illustrated in Figure 5.6, occurs where the load decreases at either a constant or increasing level of strain (given that the tests were performed in stroke control).

Values for the longitudinal modulus of a specimen are determined using a program called LIN6 [33]. This is a program developed within TELAC which takes the load and strain data and outputs the linear regions of the curve, their slopes, and correlation coefficients. The longitudianl modulus was taken as the slope of the initial linear portion of the stress-strain curve.

Gage numbering was standardized for the coupons with ply dropoffs. Gage numbers three and five were on the flat side of the specimen, with three being centered on the undropped end of the specimen and five on the dropped end. Gages two and four were on the other side, or tapered side of the laminate, with two being centered on the undropped end of the specimen and four on the dropped end. Note that there was no gage numbered

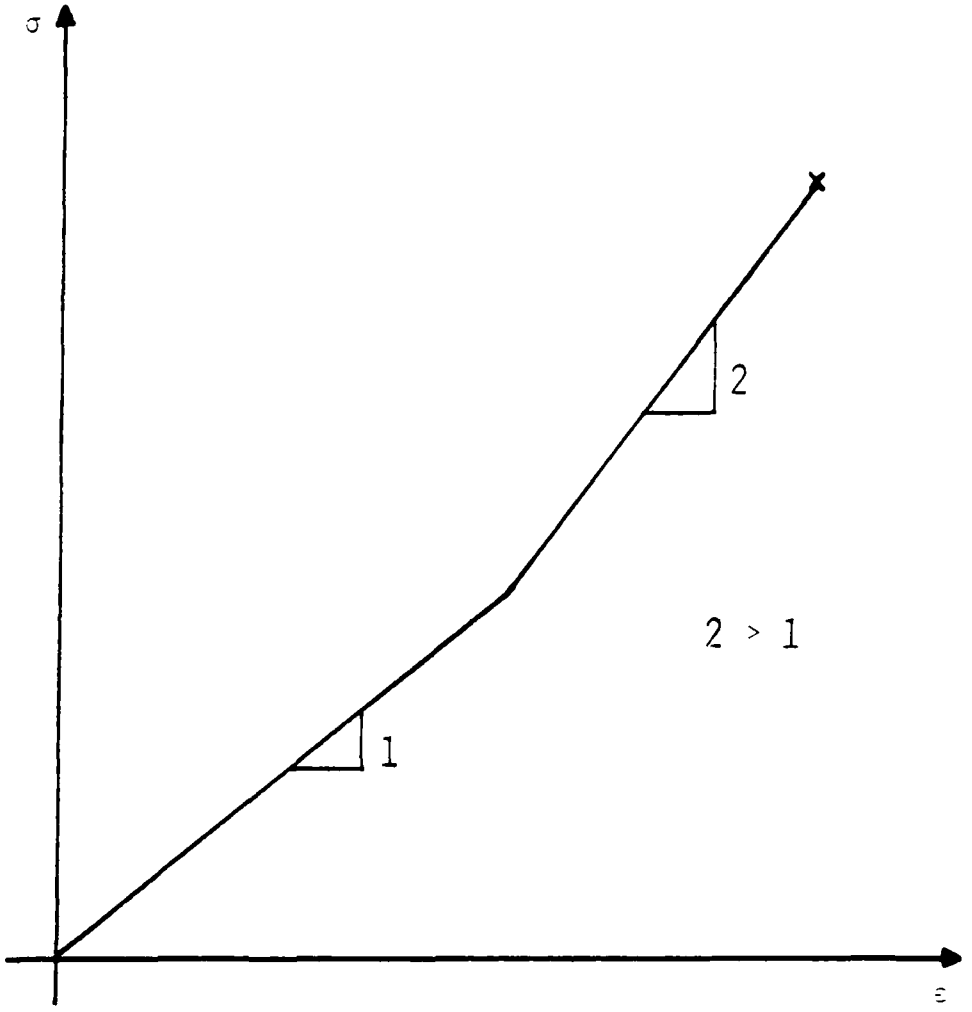

Figure 5.3 Stress-Strain Plot Showing "Stiffening"

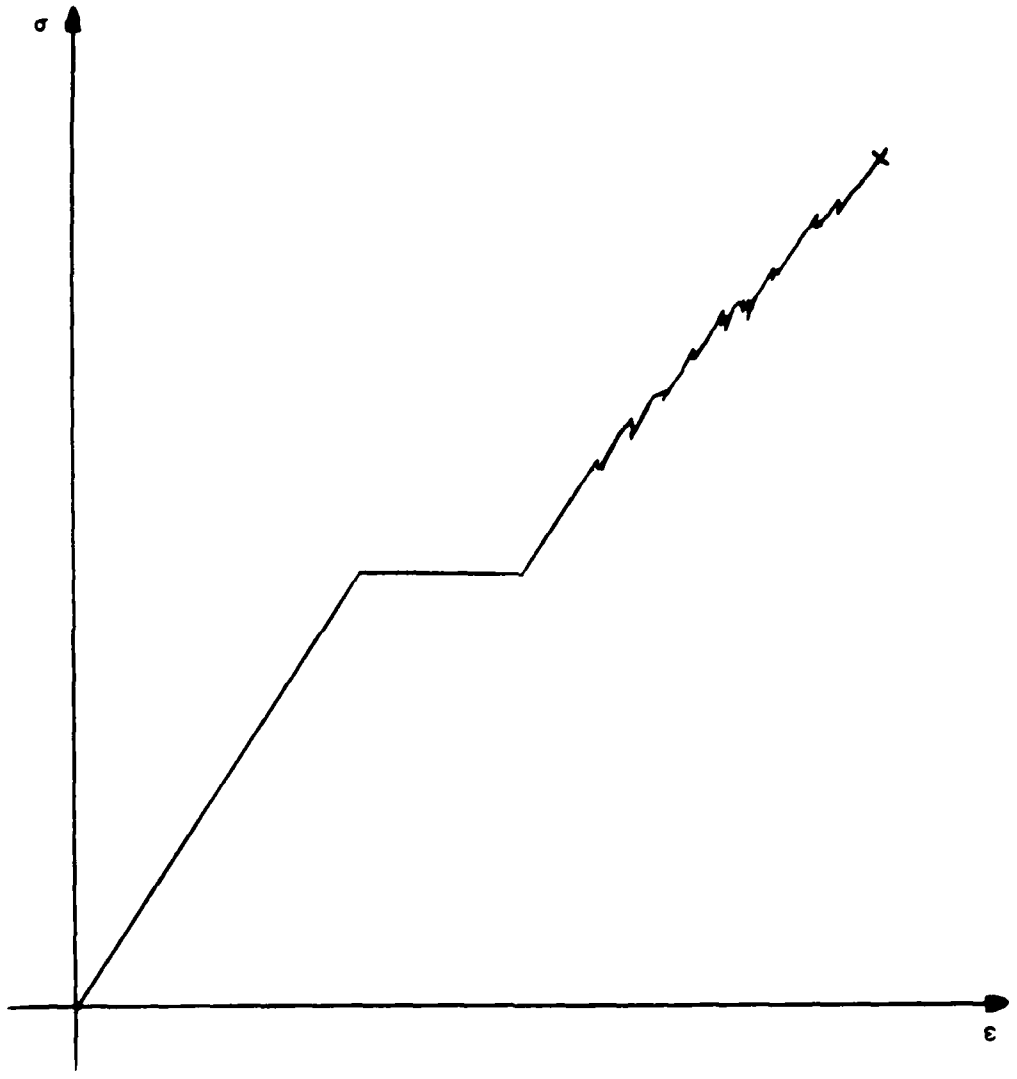

Figure 5.4 Stress-Strain Plot Showing Strain Discontinuity Points

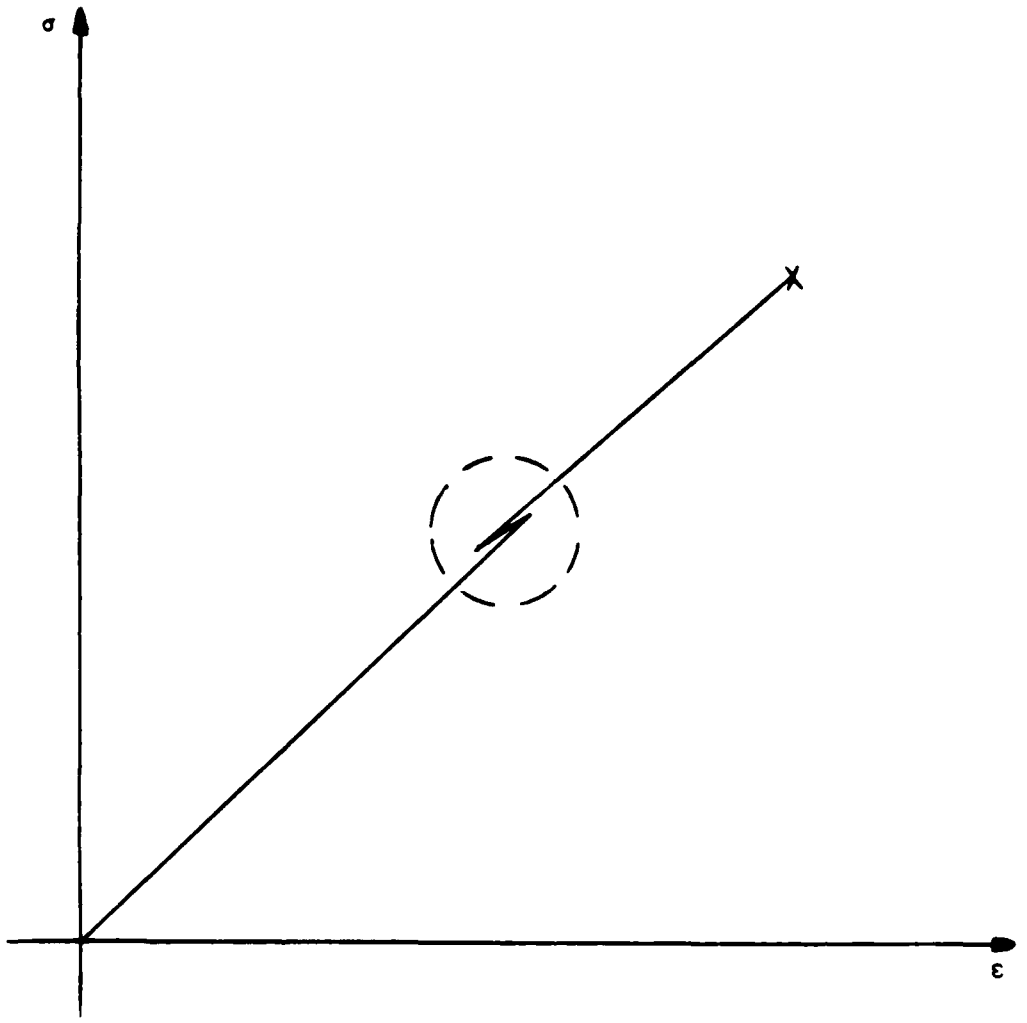

Figure 5.5 Stress-Strain Plot Showing a Reversal Point

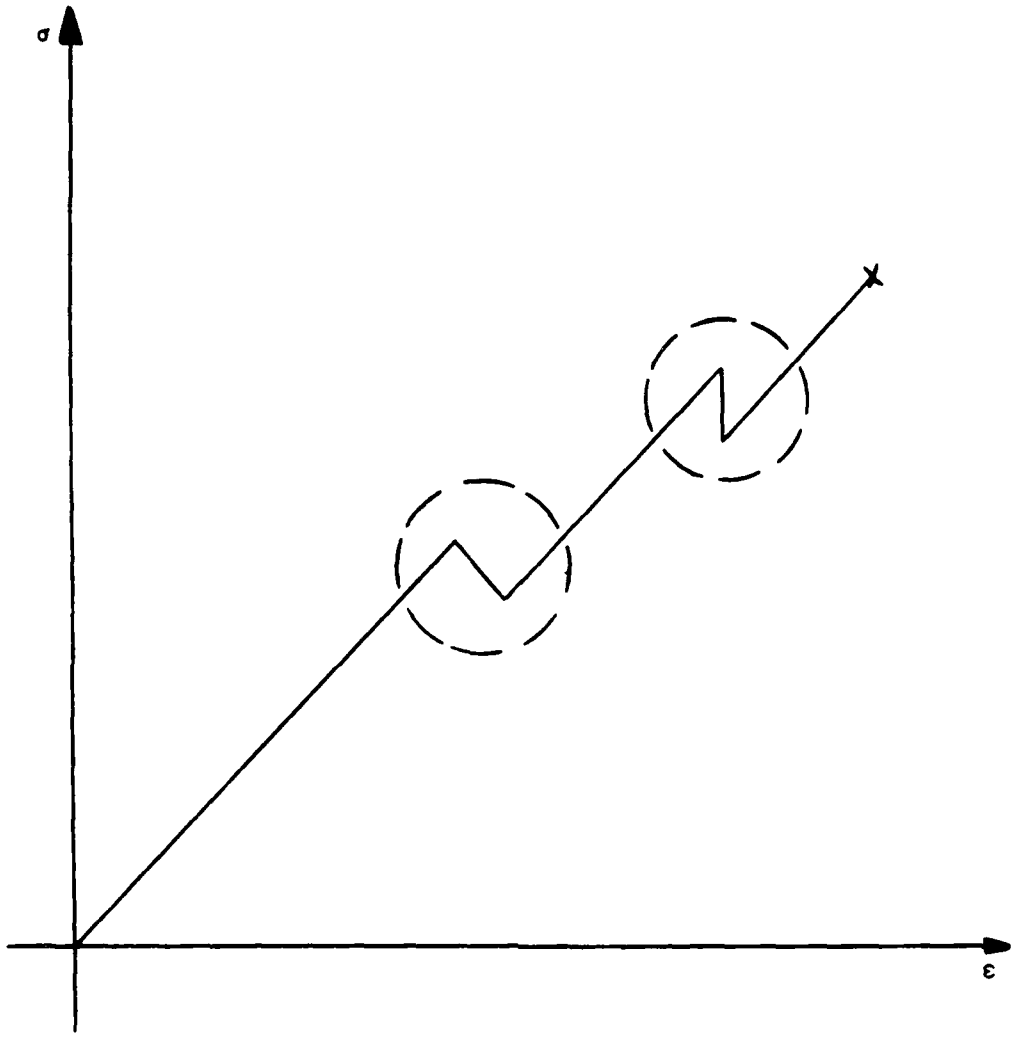

Figure 5.6 Stress-Strain Plot Showing Load Drops

one.

Longitudinal moduli for the flat specimens are listed in Table 5.1. Data for individual specimens are listed in the Data Tables. Longitudinal moduli predicted for the flat specimen using classical laminated plate theory are given in the third column. The data agrees well with the predicted values. The second column contains the coefficient of variation for each laminate, with the average coefficient of variation for all the flat specimens being about 5%.

Table 5.2 contains longitudinal moduli for the ply dropoff laminates. Each column of this table corresponds to a single gage position. The first two columns contain modulus data for the undropped end of the specimen, column one being the data for the tapered side of the specimen, or gage two, and column two being the flat side of the specimen, or gage four. The last two columns contain modulus data for the dropped end of the laminate. The data from strain gage three, the tapered side of the laminate, is in column three, while the data from gage five, the flat side of the dropped section, is in column four. The stress used in this calculation is based on the area for that particular part of the specimen. The average coefficient of variation for the ply dropoff laminates was also about 5%.

Table 5.3 is a comparison of longitudinal moduli for ply dropoff laminates and the corresponding flat laminates. The first column of this table is the average moduli for the undropped section of the laminate and is the average of the

TABLE 5.1

LONGITUDINAL MODULI FOR FLAT SPECIMENS

	E_L [GPa]	Coefficient of Variation	Predicted [GPa]
$[\pm 45/0]_S$	58.4	5.9%	61.0
$[\pm 45/0/-+45]_T$	45.2	3.5%	44.9
$[\pm(45_2)/0_2]_S$	60.4	0.8%	61.0
$[\pm(45_2)/0]_S$	46.0	1.7%	44.9
$[(\pm 45)_2/0_2]_S$	60.6	7.4%	61.0
$[\pm 45/0_2]_S$	83.7	5.0%	80.9
$[\pm 45/0]_{2S}$	62.9	0.9%	61.0
$[\pm(15_2)/0_2]_S$	123.6	2.1%	125.7
$[\pm 15/0]_S$	122.2	1.5%	125.7

TABLE 5.2

LONGITUDINAL MODULI FOR DROPPED AND UNDROPPED SECTIONS, FLAT AND TAPERED SIDES OF PLY DROPOFF LAMINATES

Laminate	LONGITUDINAL MODULUS [GPa]			
	UNDROPPED SECTION		DROPPED SECTION	
	Tapered Side	Flat Side	Tapered Side	Flat Side
$[\pm 45/0_D/0/-+45]_T$	57.8 (4.5%)[a]	60.4 (4.8%)	42.6 (6.7%)	42.6 (4.5%)
$[\pm(45_2)/0/0_D]_S$	60.3 (6.2%)	58.9 (3.4%)	42.5 (3.0%)	41.2 (14.4%)
$[+45/+45_D/-45/-45_D/0/0_D]_S$	58.6 (9.6%)	59.4 (7.2%)	57.5 (5.4%)	56.9 (5.8%)
$[\pm 45/(\pm 45)_D/0_2]_S$	59.9 (6.8%)	60.5 (3.9%)	83.2 (2.2%)	80.6 (3.1%)
$[\pm 45/(\pm 45)_D/0/0_D]_S$	59.5 (6.5%)	60.1 (6.1%)	56.3 (6.4%)	59.6 (3.2%)
$[\pm 45/0/(\pm 45/0)_D]_S$	61.0 (1.3%)	63.0 (4.1%)	59.1 (2.5%)	59.3 (1.7%)
$[+15/+15_D/-15/-15_D/0/0_D]_S$[b]	124.7 (2.0%)	125.2 (2.2%)	126.3 (1.5%)	128.0 (1.3%)

[a] Numbers in parentheses are coefficients of variation
[b] Geometrically symmetric specimen, no flat or tapered side

TABLE 5.3

COMPARISON OF EXPERIMENTAL AND PREDICTED LONGITUDINAL MODULI FOR PLY DROPOFF LAMINATES

Laminate	LONGITUDINAL MODULUS [GPA]			
	Undropped Section	Predicted	Dropped Section	Predicted
$[\pm 45/0_D/0/-+45]_T$	59.1 (4.9%)[a]	61.0	42.6 (5.3%)	44.9
$[\pm(45_2)/0/0_D]_S$	59.6 (4.9%)	61.0	41.9 (9.8%)	44.9
$[+45/+45_D/-45/-45_D/0/0_D]_S$	59.0 (8.0%)	61.0	57.2 (5.3%)	61.0
$[\pm 45/(\pm 45)_D/0_2]_S$	60.2 (5.0%)	61.0	81.9 (3.0%)	80.9
$[\pm 45/(\pm 45)_D/0/0_D]_S$	59.8 (6.0%)	61.0	57.9 (5.6%)	61.0
$[\pm 45/0/(\pm 45/0)_D]_S$	62.0 (3.3%)	61.0	59.2 (2.0%)	61.0
$[+15/+15_D/-15/-15_D/0/0_D]_S$	124.9 (2.0%)	125.7	127.3 (1.4%)	125.7

[a] Numbers in parentheses are coefficients of variations

first two columns of Table 5.2. The second column is the longitudinal moduli of the undropped section predicted via CLPT. The third column contains the average moduli for the dropped section of the laminate and is the average of the last two columns of Table 5.2. The last column of Table 5.3 contains the moduli of the dropped section predicted via CLPT.

As predicted by the analysis in Chapter 4, the far-field strain gages were too far away from the ply dropoff region to pick up any induced bending. The strain differences between the front to back gages on the dropped and undropped section of the ply dropoff laminates did not provide any consistent or significant curvature information. Thus, in all cases the measured moduli correspond well with the predicted moduli.

The stress-strain curves of the $[\pm 45/0]_S$ laminates can most generally be described as being linear. Typically these specimens showed a drop in modulus of about 3% at about 50% of the ultimate load, essentially a linear curve, as can be seen in Figure 5.7. All but one of the specimens had an audible pop at about 50% of ultimate load, with the first occurrence of an audible pop in the last specimen being at 70% of ultimate load. Typically two or three more of these pops were heard before final failure.

The stress-strain curves of the $[\pm 45/0_D/0/-+45]_T$ laminates were quite consistent from coupon to coupon. The curves for gages two and four on the undropped end of the laminates were linear curves with a 3% or less reduction in modulus for all but one of these curves, with the one exception showing a 6%

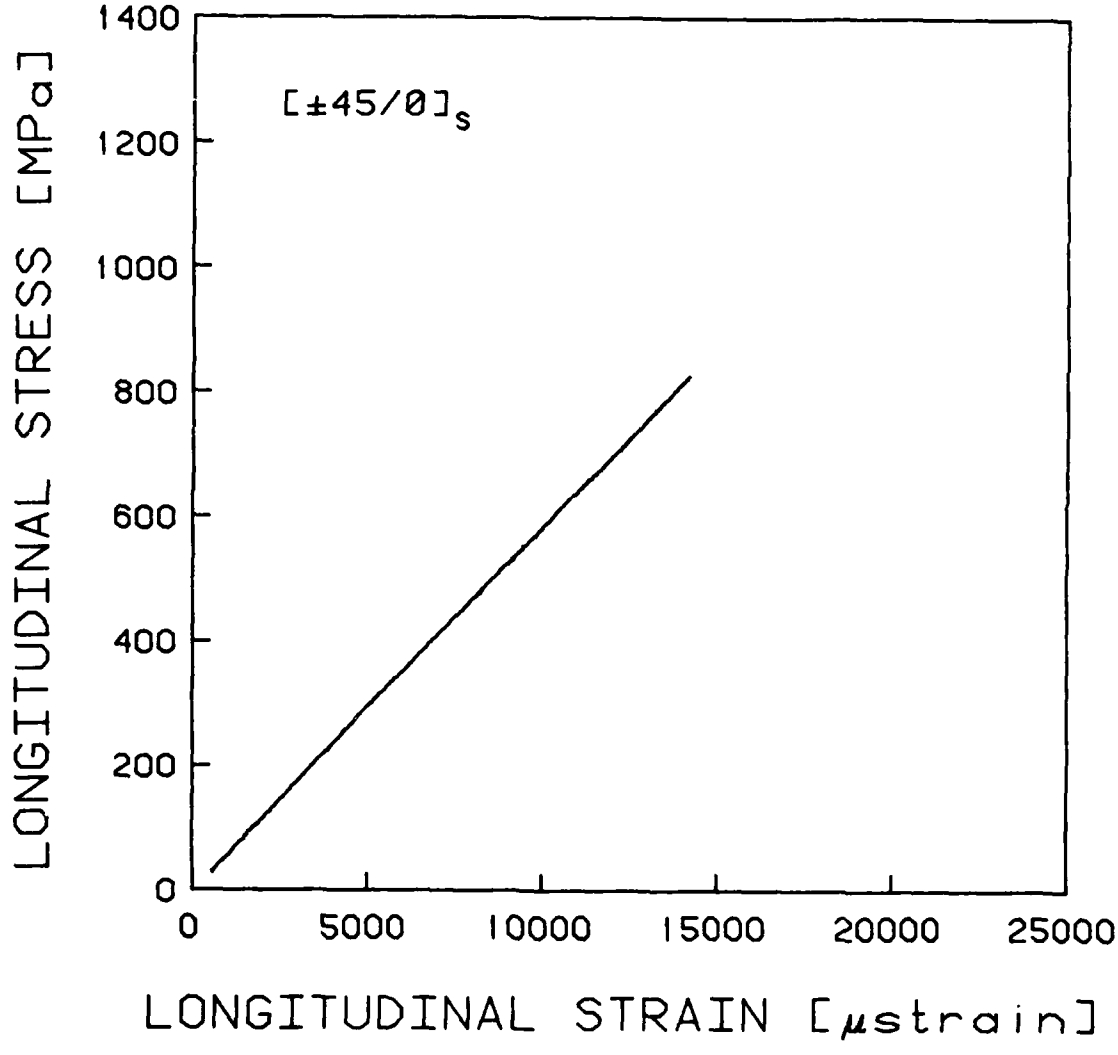

Figure 5.7 Typical Stress-Strain Plot for a $[\pm 45/0]_S$ Specimen

reduction in modulus. The stress-strain curves from gages three and five on the dropped end of the laminate showed significant softening, typically beginning at about 15% of ultimate load with about a 10% reduction in modulus and decreasing to about 80% of the original modulus value near 60% of ultimate. This can be seen in Figure 5.8. These specimens were fairly quiet during testing, with half not emitting any significant audible sounds, and half emitting loud pops only after 95% of ultimate load was reached.

The $[\pm 45/0/-+45]_T$ laminates all had a softening type of stress-strain curve. This softening is expected since the majority of plies are $\pm 45^{\circ}$ which exhibit softening behavior [35]. While the amount of softening varied between the coupons, each showed a modulus of at least 20% less upon failure than the inital linear region, with the average break stress occurring at about 25% of ultimate load. The tangent modulus of one of the specimens became horizontal, or zero, before failure. These laminates were also quiet during testing, with three of the five tested emitting one loud pop each at about 65% of ultimate load, and the other two emitting no significant sounds before failure. A typical curve is shown in Figure 5.9.

The basic laminate of the second group is the $[\pm(45_2)/0_2]_S$ layup. All but one of these laminates exhibited a slightly softening stress-strain curve, an example of which can be seen in Figure 5.10. The tangent modulus typically decreases in these specimens by about 5% after about 50% of ultimate load.

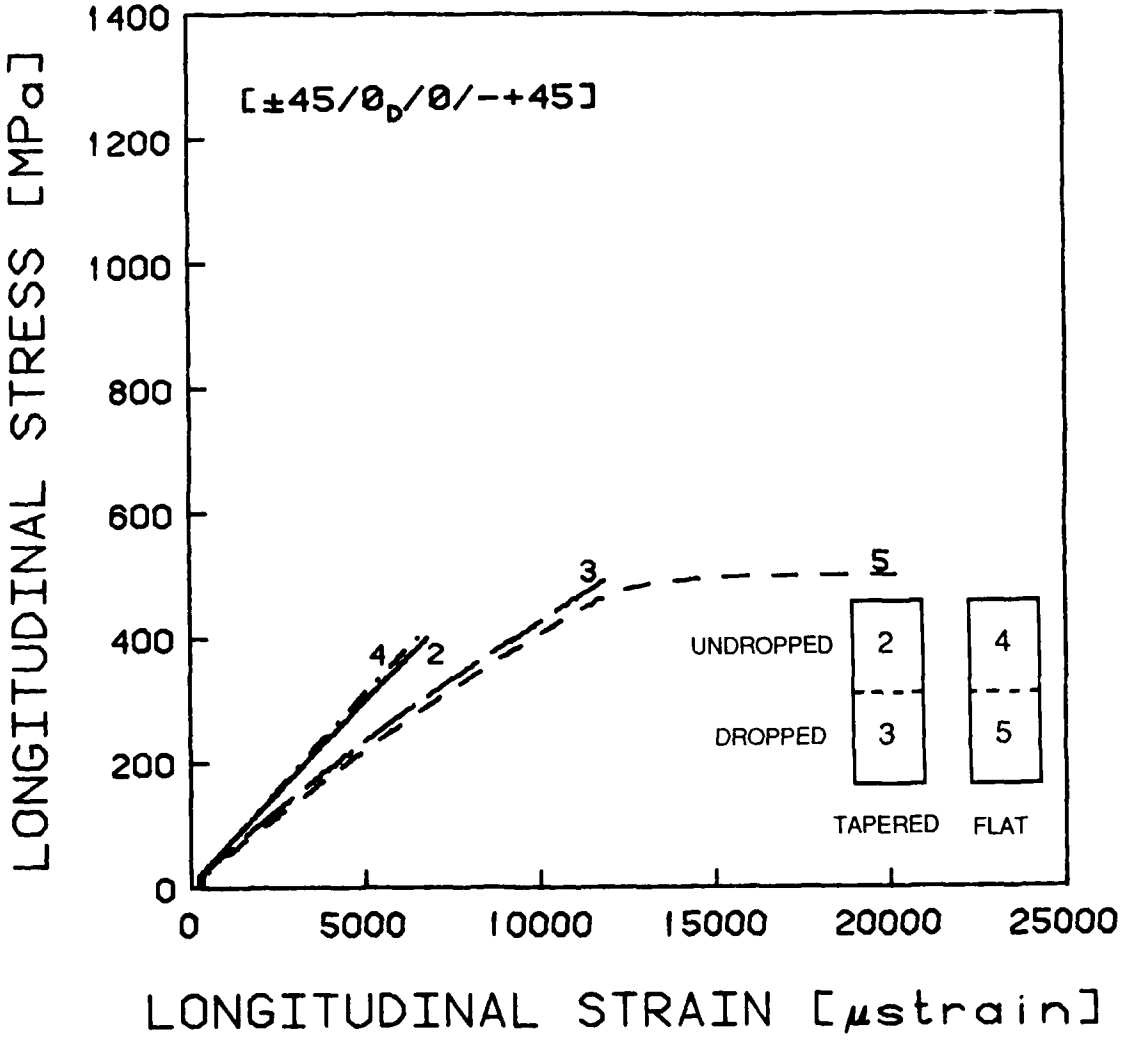

Figure 5.8 Typical Stress-Strain Plot for a $[\pm 45/0_D/0/-+45]_T$ Specimen

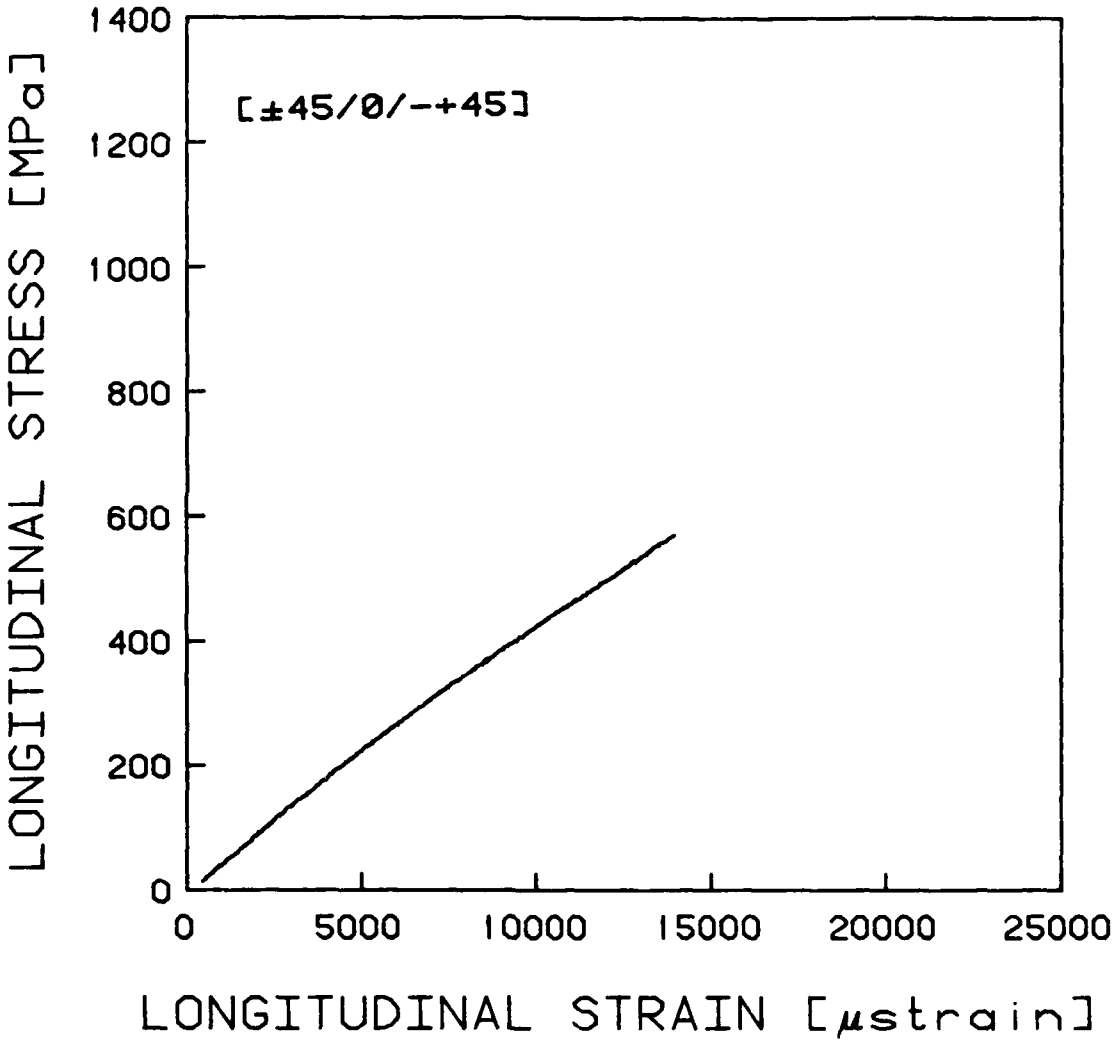

Figure 5.9 Typical Stress-Strain Plot for a $[\pm 45/0/-+45]_T$ Specimen

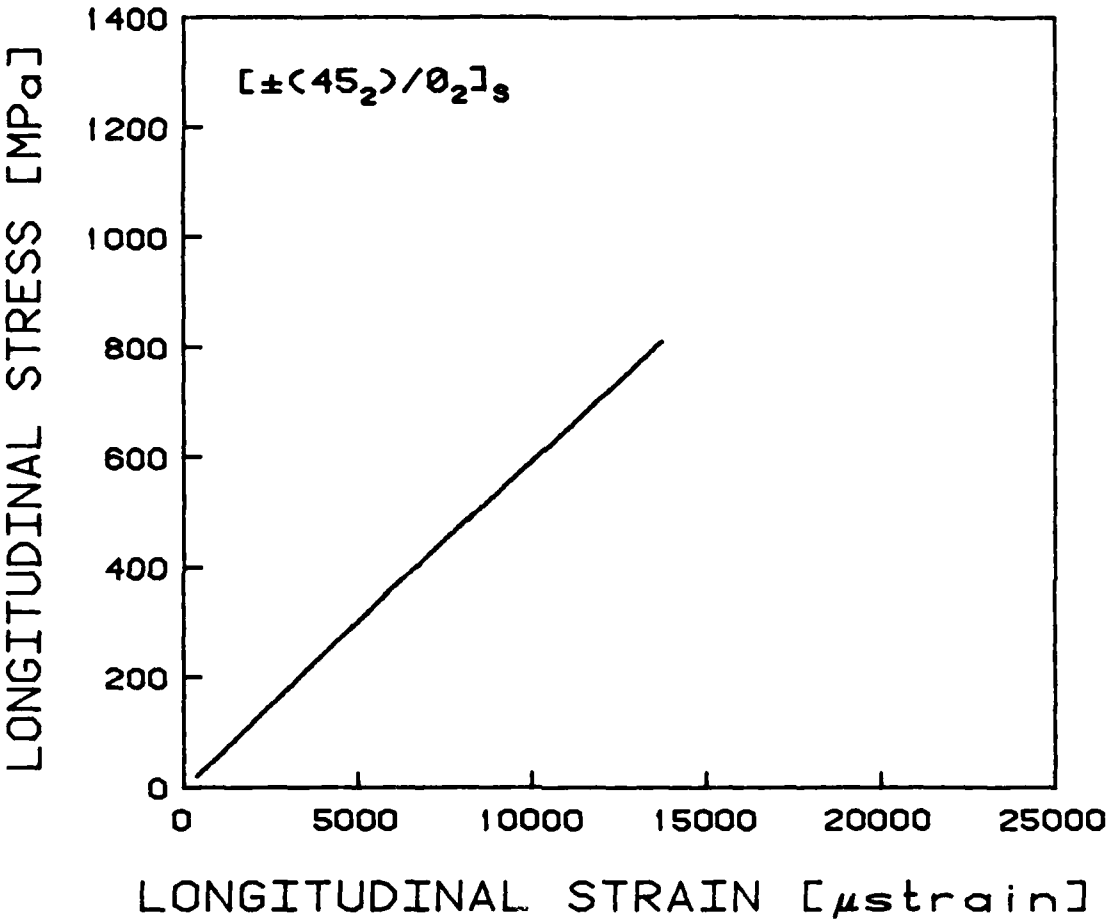

Figure 5.10 Typical Stress-Strain Plot for a $[\pm(45_2)/0_2]_S$ Specimen

The stress-strain response of this laminate should be very similar to that of the $[\pm 45/0]_S$ laminate, as it is, since effective ply thickness is not important in stress-strain response. Each of these coupons gave off several loud pops during testing, beginning at about 35% and continuing until about 85% of ultimate load, at about 10% intervals.

The $[\pm(45_2)/0/0_D]_S$ specimens exhibited linear stress-strain behavior for the most part. Two of the coupons were linear all the way through to failure while three coupons were basically linear, but showed some anomalies along the way. These normally occurred from about 85% of ultimate to failure, with the undropped end of the laminate softening sligthly, and the dropped end having very small irregularities of both stiffening and softening. An example of this type of curve is shown in Figure 5.11. These laminates were also quite noisy, with loud pops typically beginning at about 50% of ultimate load, and about four such pops occurring until 90% to 95% of ultimate load is reached.

The $[+45/+45_D/-45/-45_D/0/0_D]_S$ laminates behaved similarly to the above laminates, but with less variation from linear behavior in the sections that did soften. The stress-strain curves were basically linear, with some slight softening in the dropped section of the laminate. Break stresses are typically in the 50% of ultimate range with softening of about 7%. A stress-strain curve of this type can be seen in Figure 5.12. Loud pops were heard from all specimens between 50% and 60% of ultimate load. One other pop was heard in three of the

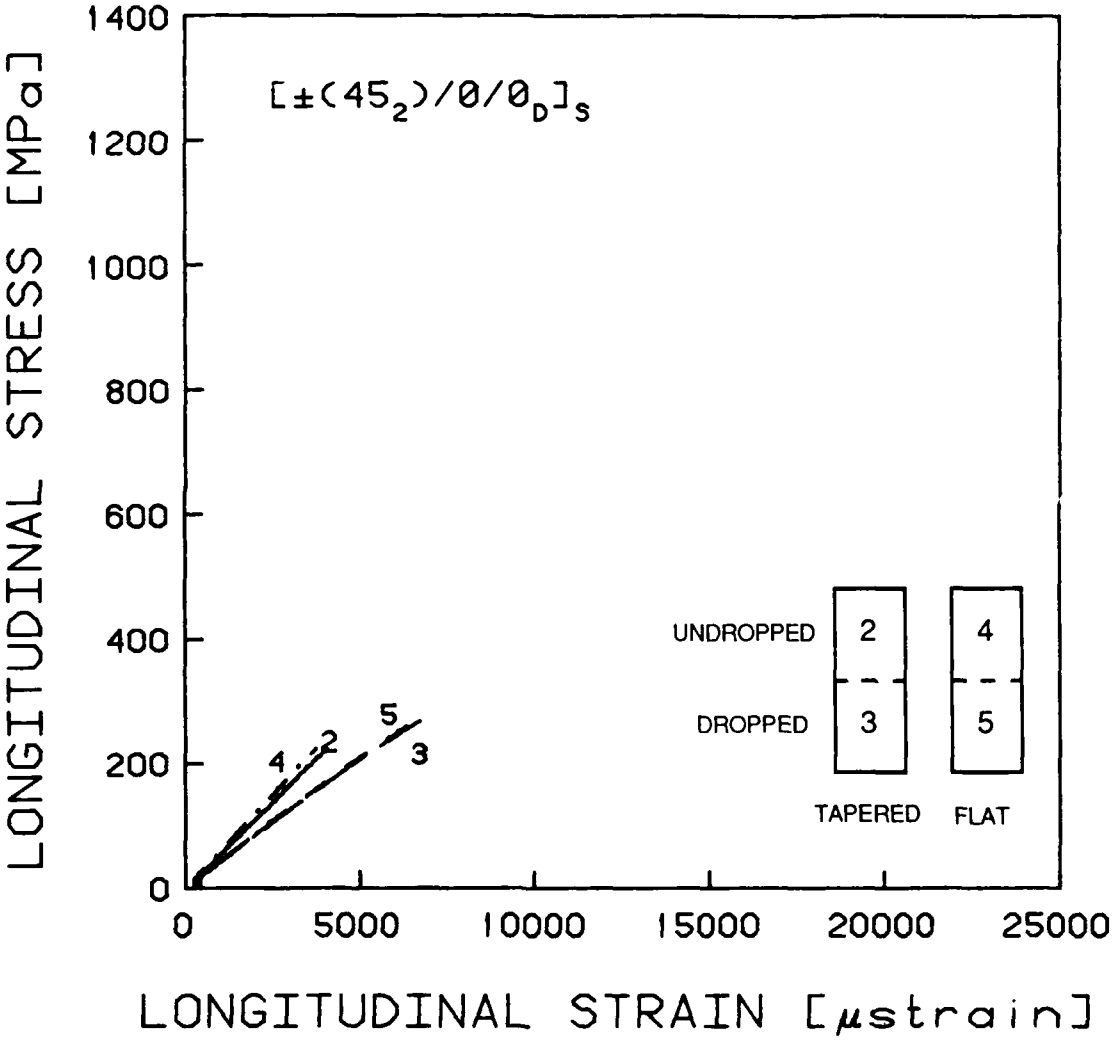

Figure 5.11 Typical Stress-Strain Plot for a $[\pm(45_2)/0/0_D]_S$ Specimen

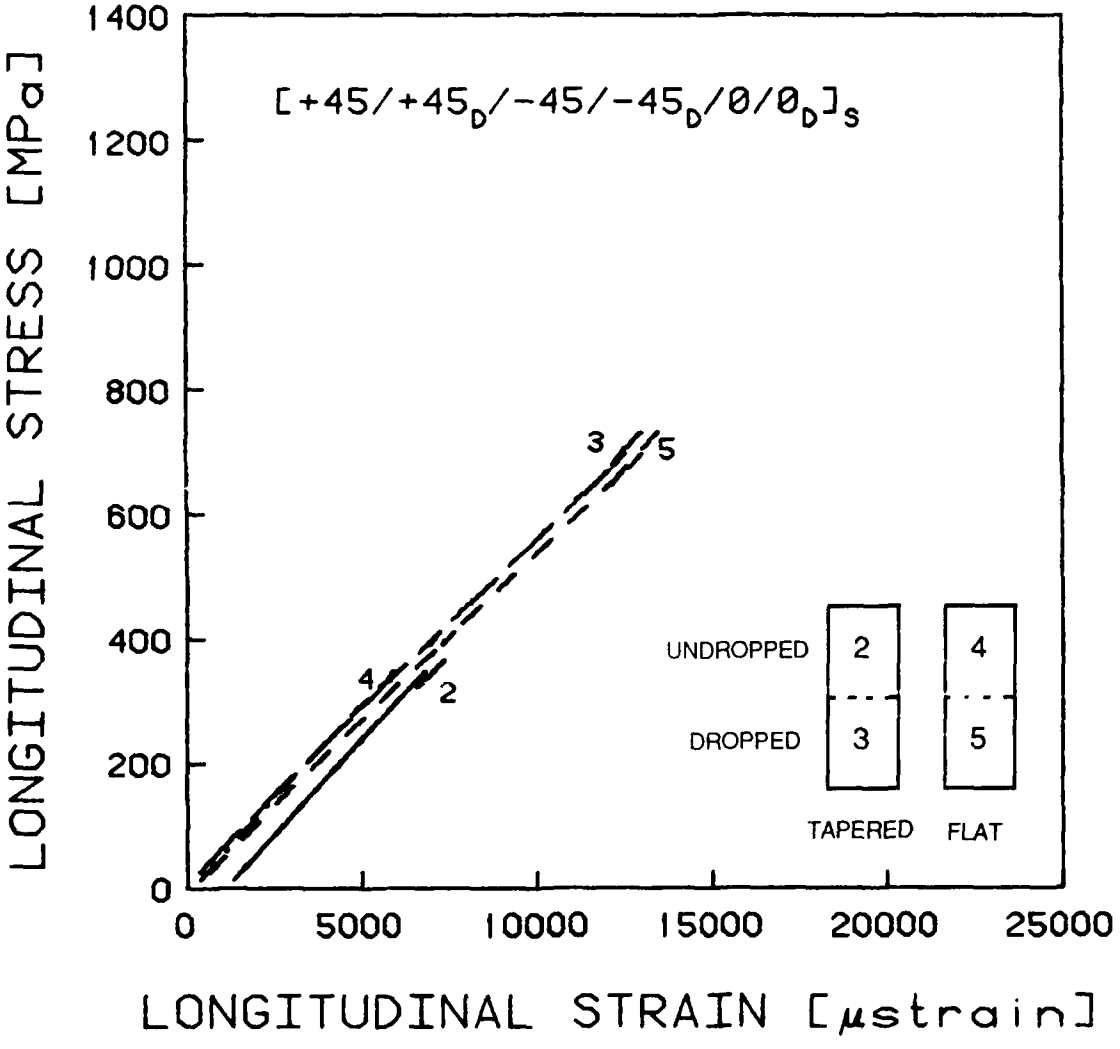

Figure 5.12 Typical Stress-Strain Plot for a $[+45/+45_D/-45/-45_D/0/0_D]_S$ Specimen

specimens between 80% and 90% of ultimate.

The other flat laminate in the second group is the $[\pm(45_2)/0]_S$ laminate. These laminates all had a softening type of stress-strain curve, with a break stress of roughly 30% of ultimate load. Maximum softening in these coupons was typically in the 20% range of the initial linear portion of the curve. A typical curve is shown in Figure 5.13. Several loud pops were commonly heard during the testing of these laminates, with the first one being heard between 50% and 75% of ultimate load.

Three of the $[(\pm45)_2/0_2]_S$ specimens had a slight softening in the stress-strain curve with modulus values decreasing in the 3% to 5% range. One of these also had a strain discontinuity at about 40% of its ultimate load. Break stresses were about 50% of ultimate. The other two coupons showed more significant softening, beginning with reductions of 3% and 6% at about 40% of ultimate and running to about 10%. Loud pops were heard beginning at 40% to 50% of ultimate load. A typical curve is shown in Figure 5.14. These curves should be, and are, similar to those of the $[\pm45/0]_S$ and $[\pm(45_2)/0_2]_S$ laminates.

The $[\pm45/(\pm45)_D/0_2]_S$ laminates were mostly linear in their stress-strain response through to failure both in the undropped and dropped sections. One of the coupons exhibited slight softening in the undropped section of the laminate. This curve is shown in Figure 5.15. Audible pops were heard from each of these coupons at about 33% of ultimate load.

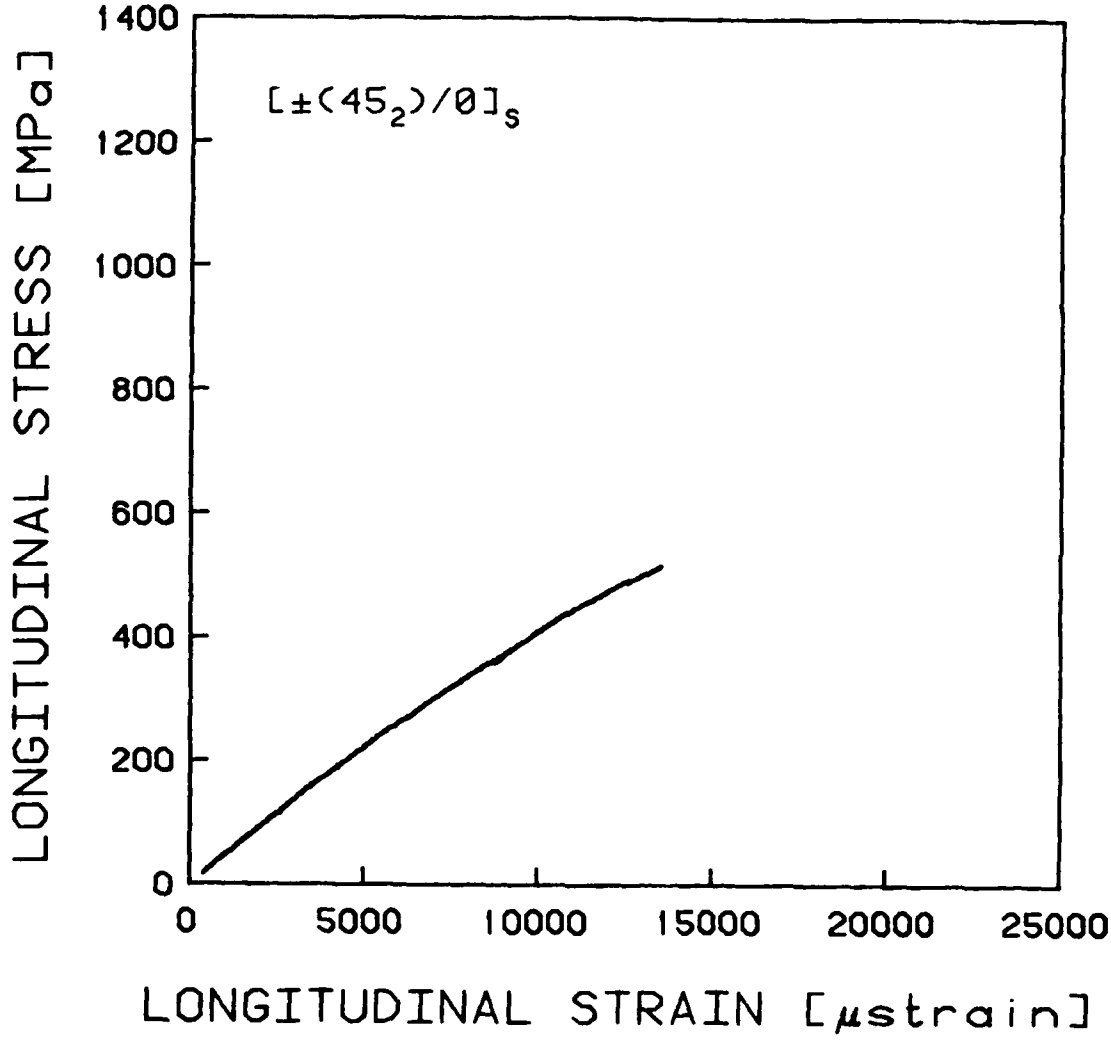

Figure 5.13 Typical Stress-Strain Plot for a $[\pm(45_2)/0]_S$ Specimen

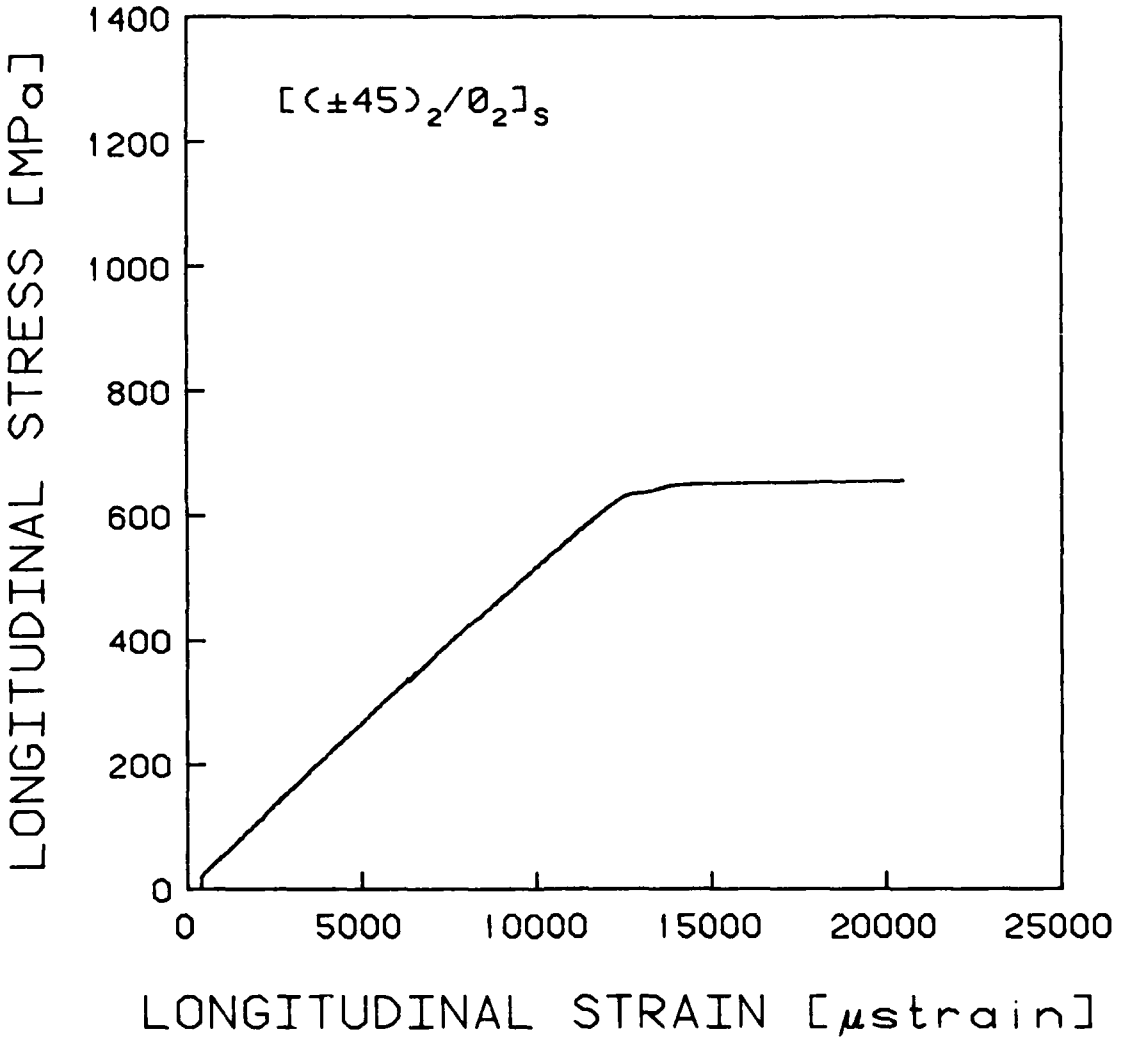

Figure 5.14 Typical Stress-Strain Plot for a $[(\pm 45)_2/0_2]_S$ Specimen

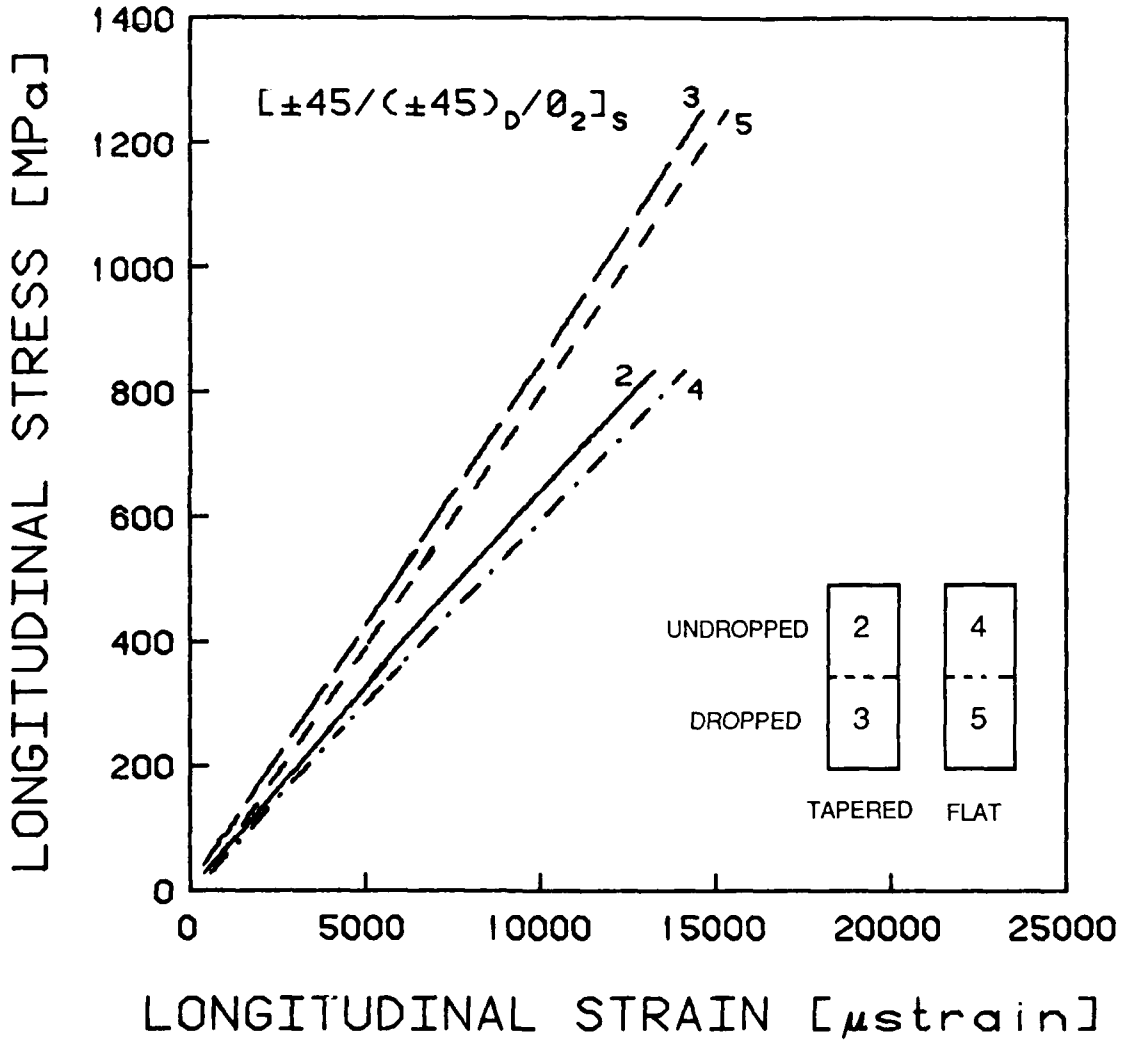

Figure 5.15 Typical Stress-Strain Plot for a $[\pm 45/(\pm 45)_D/0_2]_S$ Specimen

The undropped ends of the $[\pm 45/(\pm 45)_{D/0/0_D}]_S$ specimens were all essentially linear with respect to stress-strain behavior. The dropped sections of the coupons were not quite as consistent. On the average, these curves could also best be described as linear, although some of the curves either stiffened slightly or softened slightly, with no real pattern emerging between the flat and tapered sides of the dropped section of the specimen. Most of these changes in the dropped ends of the specimens were in the 5% to 7% range which is within data scatter. Loud pops were heard at about 50% of ultimate load for all but one specimen, where a loud pop occurred at about 80% of the ultimate load. A typical stress-strain curve is shown in Figure 5.16.

The stress-strain curves of the $[\pm 45/0_2]_S$ specimens were mostly linear, with three of the five curves having no more than 3% softening. Three to four loud pops were typically heard between 80% and 90% of ultimate load.

The basic laminate in the fourth group is the $[\pm 45/0]_{2S}$ laminate. A typical stress-strain curve is shown in Figure 5.17. The curves of this laminate show softening of a maximum of about 10% with a break stress in the 40% range of ultimate load. One of the curves had a load drop at about 75% of ultimate, as can be seen in Figure 5.18. Initial loud pops were heard at about 40% of ultimate, with another one or two pops typically in the 80% to 90% load of ultimate load. These curves are similar to those of the $[\pm 45/0]_S$ and $[\pm(45_2)/0_2]_S$ laminates, as expected.

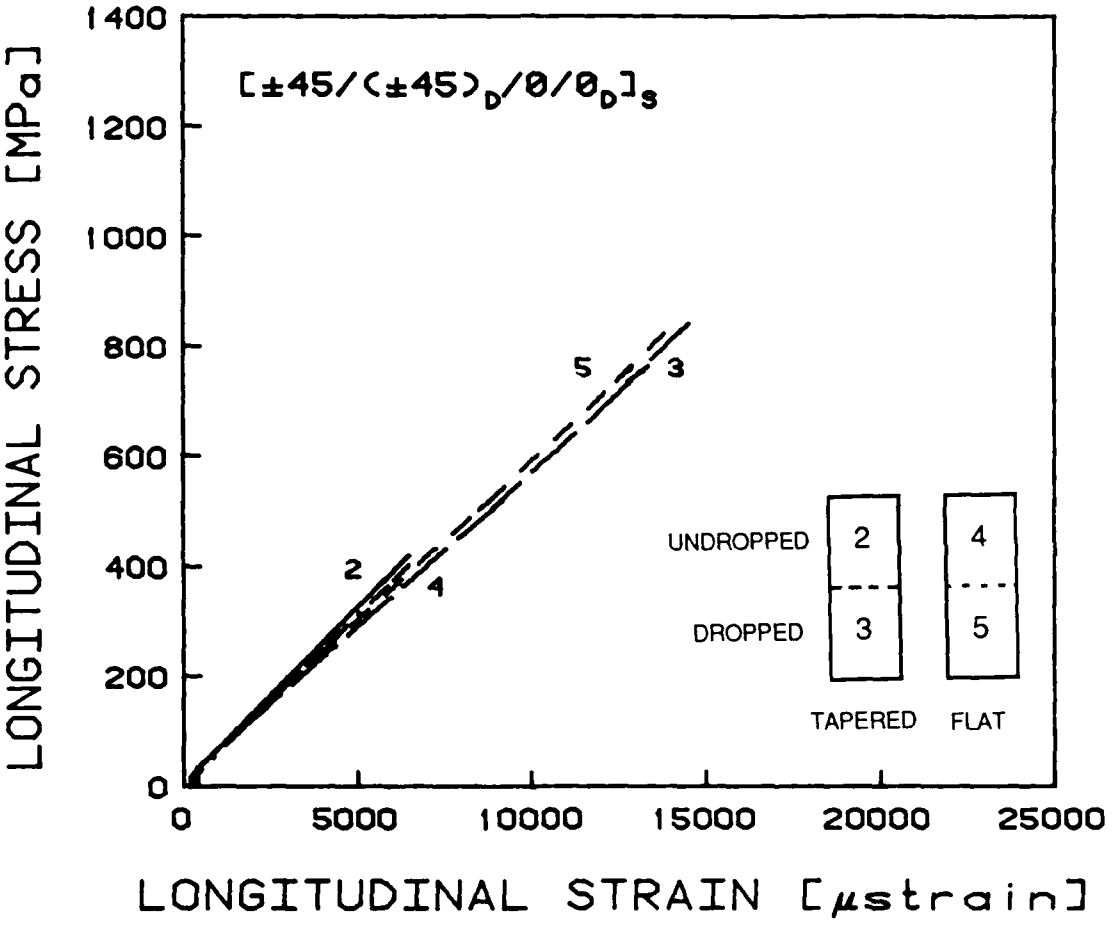

Figure 5.16 Typical Stress-Strain Plot for a $[\pm 45/(\pm 45)_D/0/0_D]_S$ Specimen

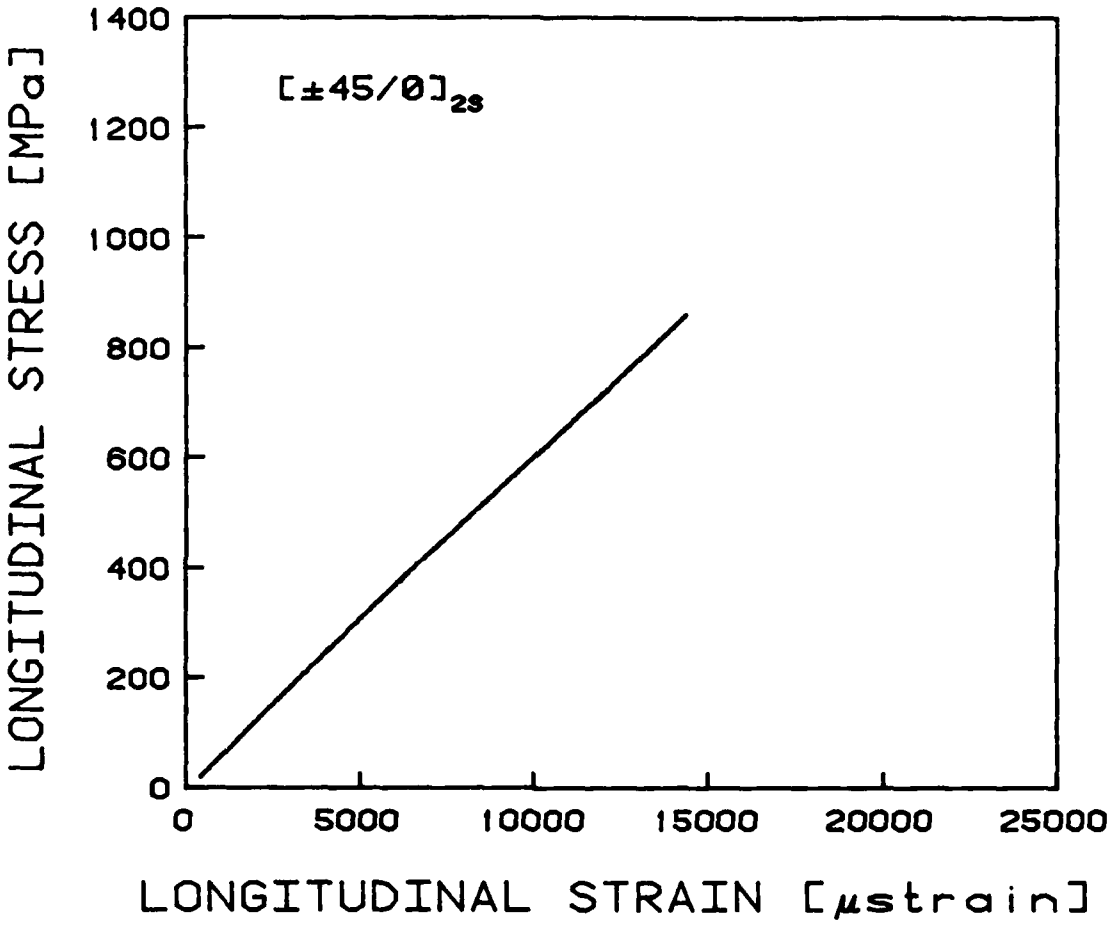

Figure 5.17 Typical Stress-Strain Plot for a $[\pm 45/0]_{2S}$ Specimen

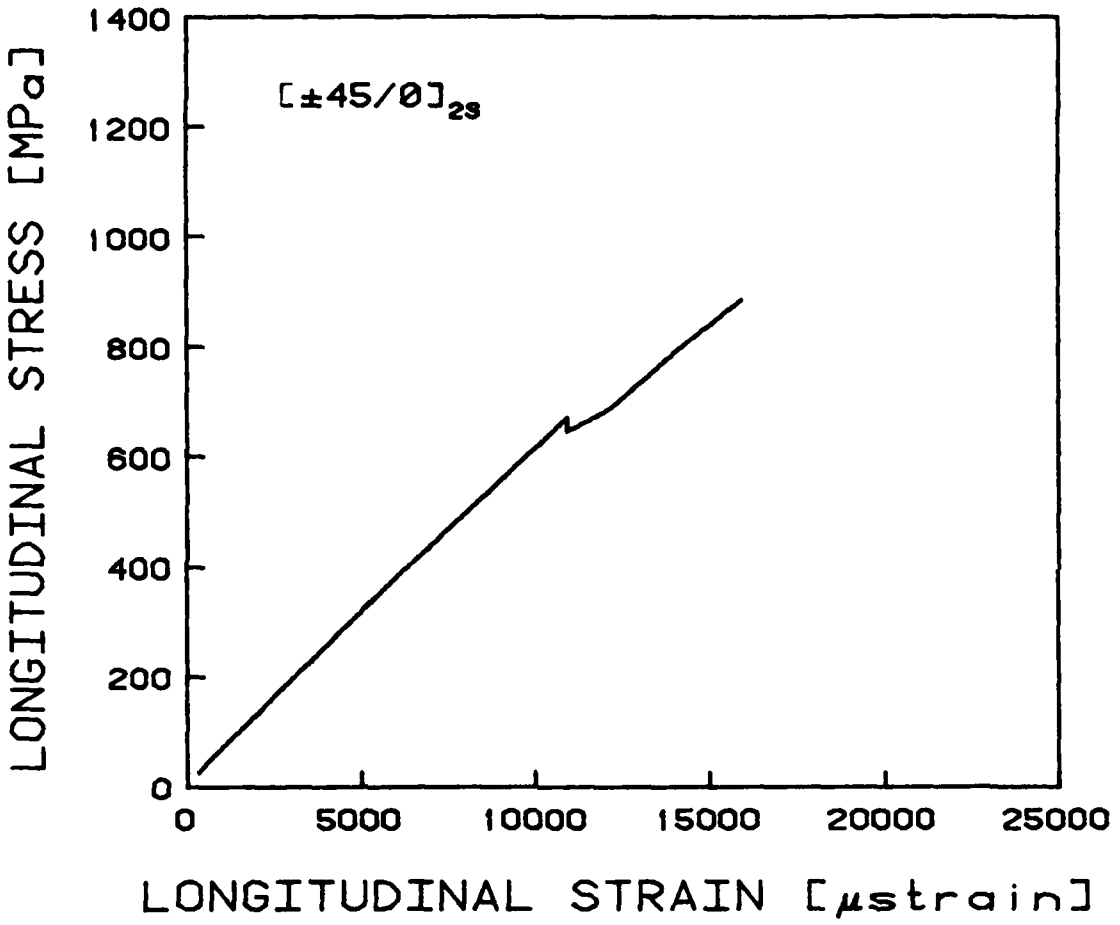

Figure 5.18 Stress-Strain Plot for a $[\pm 45/0]_{2S}$ With a Load Drop

The $[+45/0/(\pm 45/0)_D]_S$ laminates had varying types of stress-strain curves. One laminate was entirely linear in its stiffness response. One coupon was linear except for the flat side of the dropped end of the specimen, where it softened by about 25% at about 25% of its ultimate load. The dropped end of the other two specimens initially softened and then stiffened, while the undropped ends of the specimens softened. This can be seen in Figure 5.19. Initial loud pops were typically heard in the 60% range of ultimate load.

The basic laminate of the last group is the $[\pm(15_2)/0_2]_S$ laminate. These laminates all exhibited stiffening stress-strain curves, with stiffness increasing in the range of 1% to 8%, as can be seen in Figure 5.20. Two of these specimens softened at about 90% of ultimate load. Break stresses are about 60% of ultimate. Initial loud pops were heard at 50% of ultimate for three of the coupons, and 65% and 75% for the other two. Between one and three more pops were heard up to the 90% range of ultimate.

The next specimen in this group is the only geometrically symmetric secimen. The $[+15/+15_D/-15/-15_D/0/0_D]_S$ laminates were linear in their stress-strain response for all the coupons in the undropped end of the specimen and for one coupon in the dropped end. The other three coupons stiffened in their stress-strain curves, 1% to 5% in one coupon with a break stress of about 80%, 12% in a small section of the curve at about 90% of ultimate load in another coupon, and 3% to 4% in a third. Initial loud pops were heard at 30% to 40% of ultimate

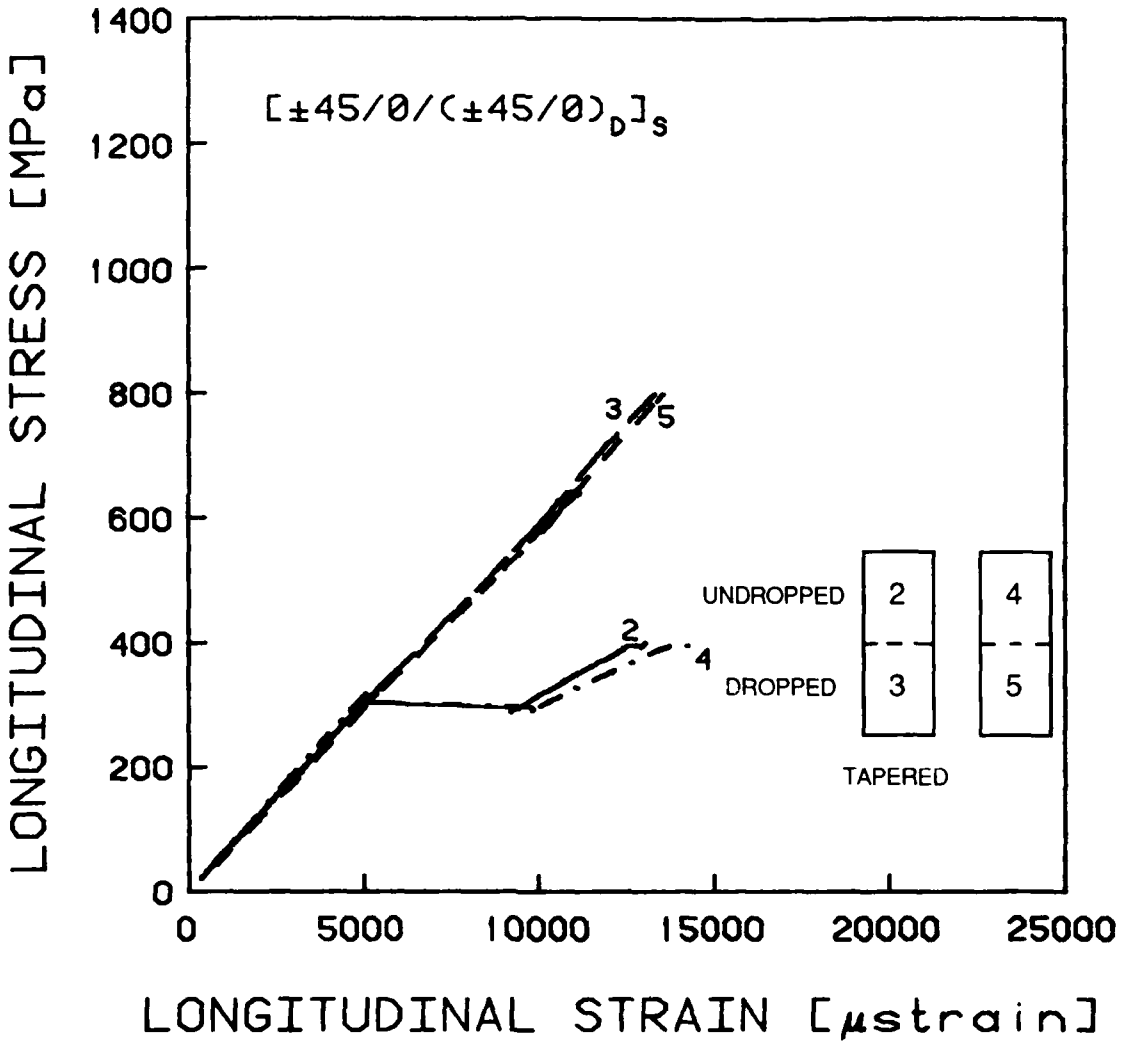

Figure 5.19 Typical Stress-Strain Plot for a $[\pm 45/0/(\pm 45/0)_D]_S$ Specimen

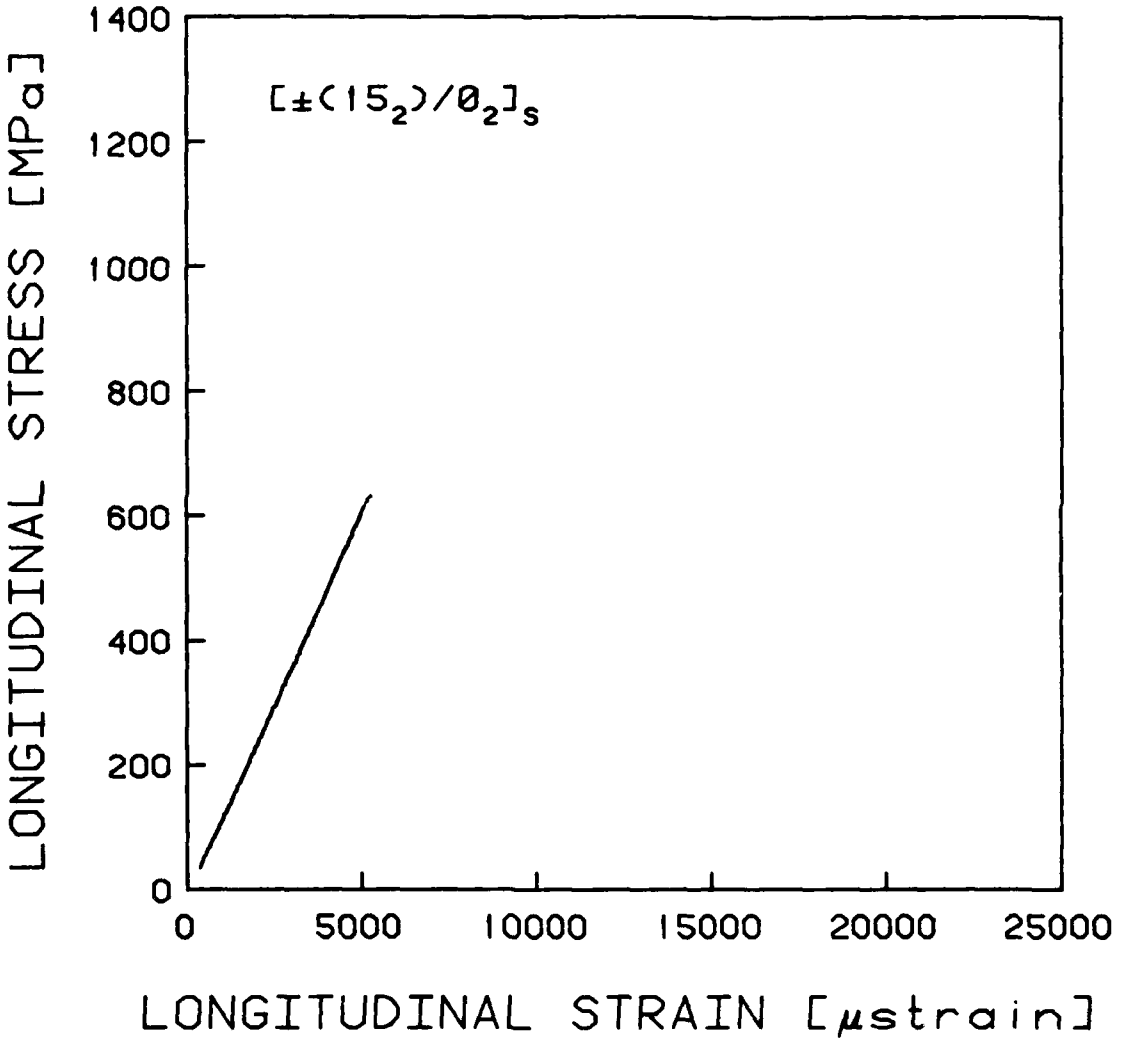

Figure 5.20 Typical Stress-Strain Plot for a $[\pm(15)_2/0_2]_S$ Specimen

load for three of the specimens (one linear, one stiffening) and at about 90% for one coupon. No loud pops were heard with one coupon, only lower level crackling noises at about 95% of ultimate load were heard when testing this coupon. A typical curve can be seen in Figure 5.21.

All of the $[\pm 15/0]_S$ specimens initially stiffened at about 5% above the initial linear modulus value, and most softened up close to failure. A typical curve is shown in Figure 5.22. Initial loud pops were heard between 50% and 60% of ultimate load.

In summary, it would be fair to say that the dropped and undropped sections of the ply dropoffs have far-field stress-strain behavior comparable to that of the flat specimens with matching layups. There were more variations from the "average" behavior in the ply dropoff specimens than in the flat specimens.

5.2 Photoelastic Tests

Four specimens were tested with photoelastic coating bonded to one side of the coupon. The laminates tested were $[\pm 45/0_D/0/-+45]_T$, $[\pm 45/(\pm 45)_D/0_2]_S$, $[\pm 45/0/(\pm 45/0)_D]_S$, and $[\pm 45/0]_{2S}$. The purpose of these tests was to get an initial qualitative feel of how a ply dropoff affects the strain field of a laminate.

Figure 5.23 is a photograph of a loaded flat laminate with a layup of $[\pm 45/0]_{2S}$. Note that the center section of the coupon, the test section, is uniform in strain. The changes at

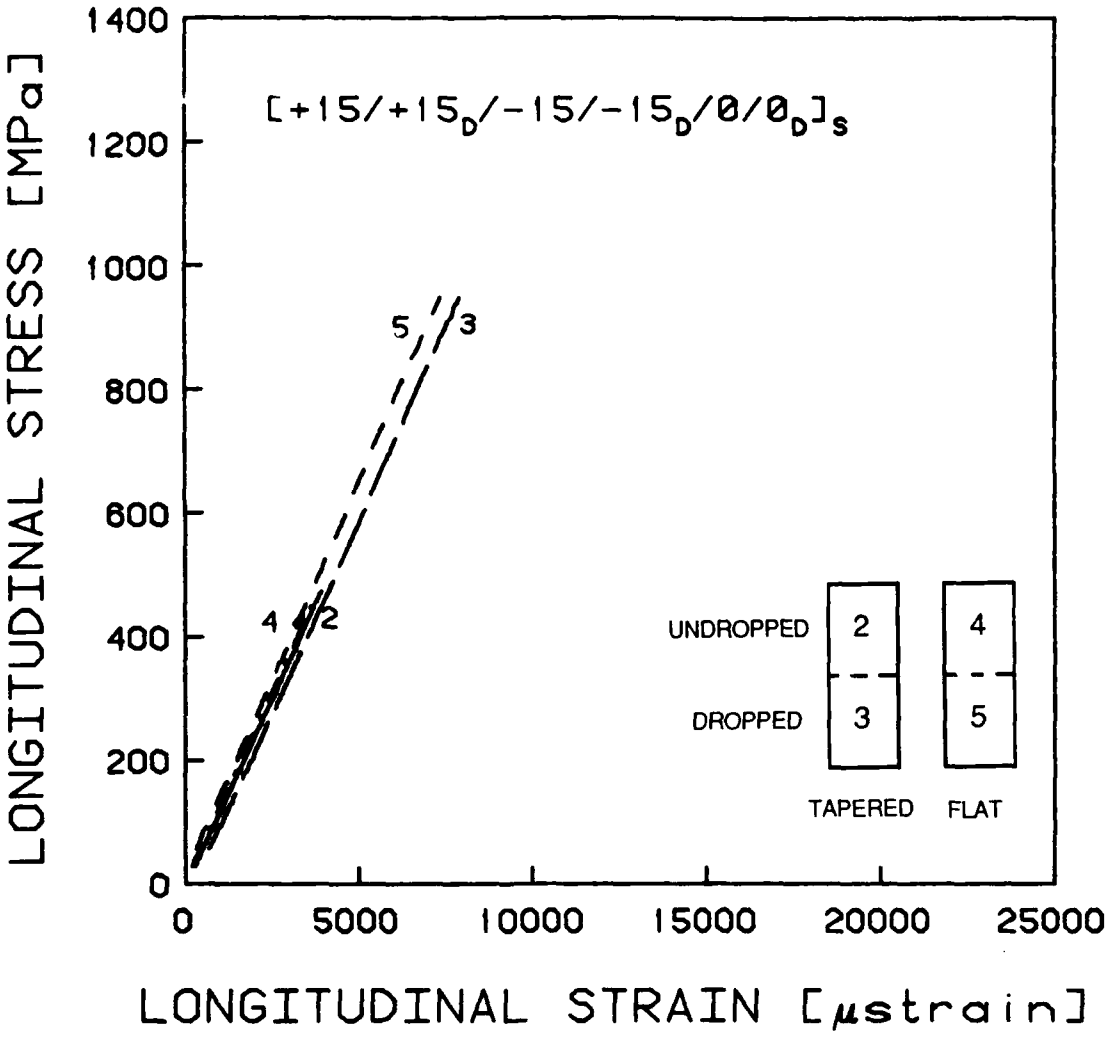

Figure 5.21 Typical Stress-Strain Plot for a $[+15/+15_D/-15/-15_D/0/0_D]_S$ Specimen

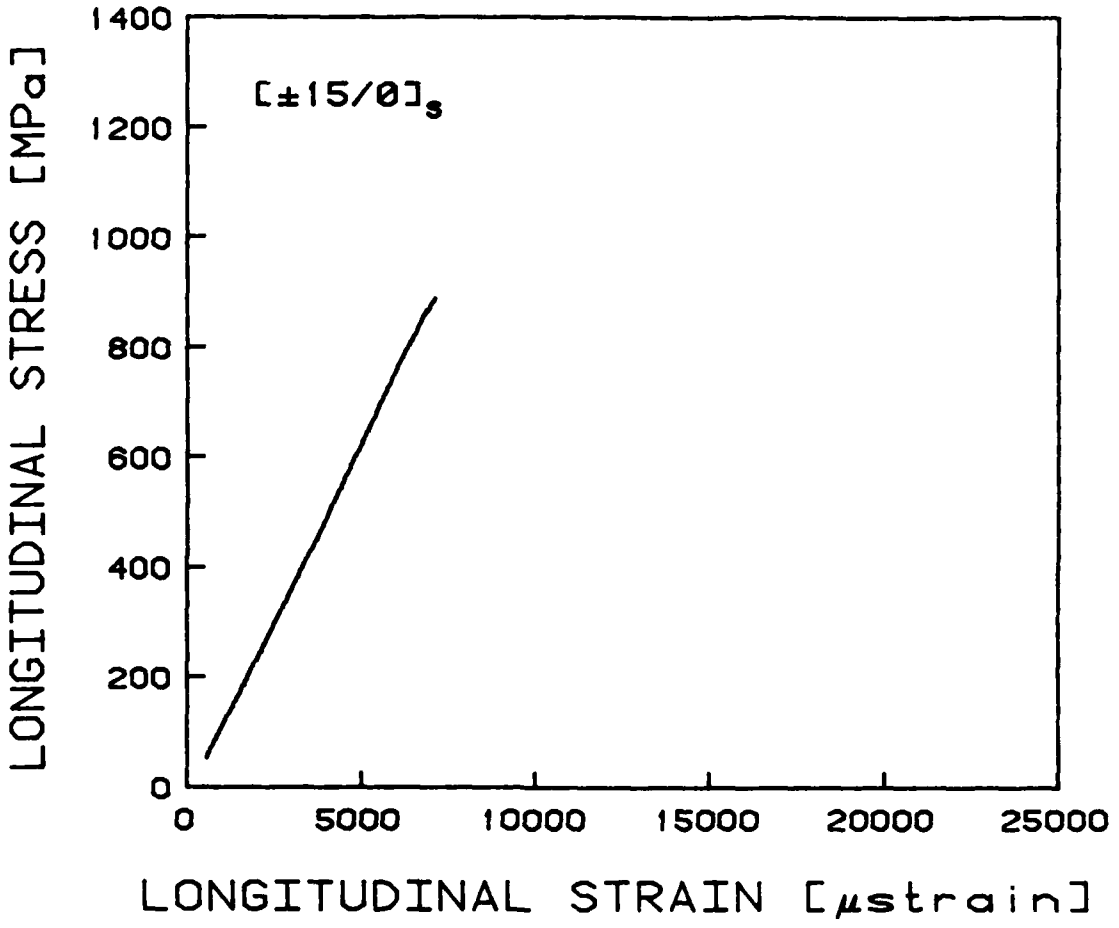

Figure 5.22 Typical Stress-Strain Plot for a $[\pm 15/0]_S$

Figure 5.23 Photoelastic Photograph of the $[\pm 45/0]_{2S}$ Specimen Loaded with 17.9 KN

the free edges of the specimen are due to bonding irregularities of the photoelastic coating. The changes in strain (and thus stress) which occur at the ply dropoff can be readily seen in Figures 5.24-5.29. Figures 5.24 and 5.25 show the $[\pm 45/0_D/0/-+45]_T$ laminate, with the coupon in the second figure under the higher load. Figures 5.26 and 5.27 show the $[\pm 45/(\pm 45)_D/0_2]_S$ laminate with the laminate in the first figure lightly loaded. Figures 5.28 and 5.29 are photographs of the $[\pm 45/0/(\pm 45/0)_D]_S$ laminate, again with the coupon in the first photo lightly loaded.

The stress gradient in the region of the ply dropoff can be easily seen in all of these photographs. The length of this region in the $[\pm 45/0_D/0/-+45]_T$ laminate was about 60 mm, and about 70 mm in the other two ply dropoff laminates. These numbers remain fairly constant over the loading range. Two important caveats must be stated. First, these measurements are very rough in that they were taken off of three inch by five inch photographs with a ruler in a relatively subjective manner. These regions were not perfectly straight across the width of the specimen, so an average value was estimated. The second point is that the photoelastic coating started to debond at about 40% of ultimate load with the $[\pm 45/(\pm 45)_D/0_2]_S$ laminate, about 50% of ultimate load with the $[\pm 45/0/(\pm 45/0)_D]_S$ laminate, and about 60% with the $[\pm 45/0_D/0/-+45]_T$ laminate. This restricted the number of photographs which could be expected to give accurate results. These values for the length of the stress gradient of the ply dropoff region are on the

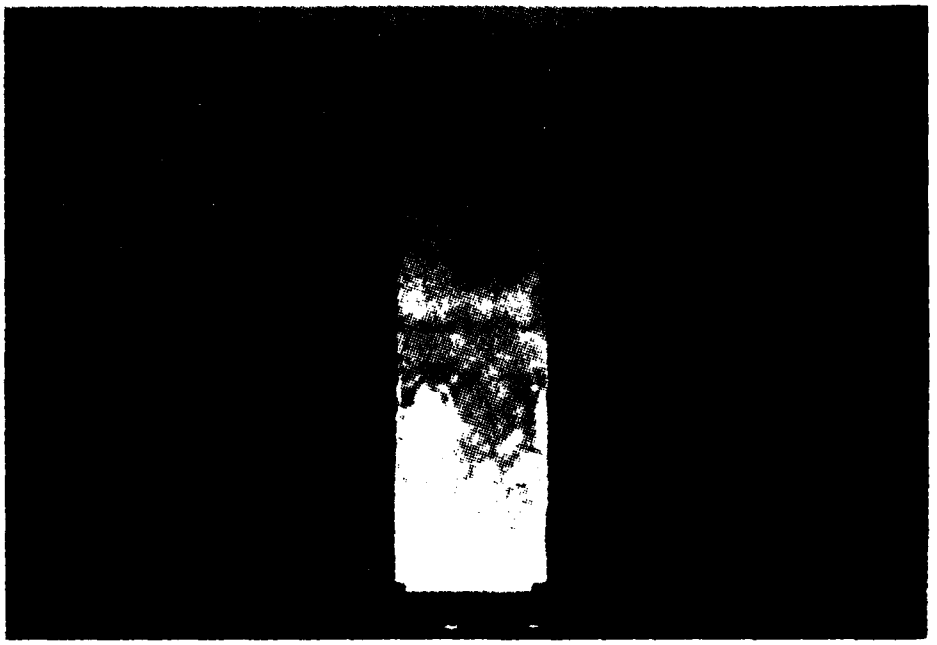

Figure 5.24 Photoelastic Photograph of the $[\pm 45/0_D/0/-+45]_T$ Specimen Loaded with 5.70 KN

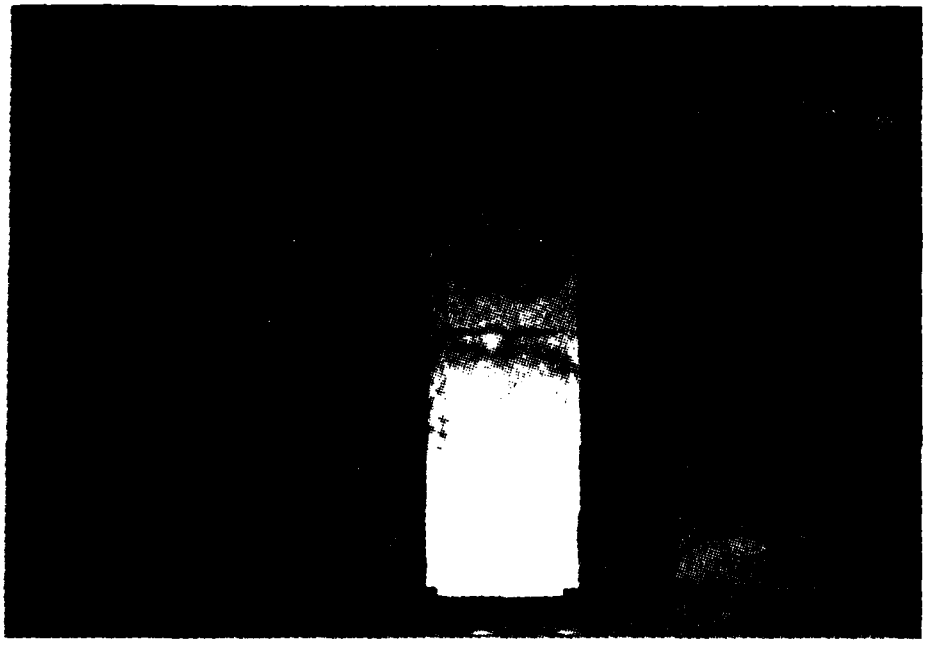

Figure 5.25 Photoelastic Photograph of the $[\pm 45/0_D/0/-+45]_T$ Specimen Loaded with 9.36 KN

Figure 5.26 Photoelastic Photograph of the $[\pm 45/(\pm 45)_D/0_2]_S$ Specimen Loaded with 5.89 KN

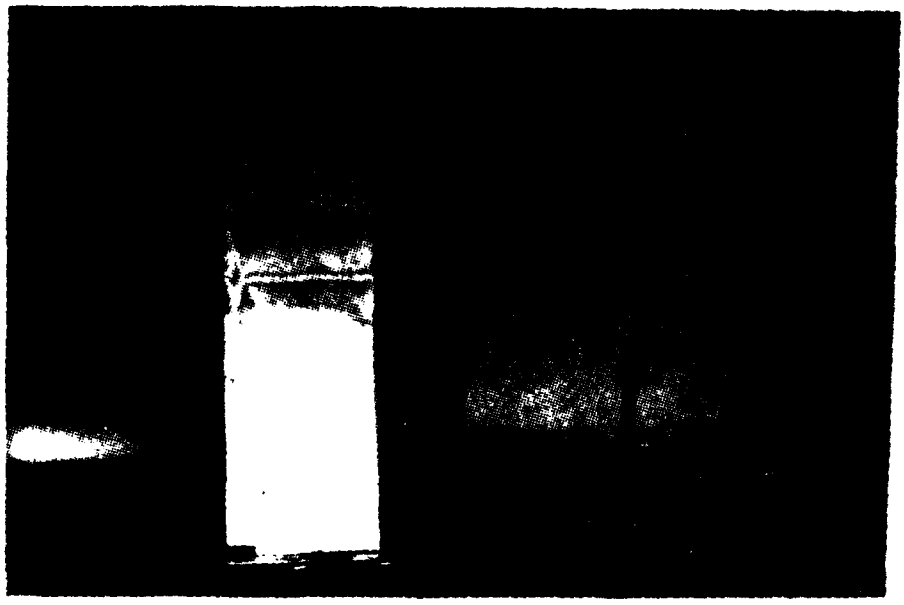

Figure 5.27 Photoelastic Photograph of the $[\pm 45/(\pm 45)_D/0_2]_S$ Specimen Loaded with 27.6 KN

Figure 5.28 Photoelastic Photograph of the $[\pm 45/0/(\pm 45/0)_D]_S$ Specimen Loaded with 464 KN

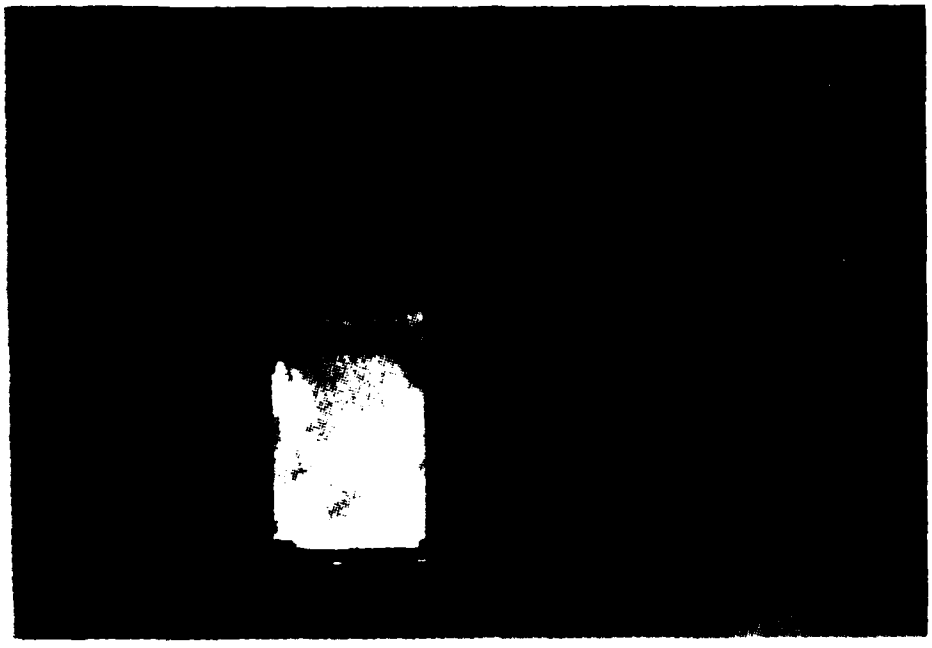

Figure 5.29 Photoelastic Photograph of the $[\pm 45/0/(\pm 45/0)_D]_S$ Specimen Loaded with 11.2 KN

same order as that obtained by the curvature analysis done in Chapter 4 to determine where the longitudinal curvature becomes insignificant. This was calculated to be about 70 mm for the $[\pm 45/0/(\pm 45/0)_D]_S$ and $[\pm 45/(\pm 45)_D/0_2]_S$ laminates and about 45 mm for the $[\pm 45/0_D/0/-+45]_T$ laminate.

5.3 Fracture Stresses

The average fracture stresses of the laminates tested in this study are listed in Table 5.4 for the flat laminates and in Table 5.5 for the ply dropoff laminates. Five coupons of each layup were tested, except for the $[\pm 45/(\pm 45)_D/0_2]_S$, of which only four were tested due to an error during the machining of this plate. Also, one of these four was used in a photoelastic test. As described in Section 3.3, the photoelastic test requires bonding of a 1.0 mm thick photoelastic coating to the surface of the laminate, which could affect the overall stiffness and strength of the coupon. Therefore, fracture stresses from photoelastic tests were not used in computing the average values. One specimen each of the $[\pm 45/0_D/0/-+45]_T$ and $[\pm 45/0/(\pm 45/0)_D]_S$ laminates was used for photoelastic testing. The coefficient of variation (C.V.), defined as the standard deviation divided by the mean, is also listed for each laminate in Tables 5.4 and 5.5. This gives information on the scatter of the data. Data for each individual specimen are contained in the Data Tables. Note that the coefficients of variation are relatively small and that the ply dropoff laminates fail at about the same stress,

TABLE 5.4

SUMMARY OF AVERAGE FRACTURE STRESSES OF FLAT LAMINATES

Laminate	Number Tested	Max Load [KN]	σ_f [MPa]	C.V.
$[\pm 45/0]_S$	5	32.3	804	12.3%
$[\pm 45/0/-+45]_T$	5	18.4	548	9.9%
$[\pm(45_2)/0_2]_S$	5	64.2	799	6.2%
$[\pm(45_2)/0]_S$	5	33.8	505	5.4%
$[(\pm 45)_2/0_2]_S$	5	63.0	783	6.9%
$[\pm 45/0_2]_S$	5	59.5	1110	6.5%
$[\pm 45/0]_{2S}$	5[a]	70.4	876	1.4%
$[\pm(15_2)/0_2]_S$	5	57.2	712	7.5%
$[\pm 15/0]_S$	5	35.3	878	1.6%

[a] Indicates one specimen from this group of the total listed was tested with a photoelastic coating

TABLE 5.5

SUMMARY OF AVERAGE FRACTURE LOADS AND FRACTURE STRESSES BASED ON UNDROPPED SECTION AND DROPPED SECTION AREA OF LAMINATES WITH PLY DROPOFFS

Laminate	Number Tested	Max Load [KN]	σ_f [MPa]	
			Undropped Area	Dropped Area
$[\pm 45/0_D/0/-+45]_T$	5[a]	18.1 (3.1%)[a]	451	541
$[\pm(45_2)/0/0_D]_S$	5	28.9 (18.8%)	359	431
$[+45/+45_D/-45/-45_D/0/0_D]_S$	5	29.0 (10.3%)	361	722
$[\pm 45/(\pm 45)_D/0_2]_S$	4[b]	64.4 (4.2%)	801	1202
$[\pm 45/(\pm 45)_D/0/0_D]_S$	5	32.2 (13.6%)	401	801
$[\pm 45/0/(\pm 45/0)_D]_S$	5[b]	29.8 (9.6%)	371	741
$[+15/+15_D/-15/-15_D/0/0_D]_S$[b]	5	37.6 (2.8%)	468	935

[a] Numbers in parenthese are coefficients of variation
[b] Indicates one specimen from this group of the total listed was tested with a photoelastic coating

basing this stress on the cross-sectional area of the dropped end of the specimen, as that of the flat laminate having the same layup as the dropped section. These results as a whole indicate that the fracture stresses of the laminates were not significantly affected by the ply dropoffs.

5.4 Fracture Modes

Fracture modes for each of the laminate types are described in this section. The descriptions are based on postmortem visual inspections. Typical photographs of each laminate are included.

The basic laminate in the first group is $[\pm 45/0]_S$. These laminates appeared to fail in a primarily in-plane mode. Fairly clean transverse cracks can be seen beneath the outer 45^o layers, where a clean fracture implies little or no delamination with matrix splitting occurring at the fracture. A secondary damage zone of outer ply splitting and delamination occurred near one tab. A typical failure can be seen in Figure 5.30. The first specimen of this laminate was fractured differently than the rest in that secondary delamination was more prevalent at the fracture surface, rather than the relatively clean in-plane fracture.

The $[\pm 45/0/-+45]_T$ specimens which models the dropped end of the $[\pm 45/0_D/0/-+45]_T$ laminate, remained in one piece after failure and was held together by outer angle plies which split but did not fracture. Outer ply splitting with some transverse cracking and delamination occurred in the major damage area of

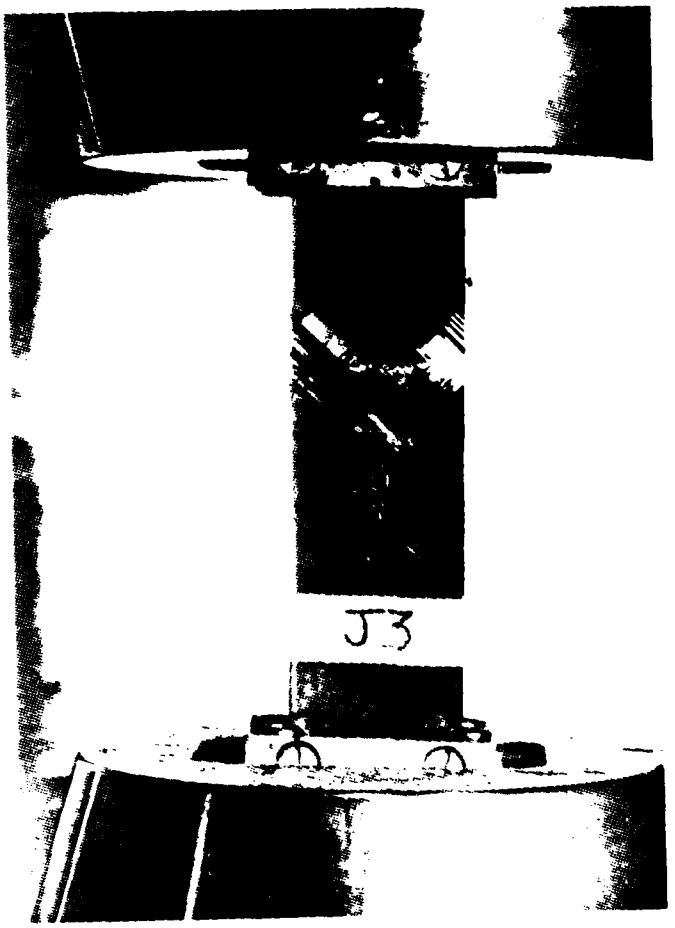

Figure 5.30 Typical Fracture Mode for a $[\pm 45/0]_S$ Specimen

these laminates. Also present in all of these coupons was some splitting and delamination of the outer plies near one tab. This failure can be seen in Figure 5.31.

The $[\pm 45/0_D/0/-+45]_T$ specimens failed in an in-plane mode. All of the specimens remained in one piece after fracture, held together by some of the outer angle plies which split but did not fracture. The main damage was splitting of the outer angle plies at 45^o at the ply dropoff, with one specimen showing the same damage mode in the dropped section of the specimen rather than at the ply dropoff region. There was also splitting of the inner plies along with some delamination close to the damage area. Figure 5.32 is a photograph of a typical failure. This is the same damage as observed in the flat $[\pm 45/0/-+45]_T$ specimens.

The basic laminate in the second group is $[\pm(45_2)/0_2]_S$. These laminates appeared to fail in a two step process, with splitting occurring first in the 0^o plies followed by major delamination along the entire length of the coupon. These fractures were quite messy, in that alot of delamination and splitting occurred along with the fracture. It was common for these specimens to fracture in more than one place along the length of the coupon, that is the coupon would often end up in three pieces. A typical failed specimen is shown in Figure 5.33.

The $[\pm(45_2)/0]_S$ laminates failed in an in-plane mode. This laminate models the dropped section of the $[\pm(45_2)/0/0_D]_S$ laminate. Typical damage here was a crisscrossed pattern of

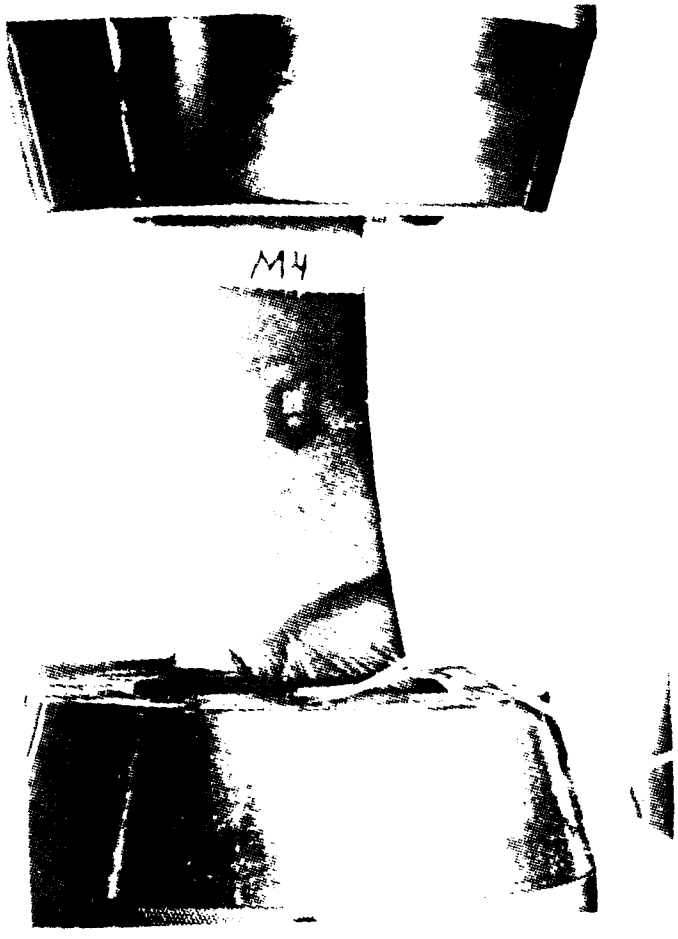

Figure 5.31 Typical Fracture Mode for a $[\pm 45/0/-+45]_T$ Specimen

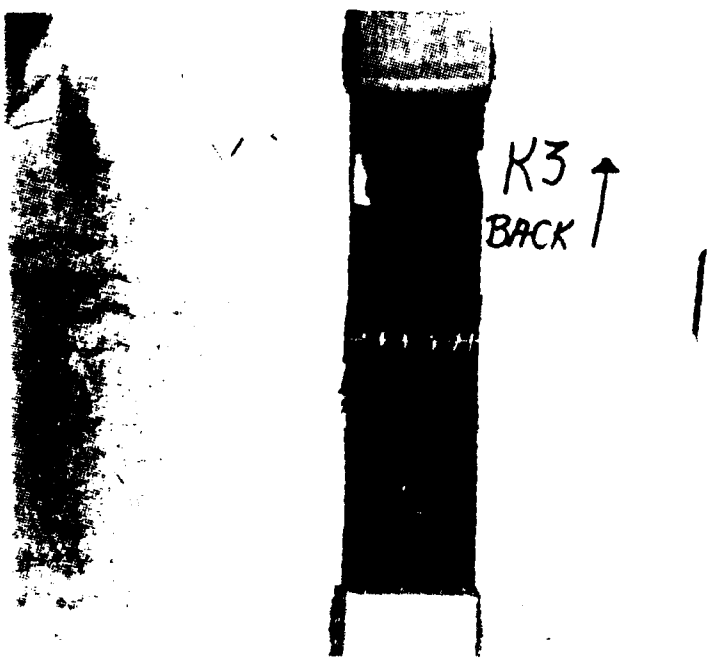

Figure 5.32 Typical Fracture Mode for a $[\pm 45/0_D/0/-+45]_T$ Specimen

Figure 5.33 Typical Fracture Mode for a $[\pm(45_2)/0_2]_S$ Specimen

$\pm 45^{\circ}$ splitting with localized delamination. This is shown in the photo in Figure 5.34.

The $[\pm(45_2)/0/0_D]_S$ coupons had two main types of damage. Fracture occurred at the ply dropoff or slightly into the dropped end of the specimen. In four of the five specimens, the two 0° plies delaminated as a single unit away form the rest of the laminate in the undropped end of the specimen. It appears that this delamination was caused by the fracture and not the other way around, and therefore can be considered secondary delamination. In this respect, the failure mode is similar to that of the $[\pm(45_2)/0/]_S$ laminate which models the dropped section. This failure mode is shown in Figure 5.35.

The $[+45/+45_D/-45/-45_D/0/0_D]_S$ coupons failed in an in-plane mode, as can be seen in a typical photo in Figure 5.36. Fracture occurred at a 45° angle with some splitting of the inner plies as well. This fracture mode was similar to that of the $[\pm 45/0]_S$ (described in the second paragraph of this section) specimen which models the dropped section of the current laminate. This fracture began at or slightly below the ply dropoff and continued into the dropped section of the laminate. A fracture at -45° also occurred, sometimes originating from the "main" fracture and sometimes running over it in an "X" pattern.

The basic laminate of the third group is $[(\pm 45)_2/0_2]_S$. These laminates had significant delamination along the free edge which appeared to be the primary cause of failure. The fractures which occurred in these specimens was quite dirty.

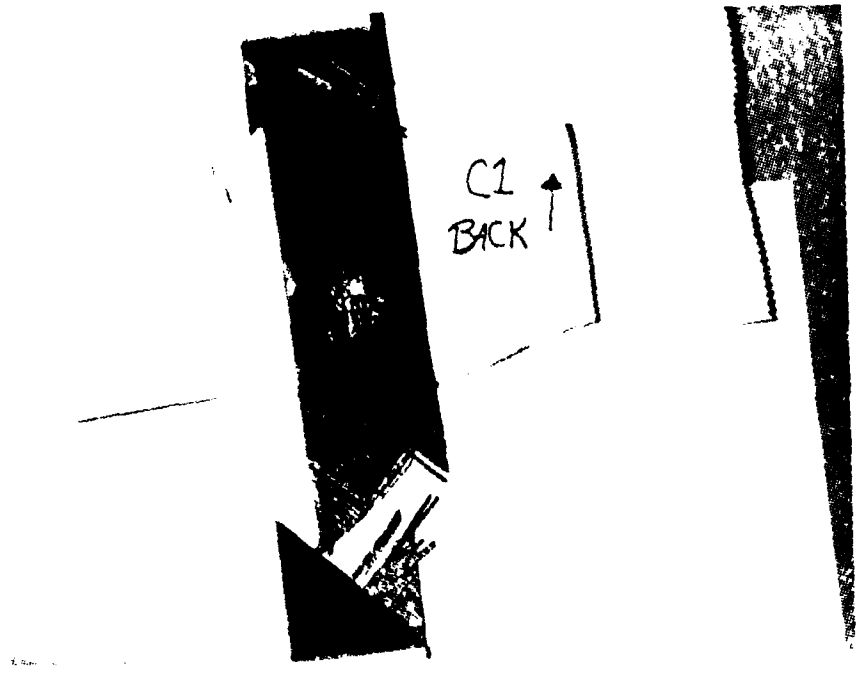

Figure 5.34 Typical Fracture Mode for a $[\pm(45_2)/0]_S$ Specimen

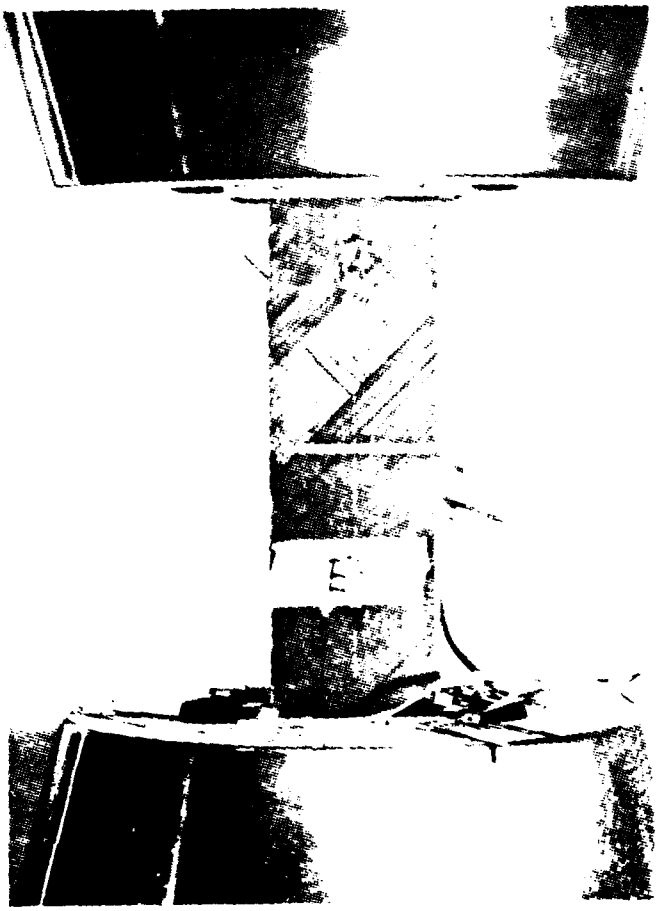

Figure 5.35 Typical Fracture Mode for a $[\pm(45_2)/0/0_D]_S$ Specimen

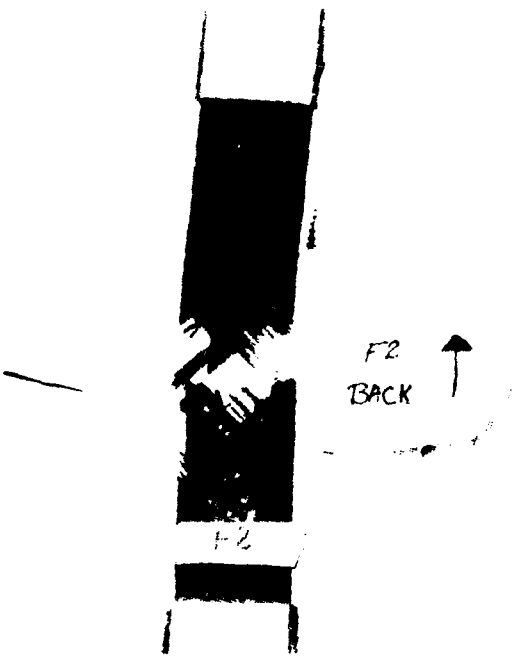

Figure 5.36 Typical Fracture Mode for a $[+45/+45_D/-45/-45_D/0/0_D]_S$ Specimen

Delamination at the $-45^{\circ}/0^{\circ}$ interface typically ran the entire length of the specimen on one side and roughly half that on the other side. This can be seen in Figure 5.37.

The $[\pm 45/0_2]_S$ laminates, which model the dropped section of the $[\pm 45/(\pm 45)_D/0_2]_S$ laminates, failed in an in-plane mode with a somewhat dirty fracture roughly perpendicular to the x-direction. A secondary damage area occurred near one of the tabs in these laminates, a fracture in two of the specimens and delamination and splitting in three of the specimens. A photo of a failure of this laminate is shown in Figure 5.38.

It could not be determined conclusively from the postmortem inspections of the $[\pm 45/(\pm 45)_D/0_2]_S$ laminates whether the failures were strictly in-plane failures or whether delaminations occurred first causing in-plane failure. Varying fractures occurred at and below (in the dropped section) the ply dropoff from a relatively clean break perpendicular to the loading direction, similar to that of the flat laminate modeling the dropped section, the $[\pm 45/0_2]_S$ laminate, to a roughly 45°, somewhat dirty fracture. One of the coupons had a free edge delamination running the length of the undropped end of the specimen. This failure is shown in the photo in Figure 5.39.

The $[\pm 45/(\pm 45)_D/0/0_D]_S$ specimens appeared to fail in an in-plane fracture mode as seen in Figure 5.40. These specimens failed at the ply dropoff for most of the specimens with a majority of the fracture perpendicular to the loading direction. One of the coupons failed at the midpoint of the

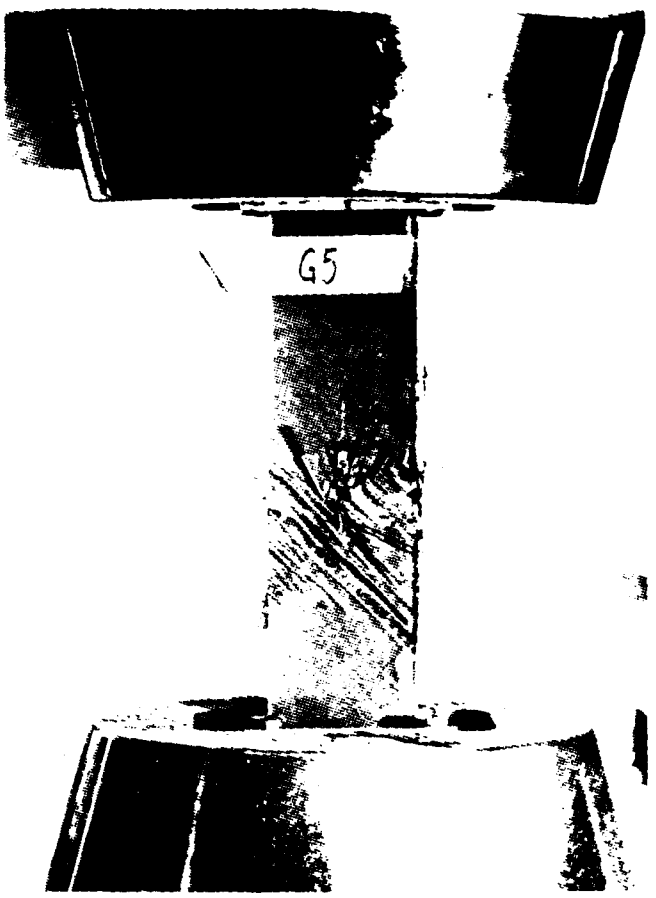

Figure 5.37 Typical Fracture Mode for a $[\pm(45)_2/0_2]_S$ Specimen

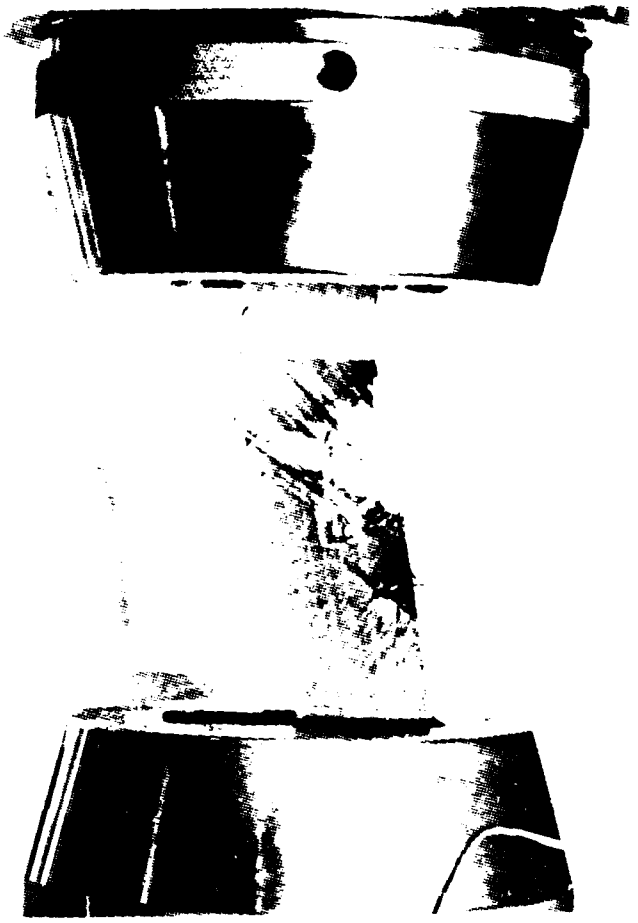

Figure 5.38 Typical Fracture Mode for a $[\pm 45/0_2]_S$ Specimen

Figure 5.39 Typical Fracture Mode for a $[\pm 45/(\pm 45)_D/0_2]_S$ Specimen

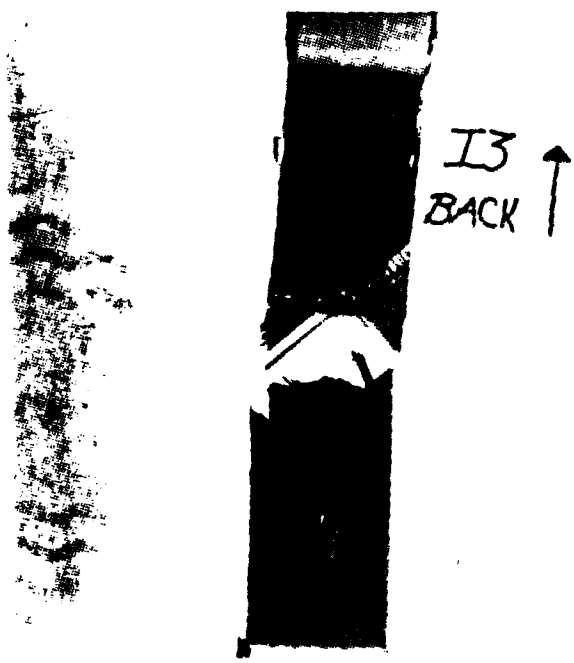

Figure 5.40 Typical Fracture Mode for a $[\pm 45/(\pm 45)_D/0/0_D]_S$ Specimen

dropped section of the laminate with a similar failure mode. Some of the breaks were cleaner than others and two of the coupons remained in one piece. Splitting of the outer plies was present near the fractures. The fracture changed from perpendicular to the loading direction to a 45^{o} angle at the free edges on two of the specimens. These fractures were similar to those of the $[\pm 45/0]_{S}$ laminates, which model the dropped section of the laminate, in that they were both in-plane and part of the fracture of the ply dropoff laminate was at a 45^{o} angle, like the fractures of the $[\pm 45/0]_{S}$ laminates. One coupon had a free edge delamination running the length of the undropped section.

The basic laminate of the fourth group was the $[\pm 45/0]_{2S}$ laminate. These laminates appeared to fail in an in-plane mode with a 45^{o} fracture, very much like that of the $[\pm 45/0]_{S}$ laminates. These fractures were relatively clean. One coupon had a somewhat dirty fracture perpendicular to the loading direction. A typical failure is shown in Figure 5.41.

Typical failure for the $[\pm 45/0/(\pm 45/0)_{D}]_{S}$ was a fracture at the ply drop mostly perpendicular to the loading direction and changing to a 45^{o} angle near the free edges. In four of the five coupons, the dropped sublaminate delaminated away from the outside of the specimen. These laminates appeared to fail in an out-of-plane mode leading away from the ply dropoffs in the undropped section of the laminate. This failure mode is therefore different from that of the $[\pm 45/0]_{2S}$ and $[\pm 45/0]_{S}$ laminates, which model the undropped and dropped sections of

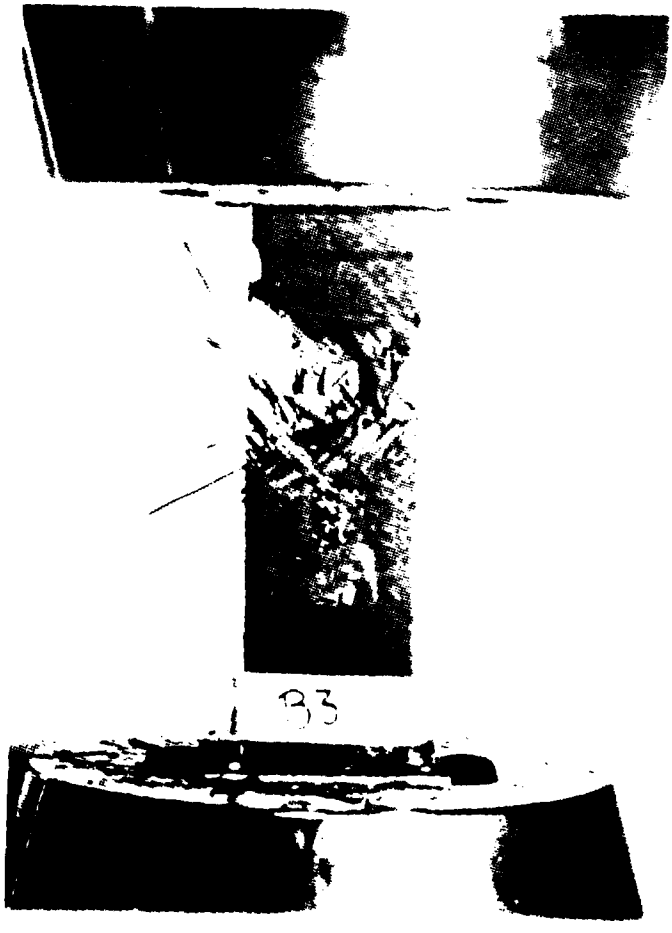

Figure 5.41 Typical Fracture Mode for a $[\pm 45/0]_{2S}$ Specimen

the ply dropoff laminate and failed in an in-plane mode. The fractures which occured at the ply dropoffs, however, were similar to those which occured in the $[\pm 45/0]_{2S}$ and $[\pm 45/0]_S$ laminates. Secondary damage occurred near the tab of the dropped end of the coupon ranging from outer ply splitting and delamination to a somewhat dirty fracture. A typical failure is shown in Figure 5.42.

The $[\pm(15_2)/0_2]_S$ laminates failed in an out-of-plane mode, as shown in the photo in Figure 5.43. Extensive delaminations could be seen running the length of the specimen on both free edges at the interface between the $+15^o$ and -15^o plies. Some of the 0^o plies did not fracture, keeping the coupons in one piece after final failure.

The $[\pm 15/0]_S$ laminates also failed in an out-of-plane mode. The delamination along the free edges at the interface between the $+15^o$ and -15^o plies was not as extensive as that on the double effective ply thickness $[\pm(15_2)/0_2]_S$ laminates. The $[\pm 15/0]_S$ laminates fractured into two pieces after final failure, with the fracture being a dirty, jagged fracture which can be seen in Figure 5.44. These laminates also exhibited slightly more outer ply splitting than the $[\pm(15_2)/0_2]_S$ specimens.

The $[+15/+15_D/-15/-15_D/0/0_D]_S$ specimens appeared to fail in an out-of-plane mode. The fracture location ranged from the ply dropoff region to near the middle of the dropped end of the specimen. The fracture was roughly perpendicular to the applied load direction, with some fractures more jagged than

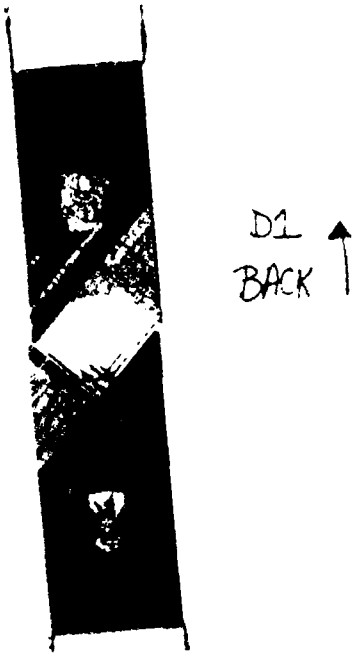

Figure 5.42 Typical Fracture Mode for a $[\pm 45/0/(\pm 45/0)_D]_S$ Specimen

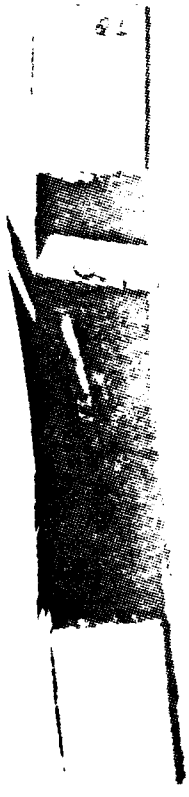

Figure 5.43 Typical Fracture Mode for a $[\pm(15_2)/0_2]_S$ Specimen

Figure 5.44 Typical Fracture Mode for a $[\pm 15/0]_S$ Specimen

other. Overall the fractures were cleaner than that of the $[\pm(15_2)/0_2]_S$ and $[\pm15/0]_S$ laminates, but did have varying degrees of delamination and outer ply splitting around the fractures and free edge delamination at the interface between the $+15^o$ and -15^o plies similar to that of the $[\pm15/0]_S$ laminates. A typical fracture can be seen in Figure 5.45.

In summary, the failure modes of the ply dropoff laminates were almost always in the dropped section of the laminate. This failure often occurred at the ply dropoff or at an angle running from the ply dropoff into the dropped section of the laminate. Failure modes of the ply dropoff laminates generally approximated that of the flat specimen with a layup equal to that of the dropped section of the laminate.

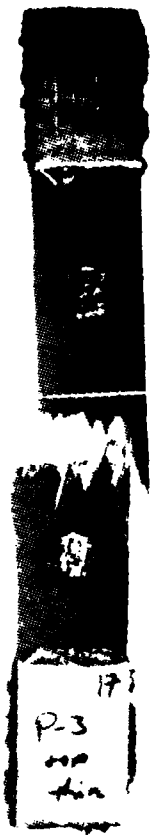

Figure 5.45 Typical Fracture Mode for a $[+15/+15_D/-15/-15_D/0/0_D]_S$ Specimen

CHAPTER 6

DISCUSSION

6.1 Effects of Ply Dropoffs on Stress-Strain Behavior

As shown in Figure 3.12, strain was measured at the center of the flat specimens and on the front and back of both the dropped and undropped sections of the coupons with ply dropoffs. Overall, the strain readings and longitudinal moduli of the ply dropoff specimens were equal to that of the flat specimens with the same layup, within the scatter of the data. As described in Chapter 4, it was determined with the analysis that the maximum longitudinal distance for the curvature to decay from its maximum value at the ply dropoff to 1% of this value was 70 mm in the undropped section and 25 mm in the dropped section. The significance of this is that the back-to-back strain gages were 75 mm from the ply dropoff and therefore would not be able to measure the curvature of the specimen. These gages were placed with the idea in mind to measure far-field strain behavior.

A good recommendation would be to place back-to-back strain gages as close as possible to the ply dropoffs to measure this curvature caused by the induced bending effect of the ply dropoff laminates with one side flat. This information could be used to see how well the curvature predicted by the analysis matches that measured experimentally. The photoelastic tests provided a rough confirmation of the

anlysis. As discussed in Chapter 5, visible stress gradients of the photelastic tests were on the order of 50 mm.

6.2 Effects of Ply Dropoffs on Failure Stresses

The average failure stresses of the laminates with ply dropoffs are summarized in Table 6.1. The second column of this table is the average value of the failure stress of the ply based on the cross-sectional area of the dropped section of the laminate. Unless it is specifically stated that the stresses are based on the undropped area of the ply dropoff laminate, the dropped section of the laminate is used for the stress calculations. The third column of this table is the first ply failure stress of the dropped section as predicted by classical laminated plate theory (CLPT). The last column of this table contains the first ply failure stresses of the dropped section taking into account the induced bending stresses, as discussed in Chapter 4. For the CLPT analysis, all first ply failures, except that of the $[+15/+15_D/-15/-15_{D\backslash 0\backslash 0_D}]_S$ laminate, were failure of the 45^o plies in shear, σ_{12}. First ply failure of the $[+15/+15_D/-15/-15_{D\backslash 0\backslash 0_D}]_S$ laminate was due to σ_{11} in the 0^o plies. When the analysis from Chapter 4 is used, the bending effect causes first ply failure in the outer 45^o ply on the flat side of the laminate due to σ_{12}. This is where the maximum additive effect of the induced bending moment with the applied tension load is felt. As mentioned in Chapter 4, these values for first ply failure are significantly below that of

TABLE 6.1

COMPARISON OF EXPERIMENTAL FRACTURE STRESSES AND PREDICTED FIRST PLY FAILURE STRESSES FOR PLY DROPOFF LAMINATES

Laminate	Experimental σ_f [MPa]	Predicted σ_f, [MPa]	
		Method A[a]	Method B[b]
$[\pm 45/0_D/0/-+45]_T$	541 (3.1%)[c]	464	252
$[\pm(45_2)/0/0_D]_S$	431 (18.8%)	464	239
$[+45/+45_D/-45/-45_D/0/0_D]_S$	722 (10.3%)	638	364
$[\pm 45/(\pm 45)_D/0_2]_S$	1202 (4.2%)	866	439
$[\pm 45/(\pm 45)_D/0/0_D]_S$	801 (13.6%)	638	364
$[\pm 45/0/(\pm 45/0)_D]_S$	741 (9.6%)	638	371
$[+15/+15_D/-15/-15_D/0/0_D]_S$	935 (2.8%)	2105	[d]

[a] Method A is based on CLPT values with no local bending effect
[b] Method B includes induced bending effects
[c] Numbers in parenthese are coefficients of variation
[d] Geometrically symmetric laminate, no bending correction

the CLPT predicted first ply failures.

This analysis is only valid for first ply failure due to the fact that after the first ply fails, the midplane of the dropped section will change, making it no longer symmetric and in turn affecting the B and D matrices of both undropped and dropped sections of the specimen. This changes the energy expression and the terms used in developing it, complicating the problem to a large degree. Note that the $[+15/+15_D/-15/-15_{D\backslash 0\backslash 0_D}]_S$ laminates were geometrically symmetric and therefore no induced bending effect was predicted. The large overprediction of the strength of the $[\pm 15/0]_S$ family by CLPT is due to the tendency of these laminates to delaminate at the free edge, as was previously discussed.

Table 6.2 is a comparative listing of the fracture stresses. The first column, after the laminate column, is the mean fracture stress and coefficient of variation for the laminates with ply dropoffs. The second column is the mean fracture stress and coefficient of variation for the flat laminate which models the dropped section of the respective ply dropoff laminate. The third column is the percentage of change from the first column to the second. The last column is the predicted fracture stress of the flat laminate modeling the ply dropoff laminate using CLPT, which does not include any induced bending effect or effect of interlaminar stresses. This is a final failure, as opposed to first ply failure, prediction accomplished with a progressive ply-by-ply analysis described

TABLE 6.2

COMPARISON OF FRACTURE STRESSES FOR PLY DROPOFF LAMINATES, FLAT LAMINATES MODELING DROPPED SECTION OF PLY DROPOFF LAMINATES, AND CLPT PREDICTED VALUES

Laminate	σ_f [MPa] Dropped Laminate	σ_f [MPa] Flat Laminate	% Change	CLPT σ_f [MPa][a]
$[\pm 45/0_D/0/-+45]_T$	541 (3.1%)	548 (9.9%)	-1.3%	471
$[\pm(45_2)/0/0_D]_S$	431 (18.8%)	505 (5.4%)	-14.7%	471
$[+45/+45_D/-45/-45_D/0/0_D]_S$	722 (10.3%)	804 (12.3%)	-10.2%	785
$[\pm 45/(\pm 45)_D/0_2]_S$	1202 (4.2%)	1110 (6.5%)	+8.3%	1178
$[\pm 45/(\pm 45)_D/0/0_D]_S$	801 (13.6%)	804 (12.3%)	-.4%	785
$[\pm 45/0/(\pm 45/0)_D]_S$	741 (9.6%)	804 (12.3%)	-7.8%	785
$[+15/+15_D/-15/-15_D/0/0_D]_S$	935 (2.8%)	878 (1.6%)	+6.5%	2105

[a] Numbers in parentheses are coefficients of variation

described in Chapter 4.

The largest reduction in fracture stress from the ply dropoff laminate to the flat laminate was that of the $[\pm(45_2)/0/0_D]_S$, which failed at about 15% lower. Note, however, that a fairly wide distribution of fracture stresses for this laminate occurred, with a coefficient of variation of about 19%. The $[+45/+45_D/-45/-45_D/0/0_D]_S$ laminate showed about a 10% decrease in fracture stress from that of the flat laminate comparable to its dropped section, but the coefficient of variation for this specimen was also about 10%. The other laminates all showed differences of less than 10%, and two laminates actually showed an increase in fracture stress over their dropped section comparable flat laminate, with the $[\pm45/(\pm45)_D/0_2]_S$ laminate showing an 8% increase and the $[+15/+15_D/-15/-15_{D\backslash 0\backslash 0_D}]_S$ laminate showing a 6.5% increase. These results as a whole indicate that the fracture stresses of the laminates were not significantly affected by the ply dropoffs.

6.3 Effects of Ply Dropoffs on Failure Modes

The general pattern which can be seen in the failure modes of the laminates with ply dropoffs is that they are matched by the failure mode of the flat laminate with a layup equal to that of the dropped section. However, three of the ply dropoff laminates did not follow this general rule as well as the other four laminates did. These were the $[\pm(45_2)/0/0_D]_S$, $[\pm45/(\pm45)_D/0_2]_S$, and $[\pm45/0/(\pm45/0)_D]_S$ laminates.

The $[\pm(45_2)/0/0_D]_S$ laminates exhibited two forms of damage, a fracture at or near the ply dropoff and, in four of the five specimens, the dropped plies delaminated away from the rest of the undropped section. It appeared that the fracture at or near the ply dropoff was the primary cause of failure, and therefore failure was classified as in-plane. The undropped section of both of these laminates was modeled by the $[\pm(45_2)/0_2]_S$ laminate. These laminates appeared to fail in a two step process, first with transverse cracking of the inner plies followed by major delamination of the along the entire length of the free edge. The dropped section of the $[\pm(45_2)/0/0_D]_S$ laminate was modeled by the $[\pm(45_2)/0]_S$ laminate, which failed in an in-plane mode. Therfore, while the primary fracture mode of the ply dropoff laminate was an in-plane fracture like that of the flat laminate modeling the dropped section, the center two dropped plies also delaminated in the undropped section of the laminate.

The $[\pm45/0/(\pm45/0)_D]_S$ laminates appeared to fail in an out-of-plane mode. The sublaminate consisting of the inner six dropped plies would normally delaminate away from the rest of the undropped section. These laminates also had a fracture at or near the ply dropoff region, showing signs of in-plane failure. The undropped section of this laminate was modeled by the $[\pm45/0]_{2S}$ laminate, which appeared to fail in an in-plane mode with a fracture at a 45^o angle. The dropped section of this ply dropoff laminate was modeled by the $[\pm45/0]_S$ laminate, which failed in an in-plane mode. This means that the

$[\pm 45/0/(\pm 45/0)_D]_S$ laminates failed in a mode different from that of the flat laminates modeling its dropped and undropped section. One possible cause of this may be that this laminate was laid up with all of the plies dropped off consecutively as a single sublaminate. It appears that dropping these plies off all at once rather than spreading them throughout the laminate is more delamination critical. It is important to note here that the failure stress of the $[\pm 45/0/(\pm 45/0)_D]_S$ laminates was only about 8% lower than that of the flat laminate modeling the dropped section. Thus, there is essentially no strength reduction when considering normal data scatter. So, although delamination does appear at the ply dropoffs, it did not appear to alter the final fracture stress.

Table 6.3 contains the first ply failure loads, rather than stresses, as predicted by CLPT. By looking at this table, it can be seen how much load is required to fail the first ply of the undropped section of the ply dropoff laminate versus the dropped section. For example, the undropped section of the $[\pm 45/0/(\pm 45/0)_D]_S$ laminate would require twice the load as the dropped section of the laminate to reach first ply failure stress. First ply failure of the dropped section of the $[\pm 45/(\pm 45)_D/0_2]_S$ laminate, however, would require 90% of the load required for first ply failure of the undropped section. This would seem to indicate that damage in the undropped section of the $[\pm 45/(\pm 45)_D/0_2]_S$ laminate would be more likely than in the $[\pm 45/0/(\pm 45/0)_D]_S$ laminate. The $[\pm 45/(\pm 45)_D/0_2]_S$ laminate did indeed fail with damage in the undropped section

TABLE 6.3

CLPT PREDICTED FIRST PLY FAILURE LOADS FOR PLY DROPOFF LAMINATES

Laminate	CLPT Predicted First Ply Failure Loads, [KN]	
	Dropped Section	Undropped Section
$[\pm 45/0_D/0/-+45]_T$	15.5	25.6
$[\pm(45_2)/0/0_D]_S$	31.1	51.3
$[+45/+45_D/-45/-45_D/0/0_D]_S$	25.6	51.3
$[\pm 45/(\pm 45)_D/0_2]_S$	46.4	51.3
$[\pm 45/(\pm 45)_D/0/0_D]_S$	25.6	51.3
$[\pm 45/0/(\pm 45/0)_D]_S$	25.6	51.3
$[+15/+15_D/-15/-15_D/0/0_D]_S$ [a]	84.6	169.

of the laminate, but so did the $[\pm 45/0/(\pm 45/0)_D]_S$ laminate. Other laminates which had the same 50% ratio between required loads for first ply damage in the dropped section to the undropped section did not show this damge in the undropped end of the specimen. The $[\pm(45_2)/0/0_D]_S$ specimens, with a 60% ratio between required first ply failure loads of the dropped to the undropped section, also showed significant damage in the undropped section. Note that the plies dropped off in this lamminate were also dropped off in one sublaminate at the center of the specimen, which gives more credence to the idea that lumping the dropped off plies into one sublaminate rather than distributing them through the thickness can lead to delamination of the dropped plies.

The fracture mode of the $[\pm 45/(\pm 45)_D/0_2]_S$ specimens was somewhat in doubt. Free edge delamination of the undropped section was common, but the fracture, which normally occurred at or near the ply dropoff, appeared fairly clean, indicating an in-plane fracture. The undropped section of this laminate was modeled by the $[(\pm 45)_2/0_2]_S$ laminate, which appeared to fail in an out-of-plane mode, with delaminations at the $-45^o/0^o$ interface typically running the length of the specimen. The dropped section of the $[\pm 45/(\pm 45)_D/0_2]_S$ laminate was modeled by the $[\pm 45/0_2]_S$ laminate, which failed in an in-plane mode. This ply dropoff laminate, then, did fail in a mode similar to that of the flat laminate modeling its dropped section but also clearly showed evidence of the failure mode of the flat laminate modeling its undropped section.

In summary, most, but not all, of the ply dropoff laminates failed in a mode similar to that of the flat specimen modeling the dropped end of the ply dropoff laminate. The ply dropoff laminate failed at about the same stress as that of the flat laminate with the same layup as the dropped section. Even the $[+15/+15_D/-15/-15_{D\backslash 0\backslash 0_D}]_S$ laminates did not show a reduction in strength from the flat laminate with the same layup, which does delaminate due to the free edge effect. However, the $[\pm 45/0/(\pm 45/0)_D]_S$ specimen showed that lumping a significant amount of dropped plies together can change the mode of failure from in-plane to delamination. Even though the failure stress was not affected in this case, the change in failure mode could be important in other instances, such as fatigue.

CHAPTER 7

CONCLUSIONS AND RECOMMENDATIONS

An investigation was performed to examine the tensile behavior of laminates with ply dropoffs. Experiments were conducted to study the effects of number, order, angular orientation, and effective ply thickness of dropped plies. An analytical model was developed to account for the induced bending effect of the geometrically unsymmetric laminates. The following conclusions are made based on this work:

1. The stress-strain behavior of the ply dropoff laminates was closely approximated by those of the flat laminates having the same layups as the dropped and undropped sections.

2. Maximum regions of significant curvature were predicted to be between 30 mm and 70 mm from the ply dropoff for the undropped sections and between 10 mm and 25 mm from the ply dropoff for the dropped section. This was verified experimentally as an upper bound value via far-field back-to-back strain gages which indicated no curvature 75 mm from the ply dropoffs.

3. The failure stresses of the ply dropoff laminates were equal to that of the flat laminate having the same layup as the dropped section of the ply dropoff laminate, within data scatter.

4. The failure modes of the ply dropoff laminates were

generally similar to those of the flat laminates modeling the dropped sections of the ply dropoff laminates.

5. Of the number, order, angular orientation, and effective ply thickness variables studied, only the order seemed to affect the ply dropoff laminates in comparison with the flat laminates. Laminates with all dropped plies placed adjacent to each other in the center of the laminate tended to delaminate away from the rest of the laminate in the undropped section. Failure stresses were still unaffected, however.

6. The analysis method developed was inadequate in that only first ply failure could be determined. Upper bound regions of significant curvature predicted with the analysis method were confirmed experimentally by the fact that no consistent curvatures were measured by the back-to-back far-field strain gages.

The following are recommendations for further work:

1. Extend the analysis method so that it would be applicable after first ply failure. This would allow a ply-by-ply failure analysis to predict final failure to be compared with CLPT solutions and experimental results.

2. Conduct testing with strain gages closer to the ply dropoffs. This would allow direct measurement of longitudinal curvature, which could be used to determine

the effects of the loading eccentricity directly and provide data to better prepare with the analysis.

3. Develop an analysis method to determine interlaminar stresses caused by ply dropoffs in composite laminates.

4. Implement a nondestructive inpection method capable of detecting delamination inside (away from the free edge) a laminate at a ply dropoff.

REFERENCES

1. Autoweek, Vol. 37, No. 14, pg. 4, 6 April 1987.

2. Lagace, P. A., 16.292 Class Notes, Massachusetts Institute of Technology, Spring 1986.

3. Pagano, N. J., and Soni, S. R., "Global-Local Laminate Variational Model," International Journal of Solids and Structures, Vol. 19, No. 3, 1983.

4. Jones, R. M., Mechanics of Composite Materials, Mc-Graw Hill, New York, 1975.

5. Pipes, R. B., and Pagano, N. J., "Interlaminar Stresses in Composite Laminates Under Uniform Axial Extension," Journal of Composite Materials, Vol. 4, 1970, pp. 538-548.

6. Rybicki, E. F., "Approximate Three-Dimensional Solutions for Symmetric Laminates Under Inplane Loading," Journal of Composite Materials, Vol. 5, 1971, pp. 354-360.

7. Wang, A. S. D., and Crossman, F. W., "Some New Results on Edge Effects in Symmetric Composite Laminates," Journal of Composite Materials, Vol. 11, 1977, pp. 92-106.

8. Puppo, A. H., and Evensen, H. A., "Interlaminar Shear in Laminated Composites Under Generalized Plane Stress," Journal of Composite Materials, Vol. 4, 1970, pp. 204-220.

9. Pagano, N. J., and Pipes, R. B., "The Influence of Stacking Sequence on Laminate Strength," Journal of Composite Materials, Vol. 5, 1971, pp. 50-57.

10. Whitney, J. M., "Free-Edge Effects in the Characterization of Composite Materials," Analysis of the Test Methods for High Modulus Fibers and Composites, ASTM STP 521, American Society for Testing and Materials, 1973, pp. 668-672.

11. Pipes, R. B., and Pagano, N. J., "Interlaminar Stresses in Composites - An Approximate Elasticity Solution," Transactions of the ASME, September 1974, pp. 668-672.

12. Lagace, P. A., and Kassapoglou, C., "An Efficient Method for the Calculation of Interlaminar Stresses," TELAC Report No. 85-4, Massachusetts Institute of Technology, March 1985.

13. Kassapoglou, C., and Lagace, P. A., "An Efficient Method for the Calculation of Interlaminar Stresses," Journal of Applied Mechanics, Vol. 53, December 1986.

14. Whitney, J. M., and Nuismer, R. J., "Stress Fracture Criteria for Laminated Composites Containing Stress Concentrations," Journal of Composite Materials, Vol. 8, January 1974, pp. 253-265.

15. Kim, R. Y., and Soni, S. R., "Experimental and Analytical Studies on the Onset of Delamination in Laminated Composites," Journal of Composite Materials, Vol. 18, January 1984, pp. 70-80.

16. Kim, R. Y., and Soni, S. R., "Delamination of Composite Laminates Stimulated by Intelaminar Shear," University of Dayton Research Institute, unpublished.

17. Brewer, J. C., "The Effect of Ply Thickness on the Free Edge Delamination of Graphite/Epoxy Laminates", TELAC Report No. 85-9, Massachusetts Institute of Technology, May 1985.

18. Rybicki, E. F., Schmeuser, D. W., and Fox, J., "An Energy Release Rate Approach for Stable Crack Growth in the Free-Edge Delamination Problem," Journal of Composite Materials, Vol. 14 Supplement, 1980, pp. 71-87.

19. Crossman, F. W., Warren, W. J., Wang, A. S. D., and Law, G. E., Jr., "Initiation and Growth of Transverse Cracks and Edge Delamination in Composite Laminates. Part 2. Experimental Correlation," Journal of Composite Materials, Vol. 14 Supplement, 1980, pp. 88-108.

20. O'Brien, T. K., "Characterization of Delamination and Growth in a Composite Laminate," Damage in Composite Materials, ASTM STP 775, American Society for Testing and Materials, 1982, pp. 140-167.

21. Grimes, G. C. and Dusablon, E. G., "Study of Compressive Properties of Graphite/Epoxy Composites with Discontinuities," Composite Materials: Testing and Design, ASTM STP 787, American Society for Testing and Materials, 1982, pp. 513-538.

22. Grimes, G. C., Adams, D. F., and Dusablon, E. G., "The Effects of Discontinuities on Compression Fatigue Properties of Advanced Composites," Northrop Technical Report NOR-80-158, Northrop Corporation, Hawthorne, Calif., October 1980.

23. Ramkumar, R. L., and Adams, D. F., "Compression Properties of Porous Laminates in the Presence of Ply Drop-offs and Fastener Holes," Northrop Technical Report NOR 84-1, Northrop Corporation, Hawthorne Calif., March 1984.

24. Adams, D. F., Ramkumar, R. L., and Walrath, D. E., "Analysis of Porous Laminates in the Presence of Ply Drop-offs and Fastener Holes," Northrop Technical Report NOR 84-113, Northrop Corporation, Hawthorne, Calif., May 1984

25. Dinardo, M. T., and Lagace, P. A., "Buckling and Postbuckling of Laminated Composite Plates with Ply Dropoffs," Proceedings of the AIAA/ASME/ASCE/AHS 28th Structures, Structural Dynamics and Materials Conference, Monterey, California, April, 1987, pp. 776-782.

26. Wu, C. M. L., and Webber, J. P. H., "Analysis of Tapered (in Steps) Laminated Plates Under Uniform Inplane Load," Composite Structures, Vol. 5, 1986, pp. 87-100.

27. Kemp, B. L., and Johnson, E. R., "Response and Failure Analysis of a Graphite-Epoxy Laminate Containing Terminating Internal Plies," AIAA Paper 85-0608, 1985.

28. Curry, J. M., Johnson, E. R., and Starnes, J. H., Jr., "Effect of Dropped Plies on the Strength of Graphite-Epoxy Laminates," Proceedings of the AIAA/ASME/ASCE/AHS 28th Structures, Structural Dynamics and Materials Conference, Monterey, California, April, 1987.

29. Lagace, P. A., and Brewer, J. C., TELAC Maunfacturing Course Notes, Edition 0-2, TELAC Report 81-14, Massachusetts Institute of Technology, September 1981.

30. "Standard Test Method for Tensile Properties of Fiber-Resin Composites," ASTM Designation D 3039-76.

31. Lagace, P. A., "Static Tensile Fracture of Graphite/Epoxy, TELAC Report No. 82-5, Department of Aeronautics and Astronautics, Massachusetts Institute of Technology, June 1982.

32. Brewer, J. C., Weems, D. B., and Archard, K. A., "The Effect of Ply Thickness on Delamination Failure of Graphite/Epoxy Laminates," TELAC Report 84-20, Massachusetts Institute of Technology, 1984.

33. Vizzini, A. J., and Lagace, P. A., "Tebas-TELAC Software User's Manual," TELAC Report No. 84-14-2, 1984.

34. Vizzini, A. J., "Delamination Failure and Compression Fracture of Graphite/Epoxy", Telac Report No. 86-12, Massachusetts Institute of Technology, May 1986.

35. Lagace, P. A., "Nonlinear Stress-Strain Behavior of Graphite/Epoxy Laminates," AIAA Journal, Vol. 23, October, 1985, pp. 1583-1589.

DATA TABLE 1

SUMMARY OF DATA FOR FLAT SPECIMENS

Specimen		Thickness [mm]	E_L [GPa]	σ_f [MPa]
$[\pm(45_2)/0_2]_S$	-1	1.48	60.1	712
	-2	1.56	59.9	818
	-3	1.57	60.7	817
	-4	1.57	61.0	809
	-5	1.55	60.2	838
$[\pm45/0]_{2S}$	-1	1.58	62.2	873
	-2	1.58	63.3	886
	-3[a]	1.59	63.2	859
	-4[a]	1.59	64.6	895
	-5	1.61	62.2	885
$[\pm(45_2)/0]_S$	-1	1.29	45.4	523
	-2	1.30	47.4	532
	-3	1.32	45.6	516
	-4	1.32	45.8	470
	-5	1.31	45.7	482
$[(\pm45)_2/0_2]_S$	-1	1.49	53.5	739
	-2	1.57	62.4	846
	-3	1.56	59.2	830
	-4	1.57	64.9	773
	-5	1.56	63.3	725
$[\pm45/0]_S$	-1	.81	54.3	635
	-2	.84	62.5	893
	-3	.83	57.6	843
	-4	.84	59.4	826
	-5	.83	61.8	825
$[\pm45/0_2]_S$	-1	1.03	79.3	1034
	-2	1.06	82.5	1040
	-3	1.08	87.7	1204
	-4	1.10	88.5	1142
	-5	1.07	80.5	1128
$[\pm45/0/-+45]_s$	-1	.72	44.3	461
	-2	.72	45.5	549
	-3	.73	46.0	608
	-4	.73	43.1	559
	-5	.73	47.2	564

DATA TABLE 1 (Continued)

$[\pm(15_2)/0_2]_S$	-1	1.52	120.9	632
	-2	1.55	126.9	739
	-3	1.56	122.7	689
	-4	1.54	125.8	731
	-5	1.52	121.9	770
$[\pm 15/0]_S$	-1	.83	123.8	882
	-2	.82	121.8	854
	-3	.84	124.2	881
	-4	.83	120.3	893
	-5	.83	120.7	881

[a] Indicates specimen tested with a photoelastic coating

DATA TABLE 2

SUMMARY OF LONGITUDINAL MODULUS DATA FOR PLY DROPOFF LAMINATES

SPECIMEN		LONGITUDINAL MODULUS [GPa]			
		UNDROPPED SECTION		DROPPED SECTION	
		Tapered Side	Flat Side	Tapered Side	Flat Side
$[\pm 45/0/(\pm 45/0)_D]_S$	-1	61.5	64.8	59.2	57.9
	-2	60.4	64.2	60.6	60.3
	-3	61.8	59.2	57.1	59.2
	-4[a]	61.7	a	b	a
	-5	60.2	63.6	59.5	59.6
$[\pm(45_2)/0/0_D]_S$	-1	59.9	55.8	43.1	42.1
	-2	66.2	60.9	43.2	45.6
	-3	60.4	58.8	43.8	44.2
	-4	58.8	58.8	42.1	43.4
	-5	56.0	60.3	40.5	30.9
$[+45/+45_D/-45/-45_D/0/0_D]_S$	-1	49.6	51.9	53.0	51.9
	-2	64.9	60.2	59.3	60.2
	-3	59.0	62.5	61.2	59.5
	-4	61.1	60.9	56.8	56.7
	-5	58.2	61.5	57.1	56.1
$[\pm 45/(\pm 45)_D/0_2]_S$	-1	56.2	57.8	81.2	78.0
	-2	59.3	62.1	84.8	83.0
	-3	64.3	61.7	83.7	80.7
	-4[a]	64.3	a	83.1	a
$[\pm 45/(\pm 45)_D/0/0_D]_S$	-1	56.6	53.9	56.0	57.1
	-2	64.3	62.4	55.9	58.0
	-3	60.3	61.0	61.7	60.5
	-4	61.8	63.0	56.4	61.3
	-5	54.7	60.3	51.5	60.9
$[\pm 45/0_D/0/-+45]_T$	-1	56.5	56.1	42.0	39.7
	-2	58.9	61.7	45.7	41.4
	-3	60.9	62.2	44.3	45.4
	-4[a]	67.4	a	51.3	a
	-5	55.0	61.5	40.7	41.5

DATA TABLE 2 (Continued)

$[+15/+15_D/-15/-15_D/0/0_D]_S$	-1^c	121.1	122.6	125.6	126.1
	-2^c	124.8	124.8	124.9	127.2
	-3^c	126.3	129.1	128.4	129.7
	-4^c	126.4	124.3	b	128.9
	-5^c	b	b	b	b

[a] Indicates specimen tested with a photoelastic coating
[b] No strain data
[c] Geometrically symmetric specimen, no flat or tapered side

DATA TABLE 3

SUMMARY OF THICKNESS AND FAILURE STRESS DATA FOR PLY DROPOFF LAMINATES

SPECIMEN		THICKNESS [mm] Dropped	THICKNESS [mm] Undropped	σ_f [MPa]
$[\pm 45/0/(\pm 45/0)_D]_S$	-1	.84	1.57	657
	-2	.84	1.58	801
	-3[a]	.88	1.57	707
	-4	.86	1.55	759
	-5	.87	1.59	798
$[\pm(45_2)/0/0_D]_S$	-1	1.30	1.60	288
	-2	1.33	1.55	485
	-3	1.35	1.59	470
	-4	1.33	1.54	445
	-5	1.34	1.55	467
$[+45/+45_D/-45/-45_D/0/0_D]_S$	-1	.83	1.48	617
	-2	.86	1.56	798
	-3	.90	1.58	784
	-4	.88	1.54	730
	-5	.85	1.56	682
$[\pm 45/(\pm 45)_D/0_2]_S$	-1	1.05	1.54	1151
	-2	1.07	1.56	1202
	-3[a]	1.07	1.55	1252
	-4	1.07	1.59	1211
$[\pm 45/(\pm 45)_D/0/0_D]_S$	-i	.82	1.51	606
	-2	.85	1.56	841
	-3	.84	1.56	844
	-4	.83	1.57	858
	-5	.84	1.51	854
$[\pm 45/0_D/0/-+45]_T$	-1	.72	.85	519
	-2	.73	.84	546
	-3	.72	.83	559
	-4[a]	.74	.85	576
	-5	.74	.84	540

DATA TABLE 3 (Continued)

$[+15/+15_D/-15/-15_D/0/0_D]_S$	-1	.83	1.51	948
	-2	.84	1.53	954
	-3	.84	1.56	931
	-4	.88	1.56	891
	-5	.87	1.54	952

[a] Indicates specimen tested with a photoelastic coating